Nanoreactors for local production and release of antibiotic

Inauguraldissertation

zur
Erlangung der Würde eines Doktors der Philosophie
vorgelegt der
Philosophisch-Naturwissenschaftlichen Fakultät
der Universität Basel

von
Karolina Langowska

aus
Polen

Basel, 2013

Genehmigt von der Philosophisch-Naturwissenschaftlichen Fakultät auf Antrag von

Prof. Dr. Wolfgang Meier

und

Prof. Dr. Marcus Textor

Basel, den 26.02.2013

Prof. Dr. Jörg Schibler
Dekan

Acknowledgements

I wish to express my sincere appreciation to those who have contributed to this thesis.

I am very grateful to Prof. Dr. Wolfgang Meier for giving me opportunity to work on this project. I would also like to thank the members of my committee, Prof. Dr. Marcus Textor and Prof. Dr. Thomas Pfohl for their precious time and assistance. I would like to thank to PD Dr. Cornelia Palivan for proof reading the manuscript.

The members of the Meier group have contributed immensely to my personal and professional time at the University of Basel. The group has been a source of friendships as well as good advice and collaboration, especially Juan Liu, Patric Baumann, Dominik Dobrunz, Pascal Tanner, and Dalin Wu. Special thanks go to Gabriele Persy (TEM, GPC), Justyna Kowal (AFM), Evi Bieler form the Microscopy Center (SEM), Ruth Pfalzberger (graphics), Dr. Daniela Vasquez (assistance in the light scattering measurements), and Dr. Nico Bruns (discussions).

I wish to thank Dr. Iain Wright for helping me to present my dissertation more fluently and clearly in English.

I am also indebted to the students I had the pleasure to work with. Special thanks to Albert Hofstetter.

I gratefully acknowledge the funding sources that made my PhD work possible. I was funded by the Swiss National Science Foundation, National Research Programme 62 Smart Materials.

Abstract

Implant infections are emerging as a grave medical problem [1].The number of medical and surgical procedures involving medical implant devices will continue to grow, for example due to aging of the population. Device-associated infections are a consequence of bacterial adhesion and subsequent biofilm formation at the implantation site. Due to the importance of this problem, intense research is being focused on finding new, efficient treatments. Conventional antibiotic therapies remain ineffective and very often lead to removal of the contaminated device. Various alternative strategies have been proposed [2], however, these suffer from many drawbacks. Tackling infections associated with medical implants remain a challenge.

In this thesis, enzymatically active, covalently immobilized nanoreactors based on poly(2-methyloxazoline)-*block*-poly(dimethylsiloxane)-*block*-poly(2-methyloxazoline) (PMOXA-*b*-PDMS-*b*-PMOXA) amphiphilic block copolymer were designed and prepared. These nanoreactors catalyzed the conversion of prodrug molecules, which exhibit no antibacterial activity, to a drug active as an antibiotic. The enzymatic conversion was shown to occur only inside the nanoreactors. When these are immobilized they represent a novel, nanosized system whereby a drug will not be released to the entire body, but will be synthesized *in situ*. This strategy offers multiple advantages: long term production of antibacterial compounds due to the protection of the enzyme from proteolytic degradation, control of drug production at a specific rate for a specific period of time, and localized drug delivery.

First, cationic ring opening polymerization was employed to synthesize the polymer. The self-assembly of this polymer was studied, as was the enzymatic activity of the resulting nanoreactor. The covalent attachment of the nanoreactors to a surface was realized by two different strategies: (i) attachment *via* an amino bond, involving Schiff base formation and its further reduction (ii) attachment *via* photo-cleavage by a phenyl azido linker. Both approaches resulted in successful, stable immobilization. The attached nanoreactors were characterized by surface-sensitive techniques such as scanning electron microscopy and atomic force microscopy. Experiments with bacteria were conducted to demonstrate the antimicrobial potential of surface immobilized enzymatically active nanoreactors.

In summary, this thesis develops the concept of polymeric nanoreactors that synthesize drugs *in situ* to inhibit bacterial growth. Additionally, the immobilization methodologies elaborated within the scope of this work could be further adapted for potential applications in biotechnology and biosensing.

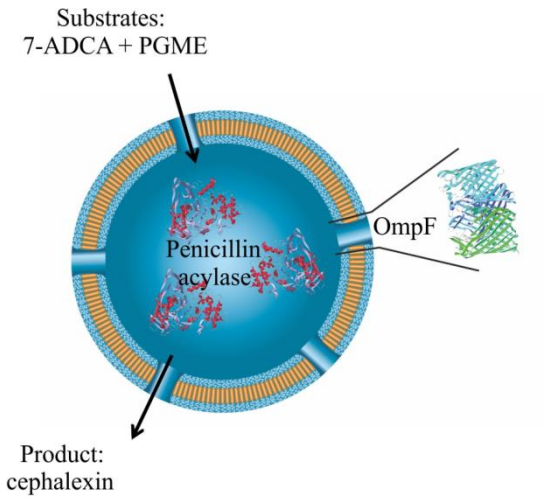

Figure 1. Schematic representation of an enzymatically active nanoreactor synthesizing an antibiotic.

Table of contents

Abbreviations and symbols

7-ADCA	7-amino-3-desacetoxy-cephalosporanic acid
APTS	3-aminopropyltriethoxysilane
Å	angstrom
a.u.	arbitrary unit
AFM	atomic force microscopy
ATR-FTIR	attenuated total reflection Fourier transform infrared spectroscopy
AqpZ	aquaporin Z
4-ABA	4-azidobenozic acid
CalB	*Candida antarctica* lipase B
CROP	cationic ring-opening polymerization
CFU	colony forming units
CMC	critical micelle concentration
DCM	dichloromethane
EDC	1-[(3-dimethylamino)-propyl]-3-ethylcarbodiimide hydrochloride
$CDCl_3$	deuterated chloroform
DNase I	deoxyribonuclease I
DMP	Dess-Martin periodinane
eq	equivalent
EE	encapsulation efficiency
E. coli	*Escherichia coli*
GPC	gel permeation chromatography
Tg	glass transition temperature

HPLC	high-performance liquid chromatography
HOPG	hydrophobic highly oriented pyrolytic graphite
Rh	hydrodynamic radius
OH	hydroxyl group
IPTG	isopropyl β-D-1-thiogalactopyranoside
kDa	kiloDalton
LB	lysogeny broth
LamB	maltose outer membrane porin
mmol	millimole
MIC	minimum inhibitory concentration
M	molar concentration
MW	molecularity
MWCO	molecular weight cut off
MHB	Mueller-Hinton broth
Octyl-POE	n-octylpolyoxyethylene
Mn	number average molecular weight
Tsx	nucleoside specific porin
OD_{600}	optical density at 600 nm
OmpF	outer membrane protein F
POPC	1-palmitoyl-2-oleoyl-s*n*-glycero-3-phosphocholine
PA	penicillin acylase
PGME	(R)-(−)-2-phenylglycine methyl ester hydrochloride
PBS	phosphate buffered saline
PAA	poly(acrylic acid)

PBD	poly(butadiene)
PCL	poly(caprolactone)
PDMS	poly(dimethylsiloxane), α,ω-bis(3-hydroxypropyl)poly(dimethylsiloxane)
PDI	polydispersity index
PEE	poly(ethyl ethylene)
PEO	poly(ethylene oxide)
PEG	poly(ethylene glycol)
PI	poly(isoprene)
PIAT	poly(3-(isocyano-L-alanylaminoethyl)tiophenone)
PIC	polyion complex
PLA	poly(lactide)
PMMA	poly(methyl methacrylate)
PMOXA	poly(2-methyloxazoline)
PSBA	poly(styrenylboronic acid)
PS	polystyrene
^{1}H-NMR	proton nuclear magnetic resonance
Rg	radius of gyration
rpm	revolutions per minute
RNase A	ribonuclease A
SEM	scanning electron microscopy
SEC	size exclusion chromatography
SDS	sodium dodecyl sulphate
SDS-PAGE	sodium dodecyl sulphate polyacrylamide gel electrophoresis
THF	tetrahydrofuran

TEM	transmission electron microscopy
Tris-Cl	tris(hydroxymethyl)amino methane hydrochloride
TfSA	trifluoromethanesulfonic acid anhydride
UV-Vis	ultraviolet-visible spectrophotometry
UVO	ultraviolet ozone
Mw	weight average molecular weight

1 Introduction

1.1 Bacterial related implant infections

Bacterial infections following implant surgeries present major problems after orthopedic, dental or other implant surgeries, and are difficult to treat [3, 4, 5]. They can usually be cured only by surgical removal of the implant, causing patient discomfort and high medical costs, estimated to exceed three billion dollars annually in the U.S.A. alone. Biomaterials, as in an implant, involve risk due to infectious microorganisms. Medical device-related infections include those associated with the biomaterials of artificial joints, e.g. dental-, knee- or hip implants, heart valves and catheters [6, 7]. Bacteria adhere to the implant surface and proliferate. Bacterial adhesion and surface colonization have been widely described in literature [8, 9, 10, 11], but the process is still poorly understood. Bacterial response to antibiotic treatment may vary and, in some cases, a harmful biofilm is created. Biofilm protects growing bacteria from the host immune system and antimicrobial chemical agents and, upon long-term exposure to drugs, microbial pathogens may develop resistance. The host immune system cannot prevent microbial colonization if bacteria adhere to an implant surface covered by biofilm [12]. An increase in medical and surgical procedures has intensified the search for new antimicrobial targeting strategies and medical device materials. Various strategies have been proposed to prevent and inhibit bacterial colonization and biofilm formation.

The six hour post-surgery implantation period is recognized as critical to the prevention of bacterial adhesion and determines the success of the implantation [13]. During this period, an implant is at risk of bacterial colonisation at the implant surface. Although sterile conditions and the use of aseptic techniques are standard, pathogenic bacteria are still present in approximately 90% of implants [14, 15]. Because bacterial adhesion plays a fundamental role in the development of implant-related infections, much research is focused on synthetic surfaces and coatings that could prevent or limit microbial colonization. A so-called "passive strategy" is based on coatings that minimize or eliminate primary bacterial colonization by modification of the physicochemical properties of surfaces. These include, for example, poly(ethylene glycol) [16] (PEG) or

poly(ethylene oxide) [17] (PEO) brushes grafted onto the surface, polyurethane coatings [18] as well as teflon coatings [19], or charge-modified surfaces [20].

Passive strategy approaches have been demonstrated to minimize bacterial adhesion. However, these modified surfaces are not free of drawbacks such as: short lifespan in some cases, unfavourable mechanical properties, low biocompatibility for mammalian cells, and harsh conditions used for coating [21]. Additionally, such modified surfaces can be masked by an adsorbed bacterial film that results in the loss of beneficial anti-adhesive properties. Also, the effectiveness of a passive coating depends greatly on the bacterial species, because bacterial physicochemical properties, e.g. negative charge of the membrane surface or morphology, vary from species to species. As an alternative to passive strategies, active strategies are proposed, which have been shown to both limit surface colonization and prevent biofilm formation [1, 22]. The aim is to avoid or inhibit primary colonising bacteria by releasing chemical agents.

Primary attention is focused on antimicrobial agents incorporated in materials or coatings [23, 22]. Some of these are commercially available – including poly(methyl methacrylate) (PMMA) antibiotic-loaded bone cement [24]. The major disadvantage here is poor control over the rate and manner in which the drug is released. When microorganisms are exposed over long periods to low doses of antibiotics, such as gentamycin or vancomycin, they eventually become resistant [25, 26]. All *in vitro* studies [27] indicate that only 5 – 8% of antibiotics incorporated in a polymeric matrix are eventually released, over up to 9 weeks. The duration of testing, sample geometry, temperature, pH or the detection assay strongly affects the amount of released drug. *In vivo* studies also confirm that only a minor portion (5 – 18%) of antibiotic incorporated in bone cements is eluted [28, 29]. Furthermore, *in vitro* studies also show bacterial growth in the interfacial gap between antibiotic-loaded bone cement and the bone [30]. Also, release of doses which are too high may cause toxicity and illicit an immune response [31]. Moreover, the incorporation or coating procedure must not damage the material (e.g. stability, mechanical properties, host compatibility) and cannot influence the stability or activity of the drug. Implant-related infections are still a challenge to medicine. Therefore, new drugs delivery systems employing nanotechnology could be more effective and safer than available ones. The use of nanotechnology to design and prepare new systems for delivery of antimicrobial drugs has been explored as a promising alternative to the current approaches [32].

1.2 Amphiphilies and general aspects of self-assembly

The interest in amphipilic block copolymers has greatly increased in the last 20 years due to their unique molecular structure. They consist of a hydrophobic (non-polar) and a hydrophilic (polar) part, which are linearly covalently linked as series of two or more blocks. Because of their amphiphilic nature (from the Greek *amphis*: of both kinds, *philic*: having an affinity for [1]) they arrange themselves at interfaces or aggregate in solution, forming supramolecular structures such as vesicles, rods, and micelles. In the classical, geometrical description of the amphiphilic aggregation the size of the hydrophobic part in relation to the size of the hydrophilic moiety is the morphogenic factor. The variety of morphologies is primarily a result of the molecular curvature and the packing of the copolymer chains (Figure 2). The "packing parameter" allows targeting of the specific self-assembled structure and it is defined as:

$$p = \frac{v}{a_o l_c} \qquad (1)$$

Where v is the volume of the hydrophobic moieties, a_o is the optimal area of the hydrophilic moieties, and l_c is the length of the hydrophobic chain. Spherical micelles are formed when $p \leq \frac{1}{3}$, cylindrical micelles when $\frac{1}{3} \leq p \leq \frac{1}{2}$, and vesicles when $\frac{1}{2} \leq p \leq 1$ [33].

The first report on self-assembly of a fully synthetic diblock copolymer was published by Zhang and Eisenberg [34]. Various structures were obtained for polystyrene-*block*-poly(acrylic acid) (PS-*b*-PAA) diblock copolymer by graduate decrease of the PAA content, which resulted in spheres, rods, vesicles, lamellae, and inverse micellar aggregates. Another example of the polymorphism of block copolymers self-assemblies is a series of poly(ethylene oxide) based di- and triblock copolymers, which demonstrated structural changes associated with variation of molecular composition, e.g. on the content of PEO blocks [35]. In brief, a decrease of the hydrophilic to hydrophobic moieties ratio result in morphological changes from spherical to cylindrical and finally to bilayers. Amphiphilic self-assembly can be also described by thermodynamic aspects, where the minimization of the total free energy is the driving force of the self-assembly [36]. For

[1] The Oxford Greek Dictionary, by Niki Watts, Oxford University Press, 2000

amphiphiles the free energy is mainly contributed to interfacial energy of the hydrophobic-hydrophilic interface and entropic loss. In aqueous solution the hydrophobic blocks of the copolymer tend to associate with each other in order to minimize their direct exposure to water, whereas the hydrophilic parts point towards water. This causes a decrease in the total entropic loss, due to the reduction in contact between hydrophobic moieties and water molecules ("hydrophobic effect"). In 1959 Kauzmann used the term "hydrophobic effect" for the first time in his review article on protein denaturation [37].

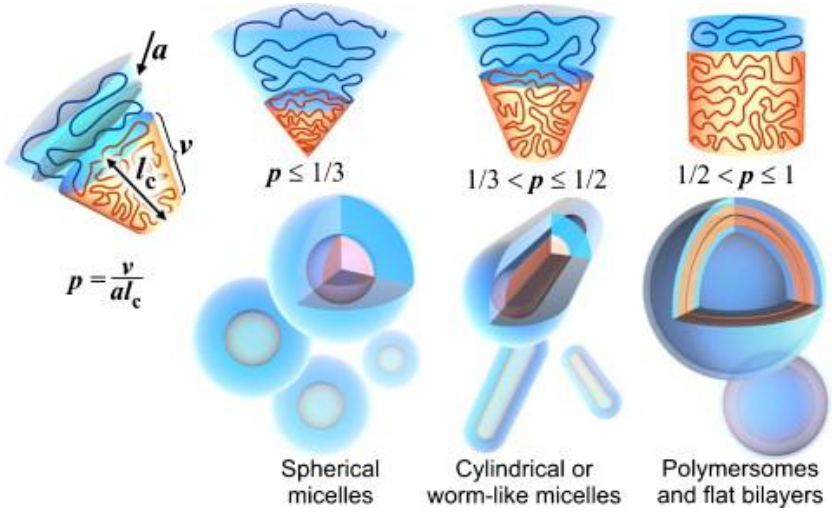

Figure 2. Various self-assembled structures formed by amphiphilic block copolymers at different packing parameters, p [38].

Decrease of the free energy is also achieved by the reduction of interfacial contact area at the hydrophobic and hydrophilic interface. This minimizes the interfacial area per unit volume. Nevertheless the self-assembly process is very complex and still not fully understood, and the debate among specialists continues.

Vesicles (*vesicula* from the Latin: bladder [2]) are closed hollow-spherical structures with an aqueous interior that is separated from the bulk by a membrane. The term vesicle is more general, and includes lipidic vesicles as well as synthetic surfactants and amphiphilic polymers. When vesicles are made of block copolymer are referred as

[2] Oxford Latin Dictionary, Edited by P. G. W. Glare, Oxford University Press, 1983

polymersomes, the term was used for the first time by Discher and co-workers in a paper on the elastic properties of poly(ethylene oxide)-poly(ethyl ethylene) (PEO-PEE) based vesicles [39]. Lipids are low molecular counterparts of amphiphilic block copolymers, and since they are derived from nature, tend to be biocompatible, and are widely used for biomedical applications, especially in the field of drug delivery [40, 41, 42]. Lipids typically have a total MW of less than 1 kDa, whereas polymers have a MW to the order of 10 kDa. Polymeric vesicles exhibit enhanced mechanical and physical properties compared to their lipidic analogues due to the higher molecular weight of the block copolymers. Polymeric amphiphiles offer some additional advantages. The critical micelle concentration (CMC) of polymeric surfactants can be controlled so that it is extremely low; hence efficiency is kept even at high dilutions. The permeability of molecules through the polymeric wall is much slower compared to lipidic wall. This is due to the higher thickness of the polymer which is between 5 to 20 nm, whereas for lipids between 3 and 5 nm. Additionally the stability of polymersomes against lysis by classical surfactants is significantly higher than that of liposomes. Also tunable membrane permeability of polymersomes was achieved for example by the reconstitution of channel proteins in polymeric membrane [43, 44, 45], membrane plasticization of the vesicle wall [46, 47], or use of stimuli responsive copolymers to induce pore-generating components [48]. A number of papers have been published illustrating the wide range of possible chemistries allowing functionalization of polymeric vesicles for potential applications in drug delivery, sensing and hybrid materials synthesis [49, 50, 51, 52]. In this respect polymersomes are more versatile then liposomes since their exhibit higher stability and toughness, and can be decorated with responsive and reactive groups.

The formation of vesicles was described theoretically by Wang [53]. The process of vesicles formation is complex but it can be shortly summarized: when a bilayer formed by two monolayers consists of diblock copolymer, vesicles may become favoured over flat bilayers when the outer block (in an outer block-like solvent) is much larger than the inner block. In other words, the vesicles formation is a two-step aggregation process, in which first a flat bilayer is formed, and in a second step, it closes to a spherical vesicle. The morphology of vesicles can be affected by any number of morphogenic factors such as relative block length, presence of solvents or surfactants, addition of salts, bases, acids, temperature etc. [54, 55, 56]. For example, morphological changes of PS-*b*-PAA were induced by addition of acid (HCl) or salts ($CaCl_2$ or NaCl) [54]. With the increasing concentration of

added ions the morphology of formed self-assembled structures changed from spheres to rods, vesicles and to large compound vesicles.

All methods developed for liposomes preparation are also valid for polymersomes. In general, preparation techniques can be either solvent free or involve organic solvents. In the first approach, the dry amphiphile is dissolved in water and is subsequently hydrated to vesicles. The advantage is that no organic solvent is present in the system, which makes this preparation method suitable for medical applications. In the solvent displacement methods, the block copolymer is first dissolved in an appropriate organic solvent and then mixed with aqueous medium. The solvent is subsequently removed by dialysis, ultrafiltration, under reduced pressure etc. It should be noted that it is not possible to completely remove all solvent. Solvent residues may interfere in biological or medical applications.

To generate well-defined nanosized vesicles usually film rehydration (film swelling) [57], direct dissolution in water (bulk swelling) [58], electroformation [59] or solvent displacement methods (involving a co-solvent) [60, 61] are used, followed by subsequent, repeated extrusion through polycarbonate filters [62], size exclusion chromatography [63] or freeze-thawing [64].

The film rehydration method, used in this work, involves the solubilisation of the block-copolymer in an organic solvent that can dissolve both blocks, and the subsequent removal of the solvent by evaporation under reduced pressure to produce a thin film on a solid surface. Ethanol and chloroform are most commonly used solvents for the preparation of vesicles based on PMOXA-*b*-PDMS-*b*-PMOXA block copolymer. Next, aqueous buffer is added, leading to the hydration of the film. This approach yields vesicles with a broad size distribution.

1.3 PMOXA-*b*-PDMS-*b*-PMOXA block copolymer and its synthesis

One of the polymerization techniques used to synthesize block copolymers is macroinitiator polymerization, where a macromolecule is capable of entering into further polymerization or other reactions through its reactive end-groups [3]. When the pre-polymer contains two active sides it is called telechelic polymerization. The telechelic polymerization is based on the polymerization of a monomer on pre-existing polymer molecule (pre-polymer) with active sides. The side chains grow on the activated side of the macroinitiator. The length of the resulting chain depends on the amount of the monomer used and the number of active sides in pre-polymer. Various examples of di- and triblock copolymer containing oxazoline block were obtained by this polymerization technique [65, 66, 67, 68].

The choice of the block copolymer was based on considerations regarding the self-assembly properties (i.e. vesicles formation). Furthermore, the hydrophobic block should display flexibility allowing for channel protein insertion. Finally, the block copolymer must be suitable for *in vivo* application.

Poly(dimethylsiloxane) α,ω-bis(3-hydroxypropyl)poly(dimethylsiloxane) (PDMS) was chosen as the middle block because of its hydrophobicity, high chain flexibility [69], low glass transition temperature (Tg = 146 K) [70], good thermal and oxidative stability [71], low surface tension and low surface activity [72], high biocompatibility [73] (it is used as coating material of plasma bottles, in contact lenses as well as in heart valves) and high chemical and biological stability [72]. PDMS unique properties are due to the fact that the siloxane backbone possesses a superior flexibility. On the one hand, the Si-O bond is very polarised, highly ionic and should lead to strong intermolecular interactions. On the other hand, the methyl groups are closely packed and interact weakly with each other. The close packing of the hydrophobic methyl side groups shields the main backbone [74].The high flexibility of the siloxane chain allows for conformational adaptation.

Poly(2-methyloxazoline) (PMOXA) was selected as hydrophilic block because it possesses protein-repellent and stealth properties [75, 76]. PMOXA is non-ionic, stable, shows excellent anti-fouling properties [77] and it was found that PMOXA graft copolymer

[3] Encyclopedia of Polymer Science and Technology, 4th Edition, Wiley

films were significantly more stable than polyethylene glycol graft copolymer [78]. PMOXA, called a peptide-mimetic polymer because of its isomeric to that of polypeptides structure. It has been shown to exhibit favourable properties for a number of biological and medical applications, e.g. stealth liposomes [79, 75], cell targeting [80] and drug delivery [81]. Polyoxazolines were developed as a food additive and animal safety studies proved its safety [82]. Numerous papers showed that polyoxazolines can be used in multiple pharmaceutical and medical applications [83, 84]. Polyoxazolines can be easily functionalised from the terminal hydroxyl, carboxyl or amino group to allow conjugation of amine, thiol, aldehyde or ketone.

2-methyl-2-oxazoline monomers can be polymerized by cationic ring opening polymerization (CROP) on PDMS pre-polymer activated with trifluoromethanesulphonic acid anhydride (TfSA) in the presence of pyridine under a dry argon atmosphere. TfSA was used to convert hydroxy end-groups of PDMA to form a highly reactive bifunctional macroinitiator. The resulting triflate ion pair is a highly reactive leaving group and a strong electrophile [85] which attacks the C-O bond of the oxazolinium ion [86].
The α,ω-telechelic PDMS macroinitiator initiates the cyclic imino ether polymerization of 2-methyl-2-oxazoline. The living cation can be terminated by the introduction of a nucleophile such as OH^-, COO^-, NH^- or S^-. Moreover, the mass ratio of hydrophilic to hydrophobic blocks was kept in the range 35% ± 10% as found to be optimal for other vesicle-forming polymers [87, 88].
Because of the very high reactivity of the macroinitator the cationic polymerization of 2-methyl-2-oxazoline has to be performed under strict anhydrous conditions. High vacuum as well as dry nitrogen or argon are necessary. The reagents and solvents used for the polymerization should be dried and the contact with air has to be avoided. In the experimental setup and methodology employed all impurities capable of deactivating the initiator and the terminating the propagating chain (moisture from air, oxygen, etc.) must be excluded from the polymerization mixture as much as possible. Moisture influences the polymerization degree considerably which can lead to macroinitiator deactivation or side reactions.

1.4 Polymersomes as nanoreactors

Cells are highly organized structures in which compartmentalisation and confinement play major role. Compartmentalisation offers many advantages: molecules stay close together, which leads to preferential interactions, and provides control and precision of biochemical processes. One the one hand, sensitive species or process are protected from harmful factors; on the other hand, processes involving highly reactive or reagents or conditions are separated and cannot influence rest of the cell components. Assembly of enzymes *in loco* enhances the efficiency of metabolic process. In other words compartmentalisation enables a cell to execute various chemical and biochemical processes in a controlled way, excluding undesired interactions. Closed, synthetic systems that mimic natural compartments and protect, transport and catalyze reactions, inspired by nature, are a challenge to scientists.

Polymersomes are an important class of nano-capsules able to encapsulate many different cargos, e.g. enzymes. They are ideal nanosized containers that can carry-out biocatalytic reactions. Permeable polymersomes containing catalytic species can be utilised as nanoreactors, able to mimic biochemical reactions.

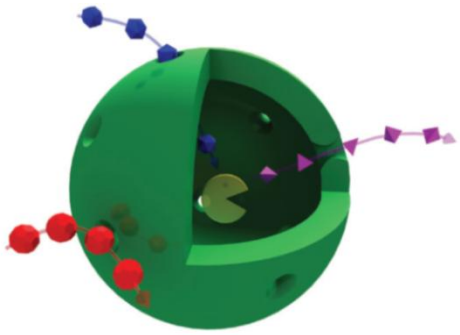

Figure 3. Schematic representation of a nanoreactor. Nanoreactors allow only specific molecules to enter the inner cavity while others are blocked from entering [89].

A polymeric shell is an essential part of a nanoreactor system and should remain intact to protect the encapsulated enzyme from degradation. At the same time, however, permeability of the vesicular wall has to be introduced to allow the transport of substrate and product molecules across the polymer membrane.

Several methods were described to obtain permeability of the polymeric membranes. Capsules produced using the layer-by-layer method and based on polyelectrolytes were shown to be permeable for substrates. In this case the porosity is an intrinsic property of the polyanions and polycations [90, 91, 92]. An interesting example of a nanoreactor based on neutral block copolymer polystyrene-*b*-poly(3-(isocyano-L-alanylaminoethyl)tiophenone) (PS-*b*-PIAT) was designed and prepared by Van Hest and co-workers [93, 94, 95]. PS-*b*-PIAT nanoreactors are porous due to the robust, helical conformation of the PIAT hydrophilic block and the relatively low molecular weight of the PS hydrophobic block. This inherently porous membranes, allows passive diffusion of small molecules, while large species such as enzymes, stay inside. Kataoka and co-workers prepared stable polymersomes with a semipermeable membrane through simple mixing of a pair of oppositely charged block copolymers in an aqueous medium. The polymersome based on a polyion complex (PIC) was called a "PICsome" [96, 97]. Semi-permeable polymersomes obtained by a synthetic approach have been also reported. The polymersomes, were prepared by aqueous assembly of a mixture of polymerizable amphiphillic diblock copolymer poly(ethylene oxide)-*b*-poly(butadiene) (PEO-*b*-PBD), and phospholipids, 1-palmitoyl-2-oleoyl-s*n*-glycero-3-phosphocholine (POPC). After crosslinking with the use of a chemical initiator, the phospholipids were extracted with a surfactant (Triton X-100), leaving behind a highly porous outer membrane [98]. Also, porous polymersomes based on poly(caprolactone)-PEG were obtained by removal of POPC [99]. A sacrificial block copolymer, poly(styrenylboronic acid)-*b*-poly(ethylene glycol) (PSBA-*b*-PEG) was mixed with a traditional amphihilic block copolymer poly(styrene)-*b*-poly(ethylene glycol) (PS-*b*-PEG) [48]. Upon increasing the pH and the concentration of monosaccharide, the sacrificial block was solubilised in an aqueous solution, creating porosity in the membrane. This system offers control of membrane permeability by varying the amount of PSBA-*b*-PEG. In cells, membrane permeability is mainly due to the presence of channel proteins. Bio-inspired insertion of channel protein in polymeric membrane was pioneered by the group of Meier [100, 101, 102, 44]. The low glass transition temperature (*Tg*) of the hydrophobic block allows incorporation of channel proteins. Various channel proteins

have been successfully inserted in the PMOXA-*b*-PDMS-*b*-PMOXA block copolymer membrane: outer membrane protein F (OmpF) [100], maltose outer membrane porin (LamB) [102], aquaporin Z (AqpZ) [44], nucleoside specific porin (Tsx) [45]. These retain structure and thus function, allowing for passive diffusion of both substrates and products.

In the case of enzymatically active nanoreactors the enzyme is the key component. The first step towards biocatylysis inside nanoreactors was encapsulation of the proteins myoglobin, haemoglobin and fluorescein labelled bovine serum albumin inside poly(ethylene oxide)-*b*-poly(ethyl ethylene) (PEO-*b*-PEE) or poly(ethylene oxide)-*b*-poly(butadiene) (PEO-*b*-PBD) polymersomes [58].

Nanoreactors prepared from PMOXA-*b*-PDMS-*b*-PMOXA block copolymer have demonstrated a broad variety of biological applications. A fully functional nanoreactor based on PMOXA-*b*-PDMS-*b*-PMOXA encapsulating β-lactamase was used to hydrolyse an antibiotic, ampicillin, and was one of the first examples of an enzymatically active polymer-based nanoreactor [100]. A number of papers showed the versatility of PMOXA-*b*-PDMS-*b*-PMOXA based nanoreactors with channel protein inserted in the polymeric membrane. These include: prodrug-activating nanoreactors with potential application for cancer treatment [81], an antioxidant nanoreactor based on superoxide dismutase [103] (in this case without channel protein, since the block copolymer was shown to be permeable to oxygen), immobilized nanoreactors with acid phosphatase enzyme [104], thymidine phosphorylase-encapsulating nanoreactor for replacement therapy [45], superoxide dismutase and lactoperoxidase-loaded nanoreactors for an enzymatic cascade reaction to combat oxidative stress [105].

Vesicles made of PS-*b*-PIAT were loaded with *Candida antarctica* lipase B (CalB) enzyme. The activity of the entrapped enzyme was tested by adding the low molecular weight substrate 6,8-difluoro-4-methylumbelliferyl octanoate, and was analysed by fluorescence spectroscopy [93]. The enzyme was encapsulated inside the inner cavity of polymersomes or positioning inside the bilayer [94]. It was observed that when an enzyme was encapsulated in the nanoreactor, its activity was close to the activity of free enzyme in solution, this is in contrast to the CalB localised in the bilayer where steric hindrance plays a role. This system was further developed for cascade reactions of multiple catalytic species [106]. A three-enzyme cascade reaction was achieved by encapsulation of glucose oxidase in the inner part of the polymersome, localisation of CalB in the membrane, and attachment of horseradisch peroxidase to the outer periphery of the polymersome.

An additional benefit of polymeric nanoreactors is the possibility of surface functionalization, which enables specific cellular targeting and cellular uptake [80, 107, 51]. For example, PMOXA-*b*-PDMS-*b*-PMOXA based nanocontainers were functionalized with a specific ligand for a target receptor – the macrophage scavenger receptor SRA1 [80].

1.4.1 Nanoreactor immobilization

The immobilization of polymer vesicles on surfaces is of crucial importance for drug delivery and sensors. The immobilization of polymeric vesicles for *in vivo* applications must fulfil various requirements: the procedure must be implementable in aqueous, solvent-free media, the vesicular structure must be preserved, toxic agents cannot be involved, long-term stability under physiological conditions must be exhibited and, in the case of enzymatically active nanoreactors, the stability and activity of the enzyme must be retained. Therefore, a versatile, robust, mild and efficient immobilization technique is crucial for the preparation of functionalised surfaces. Several immobilization methodologies have been described in literature.

One technique to achieve immobilization is to embed nanoreactors in polysaccharide hydrogels [108]. Hyaluronic acid (a polysaccharide consisting of disaccharide units of a-1,4-glucuronic acid and b-1,3-N-acetyl glucosamine) was functionalized with either azide or acetylene moieties and subsequently gelated by the Cu (I)-catalyzed Huisgen 1,3-dipolar cycloaddition reaction [109]. $CuSO_4$ was used to form Cu (I) ions *in situ* by mixing with ascorbic acid. The gelation process did not change morphology of the polymersomes and the encapsulated enzyme remained active. However, the use of copper as the catalyst as well as the redox conditions are unfavourable for biological and pharmaceutical applications. Reversible immobilization was achieved by Coulomb interactions mediated by magnesium ions [110]. Non-ionic poly(ethylene oxide)-*b*-poly(propylene oxide)-*b*-poly-(ethylene oxide) (PEO-*b*-PPO-*b*-PEO) was mixed with poly(acrylic acid) (PAA), which is negatively charged at neutral pH, resulted in vesicles that were attached to the surface at room temperature and detached with increasing temperature.

The covalent binding of amines and aldehydes *via* formation of Schiff base and subsequent conversion to an amine bond by reductive amination has been previously used by Huang [111] for the covalent attachment of block copolymer micelles to amino-

functionalized surfaces. The aldehyde functionalised poly(ethylene glycol)-poly(DL-lactic acid) (PEG-PLA) copolymeric micelles were bound to amine-functionalised TiO_2 and Au [111]. This same methodology was used to immobilise poly(lactide-*b*-ethylene oxide) (PLA-*b*-PEO), poly(caprolactone-*b*-ethylene oxide) (PCL-*b*-PEO), and poly(isoprene-*b*-ethyleneoxide) (PI-*b*-PEO) polymersomes on aminated glass surfaces [112]. However, aliphatic imines are known to be unstable and hydrolyse to amine and aldehyde functionalities [113].

Receptor-ligand pairing, e.g. biotin-streptavidin was used to immobilize enzymatically active nanoreactors [104]. Althought biotin and strepatividin form one of the strongest non-covalent interactions (dissociation constant is 10 - 12 M) [114] there is the possibility of ligand exchange with other biotinylated molecules in response to changes of ionic strength or temperature [115]. Such an immobilization method cannot be applied to *in vivo* studies because streptavidin is known to block essential immune reactions in the human body [116].

In summary, to covalently attach nanoreactors on solid substrates is still a challenge. Furthermore, well-defined, reproducible and stable immobilization techniques for polymersomes as well as nanoreactors are important for both fundamental studies and practical applications.

In this work the covalent immobilization of nanoreactors on surface was accomplished by two strategies. The first one is based on imine formation followed by reductive amination to form a stable amine bond. In comparison to other immobilization methodologies this does not require the use of a toxic catalyst (such as copper [108]), it is not susceptible to changes in the environment (electrostatic interactions or Schiff base) [110, 112], which can lead to extensive detachment of vesicles, it lacks diffusion limits (embedded into hydrogels) [108] and does not cause an immune response [104]. Recently, Domes and colleagues [112] showed that covalent binding *via* a Schiff base can readily be used to attach block copolymer vesicles without disrupting vesicular structure. As mentioned above, aliphatic imines are known to be unstable, therefore a stronger, more stable bond is required to prevent uncontrolled vesicle detachment. To obtain a more stable bond the proposed strategy was modified by reductive amination of a Schiff base to an amine. In contrast to imines, amines show no hydrolysis and are stable in aqueous solution. A simple, non-toxic reductive amination of aldehydes was applied (with amines using 2-picoline borane as a reducing agent), as previously described [117, 118]. Because this

attachment reaction is carried out under mild conditions in aqueous buffer, without an additional catalysing agent, it is applicable for pharmaceutical and therapeutic purposes. The potential of this method for long-term, stable immobilization of polymeric vesicles has never been demonstrated.

The second immobilization strategy involves bifunctional aromatic coupling agent, which acts as a photolinker. The photolinker-mediated technique is widely used for covalent binding of proteins to solid surfaces under mild reaction conditions [119]. This method is based on a compound having at least two functional groups, one of which is essentially a photoactive group. The most commonly photoactive compounds used for covalent attachment of proteins are aromatic azides [120]. The photo-immobilization is simple and reproducible and has been proven to be efficient to immobilize various components including biomolecules [121, 122], polysaccharides [123] and nanoparticles [41, 124].

The process of the photoreaction can be divided into two steps. First, nitrene formation is triggered by UV irradiation, i.e. the azido groups are converted to nitrene and release N_2. Second, the nitrenes immediately undergo further reactions such as insertion into C-H, N-H and O-H bonds, addition to olefins, or proton abstraction reactions to give corresponding amine [125, 126]. This immobilization strategy is easy to perform and very attractive for the immobilization of molecules that do not possess any suitable functional group for attachment *via* conventional chemical reactions, as was previously reported for furanones [122] or graphenes [127]. Therefore this approach is inherently versatile and should be applicable to a variety of molecules and materials especially those that do not possess reactive functional groups. Additionall benefits include selective modification where the desired areas can be specially modified by a focused UV-light beam or by using quartz photo-mask.

Photo-immobilization results in a covalent bond between the surfaces and the immobilized molecules that can withstand fluid flow as well as variations in temperatures and pH. One of the advantages of using azides is their simple and easy preparation.

Poly(2-ethylen-2-oxazoline) is a member of the family of polyoxazolines which includes poly(2-methyloxazoline) as used in this work, was successfully immobilized *via* azido photolinker [128]. We used 4-azidobenzoic acid (4-ABA) as photolinker [120]. 4-ABA is a photoactive molecule commonly employed in biochemistry and molecular biology, as for example, a photo-affinity reagent for labeling [129] or as a photolinker to immobilize polysaccharides [130] and peptides [131]. The biggest benefits are a very short time of

immobilization (20 minutes) and lack of a catalyst. This strategy fulfils all of the requirements mentioned before and compared to the first strategy does not require polymer modification.

1.4.2 Prodrug activating nanoreactors

It is unquestionable that microbial infections associated with medical devices constitute an essential problem in modern medicine. A new antimicrobial strategy employing nanotechnology, which may turn out to be more efficient and safer than those conventionally available is highly desirable. A nanosized platform for localized, controlled drug delivery would be a promising alternative offering distinct advantages in reducing systemic toxicity, overcoming resistance, controlled delivery in regard to treatment time as well as dosage, minimized side effects via localized delivery, and delivery on-demand.

Often drugs are highly toxic and direct oral or intravenous administration causes systemic toxicity. Also part of the drug can be deactivated or cleared from the system. The concept of prodrug therapy was developed in the 1980s for anticancer treatment [132]. The goal in cancer therapy is to kill tumour cells selectively without harming healthy tissue. One of the approaches is to administer and accumulate an enzyme at the tumour site [133]. The enzyme is able to catalyze conversion of non- or less toxic prodrugs into the active, cytotoxic drugs at the tumour site. The main drawback of this methodology is that the enzyme can be immunogenic and/or degraded by proteolytic enzymes before reaching the tumour site. The elimination of secondary effects associated with systemic delivery of cytotoxic agents is achieved by site-specific release only at the site of the action which leads to high local concentrations of drug. Enzymes were demonstrated to be applicable in prodrug-antibiotic therapy [134]. β-Lactamases are naturally occurring in various pathogenic bacteria and are highly efficient and specific catalysts. Various relatively non-toxic drug precursors (such as cephalosporin-taxol prodrug) [135] were converted into drugs by hydrolytic cleavage of the β-lactam ring.

The concept of using nanoreactors as prodrug-activating nanoreactors with potential application for cancer treatment was explored by encapsulation of purine-specific nucleoside hydrolase of *Trypanosoma* V*i*V*ax* [81]. The enzymatic activity of the

nanoreactors for three natural substrates, inosine, adenosine, and guanosine, and one prodrug (2-fluoroadenosine), resulting in the release of the cytotoxic molecule, 2-fluoroadenine, was investigated. Also other potentially therapeutic enzymes were efficiently encapsulated inside permeable polymersomes yielding active nanoreactors [100, 45]. The biocatalyst – native enzymes have very short blood circulation times, are sensitive to environmental changes and small conformational changes may induce loss of activity. The encapsulation of the enzyme protects it from potentially harmful environmental factors, allows control of drug production at a specific rate for a specific period of time by adding predetermined amounts of substrate to the outer medium, minimization of dosages and therefore systemic toxicity, and limitation of immune response.

2 Scope of the thesis

The aim of this thesis is to design and prepare nanoreactors based on an amphiphilic block copolymer, and study their further immobilization on a surface, for prevention and inhibition of bacterial growth associated with surgical implants. For this purpose an enzyme will be encapsulated inside nanoreactors. Conversion of molecules without antimicrobial activity into a drug will be ensured by the biocatalyst entrapped in the inner cavity of a nanoreactor. The conversion will be controlled by the amount of pro-drugs added to the aqueous environment. Firstly, a triblock copolymer will be synthesized and characterized with well-established techniques such as ^{1}H-NMR, gel permeation chromatography (GPC) and attenuated total reflection Fourier transform infrared spectroscopy (ATR-FTIR). The obtained block copolymer should form vesicles in aqueous solution and allow functionalization of the self-assembled polymersomes through insertion of a channel protein, allowing for transport through the polymeric wall as well as encapsulation of an enzyme. The feasibility of the resulting nanoreactors, with regard to the stability necessary for long-term application, their encapsulation efficiency and their enzymatic activity will be examined. The polymersome immobilization methodologies that have been explored and employed do not meet specific criteria: reliable vesicular shape, preservation of enzyme activity, mild, non-toxic conditions, long-term stability under physiological conditions. Therefore, the bulk of this thesis is dedicated to the development of versatile, robust, and efficient nanoreactor immobilization methods, which are crucial to the creation of functionalized surfaces.

The choice of the immobilization approach will be determined by the applicability in biomedical and pharmaceutical realms. The selected methodology should fulfil particular criteria. Two strategies that achieve the above mentioned objectives will be used to covalently attach nanoreactors on a model surface. Surface functionalization and nanoreactor attachment will be studied by various complementary techniques, i.e. water contact angle, ATR-FTIR, scanning electron microscopy (SEM) and atomic force microscopy (AFM). Finally, surface immobilized nanoreactors will be tested with regard to their antibacterial activity in solution and on a surface.

3 Results and discussion

3.1 Polymer synthesis and characterization

PMOXA-*b*-PDMS-*b*-PMOXA block copolymer was synthesized by cationic ring opening polymerization (CROP) [136]. The reaction scheme is depicted in Figure 4.

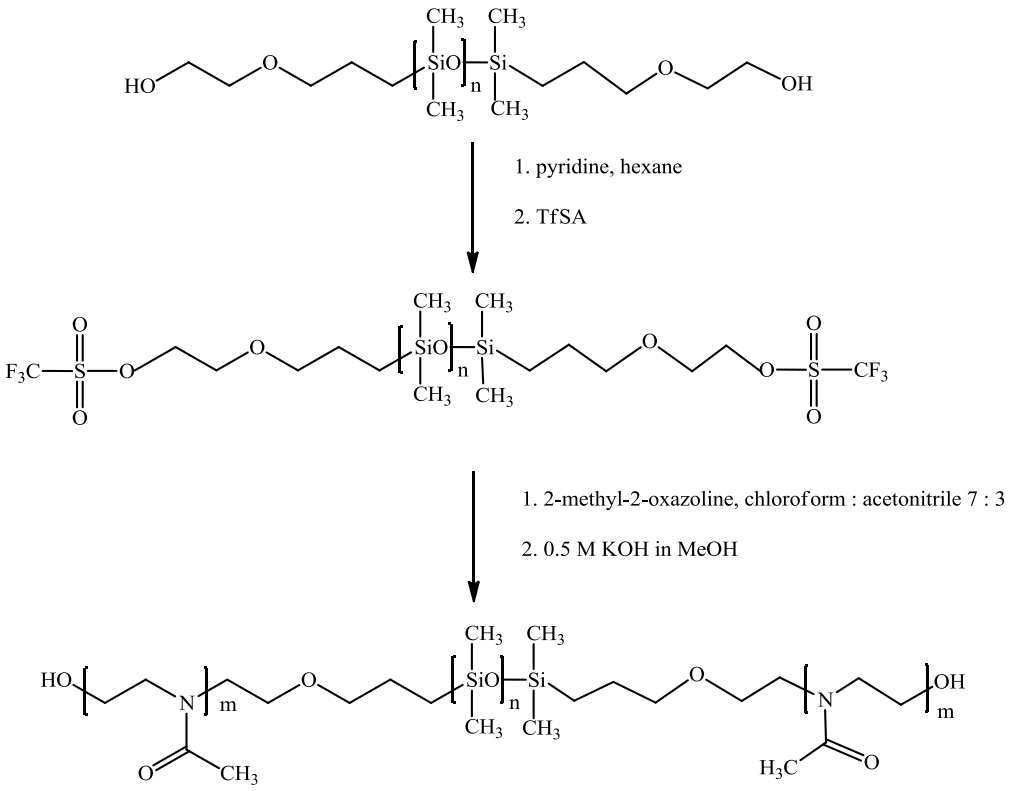

Figure 4. Reaction scheme for the PMOXA-*b*-PDMS-*b*-PMOXA block copolymer synthesis.

The α,ω-telechelic PDMS was activated by trifluoromethanesulfonic anhydride, thereby initiating the cyclic imino ether polymerization of the 2-methyl-2-oxazoline monomer. CROP is known to yield a well-defined polydispersity and molecular weight for the

PMOXA side chains [137]. The highly-living character of onium-triflates ion pairs, as demonstrated by Segusa *et al.* [138] resulted from the well-propagating triflate species. However, PDMS can also degrade in the presence of triflic acid [139]. Pyridine was added to the reaction mixture in order to form the salt of the trifluoromethanesulphonic acid, which can be filtered from of the activated PDMS macroinitator. The complete removal of this salt is essential to avoid polymerization of free poly(2-methyloxazoline) chains. To terminate the polymerization, a solution of potassium hydroxide in methanol was added to the reaction mixture, resulting in hydroxyl end groups [137]. The obtained polymer was characterized by ^{1}H-NMR, GPC and ATR-FTIR.

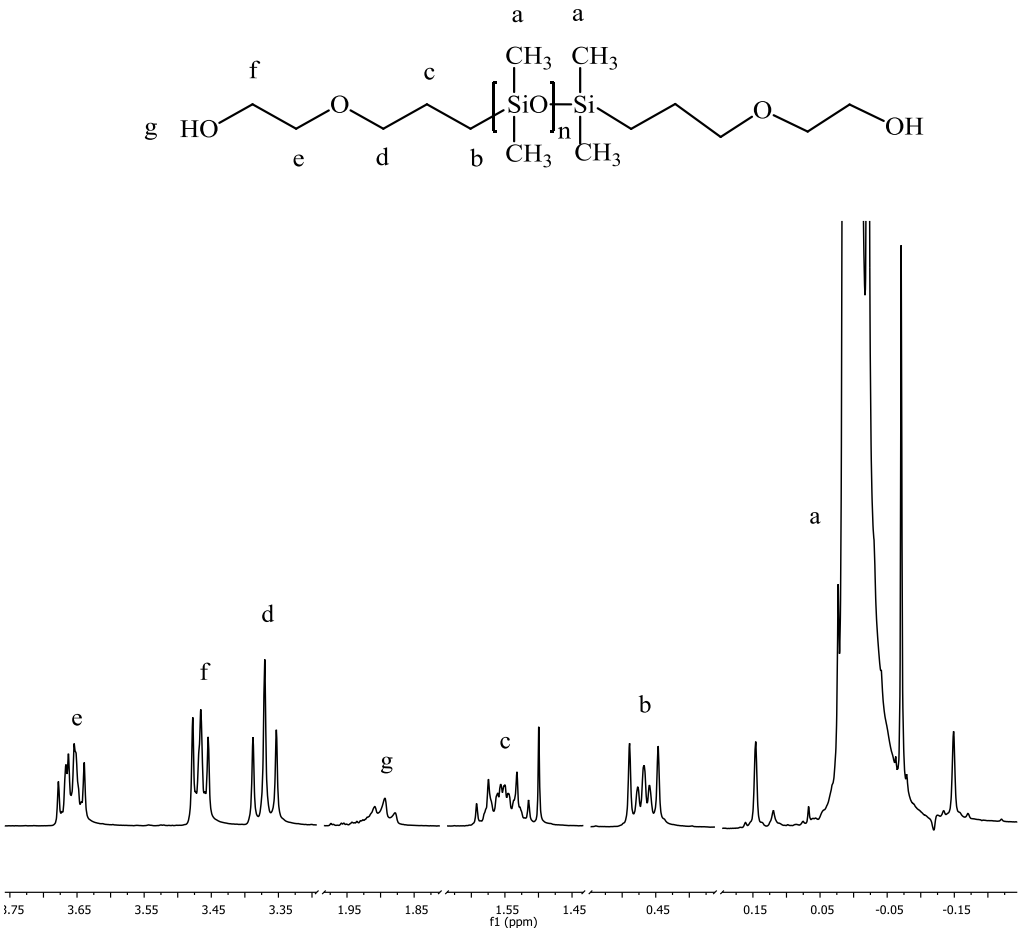

Figure 5. ^{1}H-NMR spectrum of α,ω-bis(3-hydroxypropyl)poly(dimethylsiloxane) pre-polymer in $CDCl_3$. A detailed peak assignment is presented in the Experimental part.

Compared to the spectrum of the pre-polymer (see Figure 5), new peaks, typical of poly(2-methyloxazoline), appeared at 2.0 – 2.2 ppm and at 3.3 – 3.5 ppm in the ^{1}H-NMR spectrum of the obtained block copolymer; polymerization of the 2-methyl-2-oxazoline monomer was thus confirmed. The polymerization reaction yield was 71%. *Mn* for the block copolymer was calculated based on the known *Mn* of the hydrophobic block, which is equal to 72 units. The peak at 3.3 – 3.5 ppm, attributed to the eight protons, and the peak at 2.0 – 2.2 ppm, attributed to the six protons, allowed an estimate of 32 units of 2-methyloxazoline. A representative spectrum of PMOXA-*b*-PDMS-*b*-PMOXA is depicted in Figure 6.

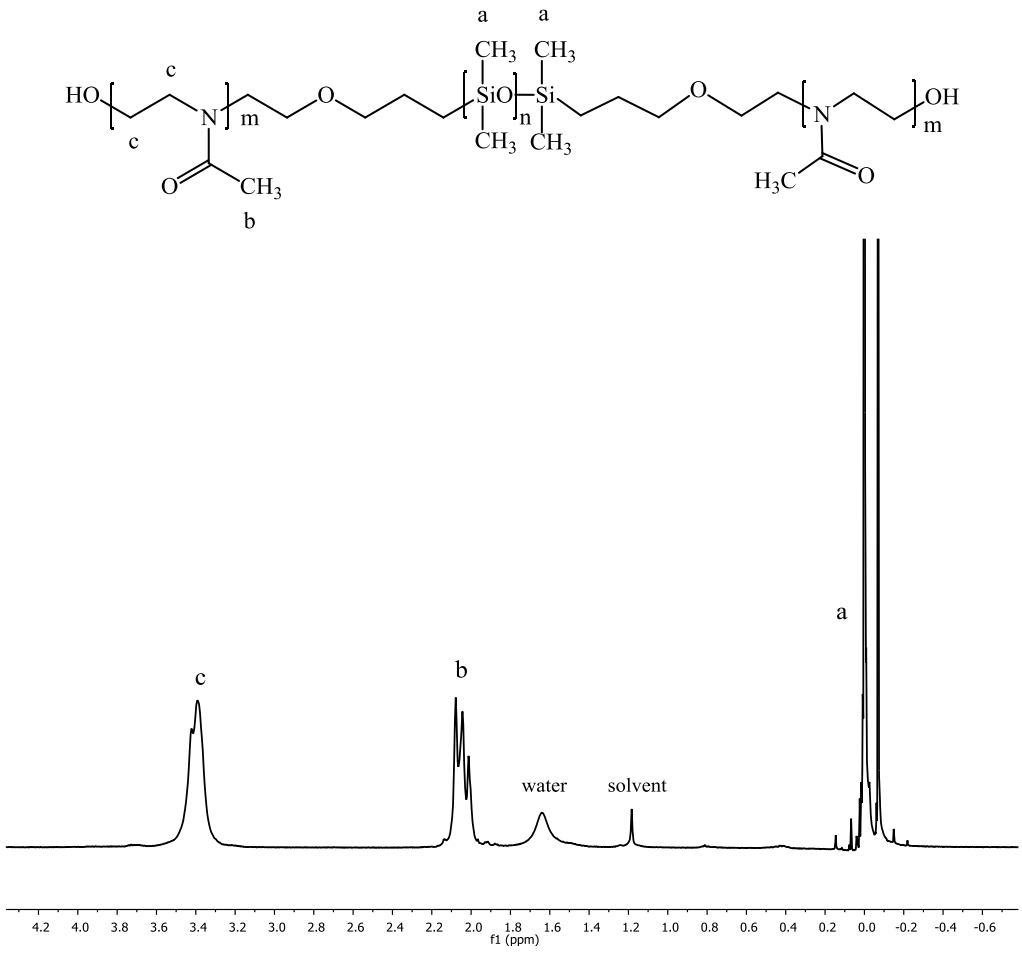

Figure 6. Representative ^{1}H-NMR spectrum of poly(2-methyloxazoline)-*block*-poly(dimethylsiloxane)-*block*-poly(2-methyloxazoline) in $CDCl_3$. A detailed peak assignment is presented in the Experimental part.

The polydispersity index (*PDI*) for the pre-polymer and the block copolymer were determined by GPC. Sample solutions (approx. 5 mg in 1 ml HPLC-grade THF) were first put through 0.2 μm filters to remove solid impurities. Samples were analysed with THF as eluent. Polystyrene standards of narrow polydispersity were used to calculate the *PDI* (Table 1). Although living polymerization should yield narrow molecular weight distributions, the obtained *PDI* (1.83) for the block copolymer was slightly higher. This value, higher than that previously published for PMOXA-*b*-PDMS-*b*-PMOXA block copolymers [136], can be attributed to the relatively high *PDI* value of the utilized pre-polymer (*PDI* = 1.62) and to the fact that the free poly(2-methyloxazoline) chains were not, as expected, entirely removed by the purification procedure.

Table 1. Polymer characterization results as obtained by ^{1}H-NMR and GPC

Polymer	***Mn* [g/mol]**	***PDI***
PDMS pre-polymer	5600	1.62
$PMOXA_{16}$-$PDMS_{72}$-$PMOXA_{16}$	8323	1.83

The transmittance spectra of pre-polymer and the block copolymer were collected and analysed. Air was measured as reference. The ATR-FTIR spectrum of the PDMS pre-polymer is presented in Figure 7. The peaks in the region of approximately 2500 cm^{-1} are attributed to C-H stretching of -CH_3 and -CH_2 groups. Peaks at 520 cm^{-1} and at 920 cm^{-1} correspond to the stretching vibrations of O-Si-O groups [140]. A strong Si-O band appears at 755 cm^{-1}; bands ascribed to long-chain methyl rock are also in this region [139].

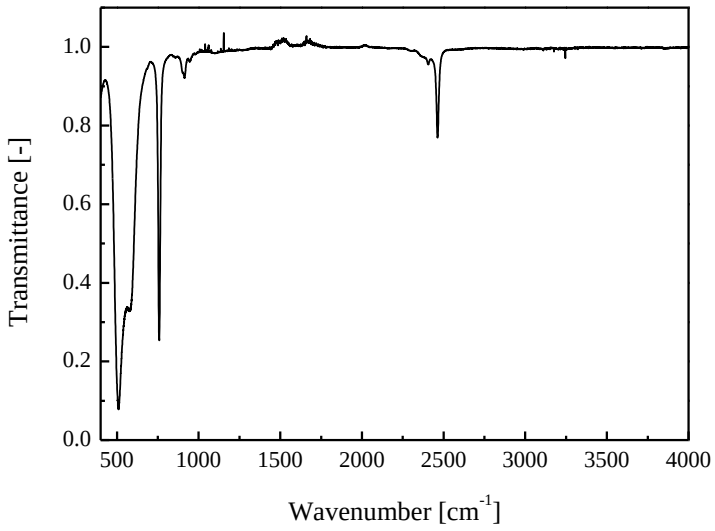

Figure 7. ATR-FTIR spectrum of α,ω-bis(3-hydroxypropyl)poly(dimethylsiloxane) pre-polymer.

The ATR-FTIR spectrum of block copolymer is shown in Figure 8. The amide band at approx. 1633 cm^{-1} is characteristic of the presence of a tertiary amide group, resulting from the ring-opening polymerization of 2-oxazolines [141]. The strong bands at 1478, 1417 and 1364 cm^{-1} are assigned to the CH_3-Si group, whereas the peak at 790 cm^{-1} is due to $(CH_3)_2$-Si. Peaks at 1081 cm^{-1} and 1010 cm^{-1} correspond to Si-O and Si-O-Si groups, respectively. The peak at 2962 cm^{-1} represents the C-H stretch of the alkyl groups of the PDMS. The broad band at 3452 cm^{-1} corresponds to an alcohol group. An ATR-FTIR spectrum of the block copolymer showed distinct peaks due to the PDMS and the PMOXA blocks, indicating successful polymerization.

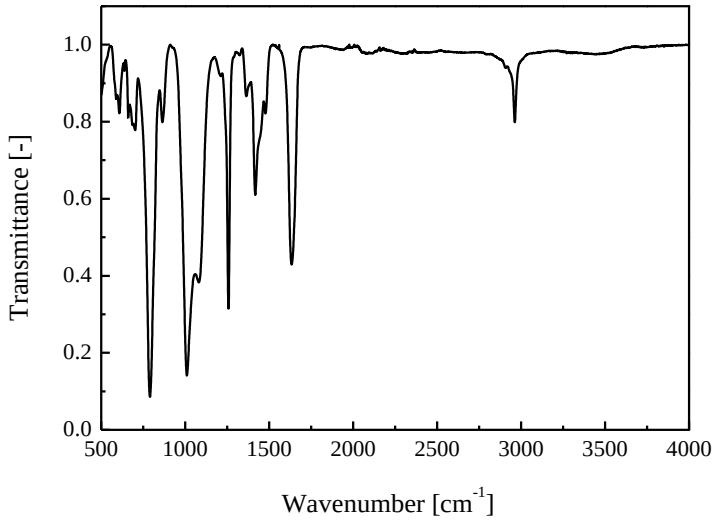

Figure 8. ATR-FTIR spectrum of $PMOXA_{16}$-$PDMS_{72}$-$PMOXA_{16}$ block copolymer.

3.2 Nanoreactor preparation and characterization

The enzymatically active nanoreactors were prepared by encapsulation of an enzyme, penicillin acylase, and insertion of a channel protein, OmpF, in the polymeric membrane, to provide membrane permeability. The self-assembly properties of the PMOXA-*b*-PDMS-*b*-PMOXA block copolymer were studied by light scattering and transmission electron microscopy **(**TEM).

The self-assembly of the block copolymers in dilute aqueous solution depends both on the hydrophilic-to-total-mass ratio and the absolute length of the polymer [88]. A minimum total length is needed for aggregation, and the ratio of the hydrophilic to hydrophobic part determines the morphology of the aggregates. Vesicular structures should form when the hydrophilic-to-total-mass ratio is 35 ± 10%. The hydrophilic-to-total-mass ratio of the polymer used was kept in this range (32.7%). The vesicle preparation method also influences the self-assembly. The presence of additives (for example ions, surfactants, proteins), the nature of the solvents, the polymer concentration in the stock solution, the water content, the speed of stirring, as well as the temperature can be used to control the resultant assembled morphology [142]. To obtain a narrow polydispersity of the vesicle solution, subsequent, repeat extrusion of the polydisperse suspension through polycarbonate filters with defined pore size is usually done. The influence of extrusion (pressure, speed, pore size, etc.) on the size and the particle size distribution was broadly described for liposomes [143, 144, 145] and it results in reduced size and lamellarity [146].

The nanoreactors (that encapsulate the penicillin acylase) and the control samples (non-permeable vesicles encapsulating enzyme and empty vesicles) were prepared *via* the film rehydration method [57]. The polymer was initially dissolved in HPLC-grade ethanol to yield a clear, homogeneous solution. A solution of the channel protein in buffer was added during the nanoreactor preparation to incorporate the channel protein in the polymeric wall. Since OmpF is a very stable membrane protein, the presence of organic solvent did not cause denaturation [147]. The solvent was removed by rotary evaporation under reduced pressure and a thin polymeric film was created on the bottom of a flask. To the resulting film a solution of the enzyme in a buffer was added, causing rehydration. Dialysis was used to remove non-encapsulated enzyme.

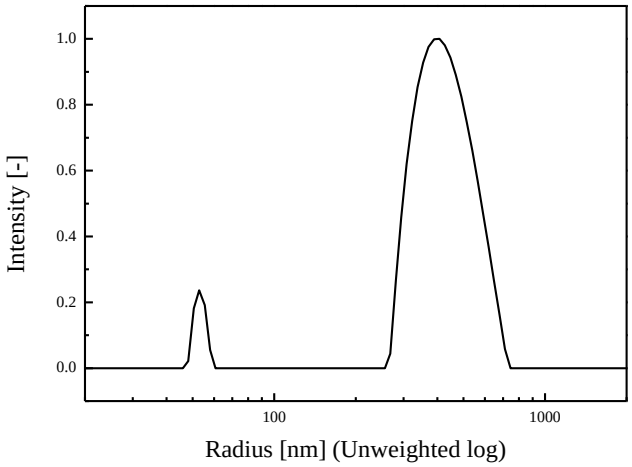

Figure 9. Size distribution of PMOXA-*b*-PDMS-*b*-PMOXA based nanoreactors obtained by DLS for 90°.

A complete light scattering (LS) study of nanoreactors was performed. The nanoreactor solution prepared in buffer revealed the presence of two populations of self-assembled structures: one population with an average hydrodynamic radius of around 255 nm, corresponding to vesicles, and the second one of around 50 nm, corresponding to small vesicles and micelles, as presented in Figure 9. This relatively high hydrodynamic radius value for the vesicles population is attributed by the fact that samples measured using DLS were not, as is typical, sequentially extruded through a membrane filter. Extrusion would lead to a more homogenous distribution, as filter pores destroy large aggregates and prevent varying sizes. Thus, the solution featured larger hydrodynamic radii. The samples were not extruded, so as to prevent the loss of material during this step, and thereby avoid lower efficiency in terms of the final concentration of antibiotic. In this case, final nanoreactor efficiency took precedence over low polydispersity. Broad size distribution and high hydrodynamic radius (*Rh*) values for non-extruded samples have been reported for PMOXA-*b*-PDMS-*b*-PMOXA based vesicles [81]. The obtained ρ-value (1.09) given as $\rho = Rg/Rh$, is close to the value for an ideal, hollow sphere – 1.0, indicating hollow-sphere morphology [148].

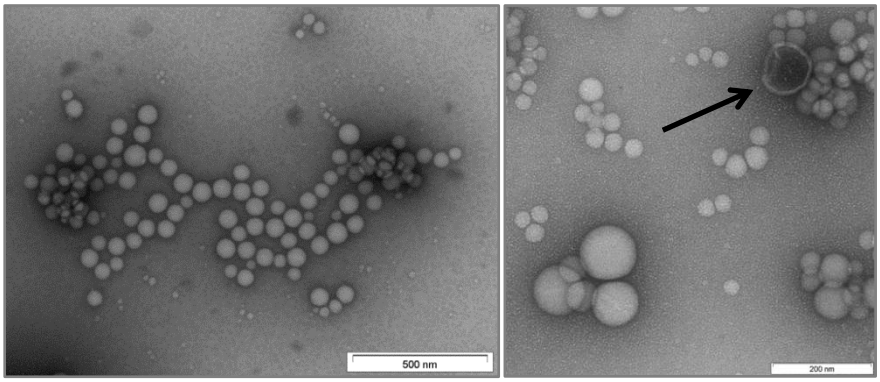

Figure 10. TEM images of PMOXA-*b*-PDMS-*b*-PMOXA based nanoreactors. Scale bar: left image 500 nm; right zoom image 200 nm, in which a broken nanoreactor can be seen, with the polymeric wall, as indicated by the arrow.

Transmission electron microscopy was used to corroborate these data. TEM showed the clear presence of two populations – spherical objects with diameters around 50 nm (corresponding to small vesicles and micelles), and with diameters between 100 nm and 200 nm (corresponding to vesicles), as can be seen in Figure 10. Aggregates of these spherical objects were observed. Collapsed and broken spherical structures are present, and the polymersome membrane can be recognized in the zoom of the image. TEM measurements repeated after three weeks of storage at room temperature and at 37 °C in PBS (phosphate buffered saline) buffer pH 7.4 did not reveal any significant morphological changes, suggesting that nanoreactors are also mechanically stable under physiological conditions (Figure 11).

The stability of another PMOXA-*b*-PDMS-*b*-PMOXA based polymersomes was reported for samples stored at room temperature for four months [149]. Stability studies of polymeric nanoreactors were carried out by adding a certain volume of nanoreactors to the same volume of naïve mouse serum [45]. Based on our and these studies, it is reasonable to conclude that polymerosmes based on PMOXA-*b*-PDMS-*b*-PMOXA block copolymer are stable under various conditions.

Encapsulation efficiency (EE) was defined as the percentage of enzyme encapsulated in the vesicles in relation to the total amount of enzyme present during the vesicle formation and encapsulation procedure [150]. The amount of enzyme encapsulated was calculated as

the difference between the total amount of enzyme present during vesicle formation and the amount of non-encapsulated enzyme remaining in the aqueous medium. This latter amount was determined following the separation of enzyme-loaded vesicles from the buffer medium by size exclusion chromatography (SEC).

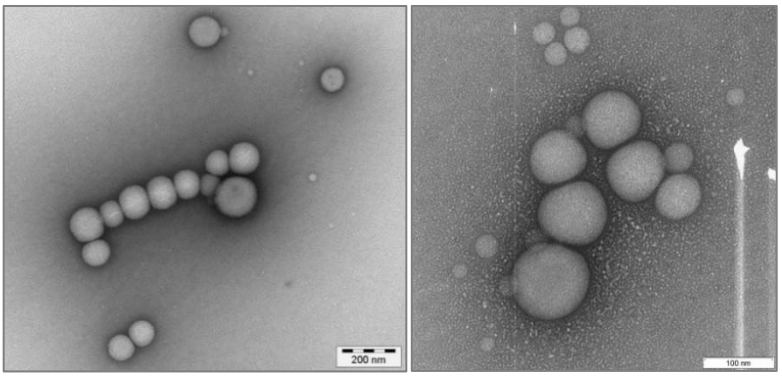

Figure 11. PMOXA-*b*-PDMS-*b*-PMOXA nanoreactors, prepared in PBS buffer, after three weeks storage, visualized by TEM. The scale bars correspond to 200 nm (left image) and 100 nm (right image).

The concentration of the encapsulated enzyme was estimated to be 9.4% for nanoreactors prepared at 8 ºC, 11% for nanoreactors prepared at RT, and 10% for polymersomes encapsulating penicillin acylase but without channel protein. In spite of various papers describing polymersomes for enzyme encapsulation, few discuss the quantification of encapsulation efficiency [81, 151, 152] which typically resides between 10% and 15% of the initial amount used for the encapsulation with the film rehydration method. Lower values of 4.5% [58] and higher values of 46% [153] can also be found in literature. Heretofore, encapsulation of catalyst has been limited to random entrapment during vesicle formation. However, the encapsulation efficiency assay, which yields what we call the apparent value, is based on evaluation of the amount of enzyme that is not encapsulated. In this regard it is important to emphasize that a certain fraction of enzyme can be encapsulated in polymersomes that are non-permeable to substrate, thereby lowering the efficiency of the system [81, 151, 152].

3.3 Enzymatic activity of nanoreactors

The penicillin acylase is a key biotechnological enzyme and it is commonly used in industrial production of semi-synthetic antibiotics [154]. It is responsible for the hydrolysis of the side chain of natural penicillins to obtain 6-aminopenicillanic acid, which is subsequently acylated to yield broad spectrum antibiotics. This enzyme can be found among many microorganisms, including bacteria and fungi, but its physiological function is still not understood. However, in the literature it has been proposed that the enzyme could be a scavenger enzyme for phenylacetylated compounds for the assimilation of aromatic compounds as carbon sources [155]. The precursor of the penicillin acylase is produced in cytoplasm and, further, it is transported to periplasm, where it becomes catalytically active [156]. The mature periplasmic *E. coli* enzyme is an 86 kDa heterodimer and it consists of two monomer subunits, referred to as A (209 amino acids) and B (566 amino acids) [157].

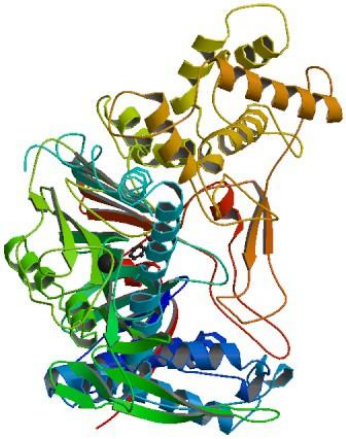

Figure 12. The three dimensional structure of penicillin acylase [154].

Penicillin acylase can also be used in the reverse reaction, i.e. in the synthesis of penicillins. Semi-synthetic β-lactam antibiotics, such as penicillins and cephalosporins, are the most important class of antimicrobial agents used in veterinary and human medicine [158]. The shared feature is the presence of the beta-lactam ring, which is responsible for their antimicrobial activity.

Cephalexin, a cephalosporin antibiotic, can be synthesised by the kinetically controlled coupling of an activated phenylglycine derivative (phenylglycine methyl ester) to a nucleus 7-amino-3-desacetoxy-cephalosporanic acid [159]. In parallel, enzyme-catalysed hydrolysis of the phenylglycine methyl ester and hydrolysis of cephalexin takes place. Cephalexin is one of the most used and effective antibacterial agents for *Staphylococcus aureus, Staphylococcus epidermidis, Escherichia coli* and *Proteus mirabilis*. This drug acts by inhibition of the last step of the bacterial cell-wall synthesis, causing cell death [160].

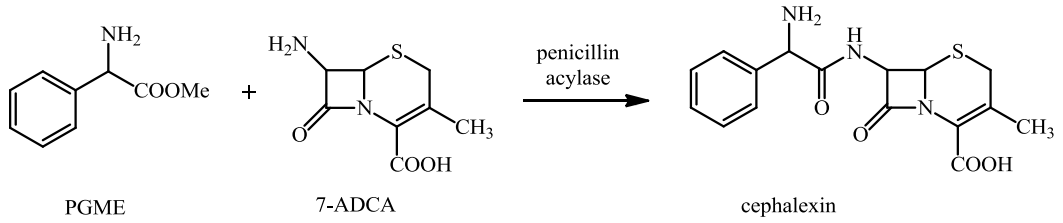

PGME 7-ADCA cephalexin

Figure 13. The reaction scheme of cephalexin deriving from phenylglycine methyl ester (PGME) and 7-amino-3-desacetoxy-cephalosporanic acid (7-ADCA), catalysed by penicillin acylase.

The penicillin acylase that catalysed the synthesis of cephalexin follows reversible bi-uni reaction kinetics [161], which is presented in Figure 14.

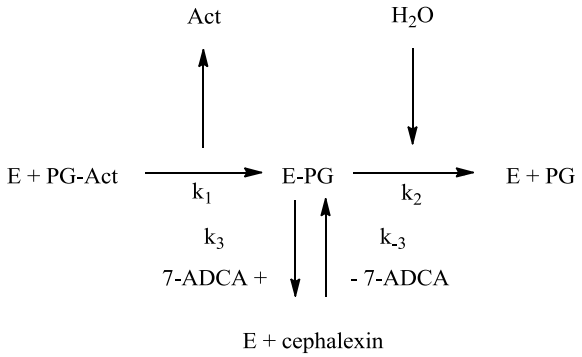

Figure 14. Simplified model for kinetically controlled cephalexin synthesis, adapted from Schroën *et al.* [162]. PG-Act denotes activated phenylglycine; E is free enzyme and E-PG is the enzyme-phenylglycine complex.

To determine the kinetic constants, the reaction rate constants as well as the concentrations of all of the side and final products need to be known. Attempts to ascertain the kinetic constants were unsuccessful, because the assay used was not suited to determining the concentrations of side products.

3.3.1 Proteolytic enzymes experiments

Two proteolytic enzymes were used to show that encapsulation of an enzyme inside polymeric nanoreactors protects them from inactivation and to eliminate the possibility that the observed enzyme activity is due to enzyme adhering to the external surface of the nanoreactors. Proteinase K and subtilisin A are serine proteases with a broad spectrum of activity, and are widely used in molecular biology to hydrolyse and denature proteins [163]. Free penicillin acylase, as the reference solution, purified nanoreactors, and purified polymersomes with enzyme encapsulated but with non-permeable membranes (without channel protein) were incubated with proteinase K ($C_{\text{proteinase K}}$ = 200 μg/ml) and subtilisin A ($C_{\text{subtilisin A}}$ = 200 μg/ml) for 2 h at 37 °C with gentle stirring. Afterwards, a freshly prepared substrate solution was added to each sample. The enzymatic activity of nanoreactors was followed by a spectroscopic assay, based on a secondary reaction of cephalexin with sorbitol solution containing zinc ions, which results in highly absorptive derivatives [164].

The enzymatic conversion occurred only when penicillin acylase was encapsulated in nanoreactors, due to the presence of OmpF reconstituted in the polymeric membrane, and to the catalytic activity of the enzyme (Figure 15). As expected, no enzymatic activity was recorded for non-permeable polymersomes or for the free enzyme reference solution. The polymersomes without channel protein could not convert substrate to antibiotic because substrates were not able to diffuse through the polymeric wall. The free enzyme solution did not display catalytic activity, due to the fact that the enzyme was deactivated by the proteases. The low conversion in the case of both of the control samples (i.e. free enzyme reference solution and non-permeable polymersomes) corresponded to the substrates reacting with self. This result indicates that polymeric vesicles are able to shield the encapsulated enzyme.

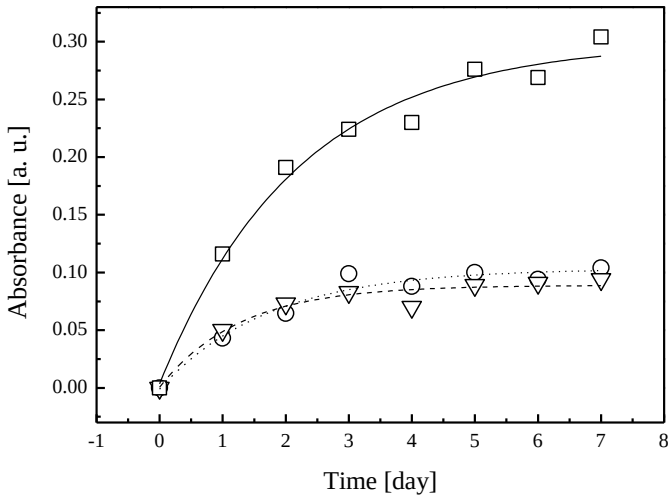

Figure 15. Reaction progress curves for: substrate solution with free enzyme solution (○,⋯), non-permeable polymersomes (∇,---), nanoreactors (□,—), after incubation with proteases. Data represent the average of three independent measurements, with an error of 5%. Fits are shown as guides and not used for kinetic analyses.

The increased catalytic activity of nanoreactors and the absence of increase in the reaction rate for the non-permeable polymersomes proves that penicillin acylase was encapsulated inside nanoreactors and not adhered to the outside, and therefore it is logical to conclude that only enzyme activity in the inside of the nanoreactors was measured.

3.3.2 Enzymatic activity assay

The enzymatic activity of nanoreactors was analysed by qualitative comparison between nanoreactor solution and free enzyme solution. For this purpose the free enzyme activity was measured for different enzyme concentrations (31.4 nM, 62.8 nM, 157 nM) at a constant concentration of substrates (C_{PGME} = 81.4 mM, $C_{7\text{-}ADCA}$ = 46.7 mM). The first concentration of enzyme used is equal to the apparent concentration of enzyme encapsulated inside nanoreactors. Because the reaction also occurs in the absence of the catalyst, the synthesis was monitored with substrate solution only. The progress of the cepahlexin formation reaction at 37 °C was monitored over time (seven days). The

enzymatic activity of nanoreactors was followed by a spectroscopic assay described above. In Figure 16, reaction progress curves for free enzyme, nanoreactors, and substrates are presented.

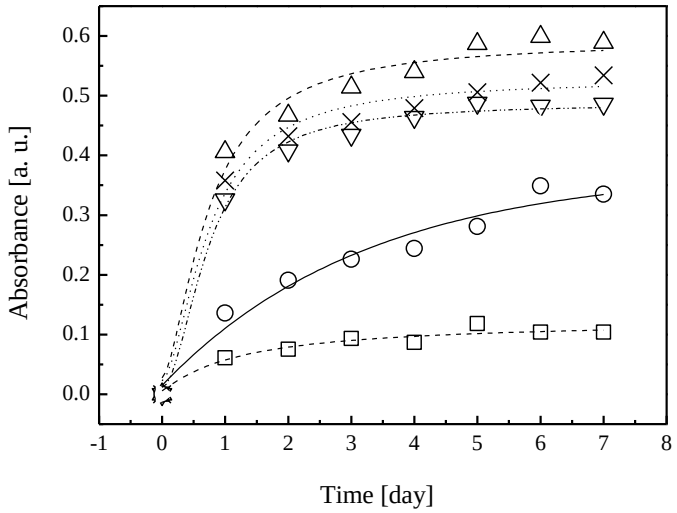

Figure 16. Reaction progress curves for: substrate solution (□,---), nanoreactors (○,—), free enzyme concentrations: 31.4 nM (∇, -··), 62.8 nM (x, ···), 157 nM (Δ, ---). Data represent the average of three independent measurements with an error of 5%. Fits are shown as guides and not used for kinetic analyses.

From the reaction progress curves it is clearly seen that the encapsulated enzyme retained its activity. However, it can be seen that encapsulated enzyme had lower activity than the free enzyme with the same concentration (estimated to be 32.4 nM), which was due to apparent encapsulation values and partial enzyme deactivation during nanoreactor preparation and purification. The nanoreactor sample was prepared and purified at room temperature for four days. During these steps penicillin acylase lost some activity because the enzyme is sensitive to temperature [165]. The conversion in the case of sample containing substrates only was significantly lower than for the free enzyme or nanoreactors.

To verify this assumption, cephalexin synthesis was performed for nanoreactor samples prepared and purified at two temperatures – room temperature and 8 °C. The results are presented in Figure 17. The results were compared with the results obtained for the

sample containing substrates only and the non-permeable polymersomes. The final cephalexin concentration for the sample containing substrates only was 3.1 mM; for the non-permeable polymersomes, 2.4 mM; nanoreactors prepared at room temperature, 9.7 mM; and for the nanoreactors prepared at 8 °C, 11.8 mM.

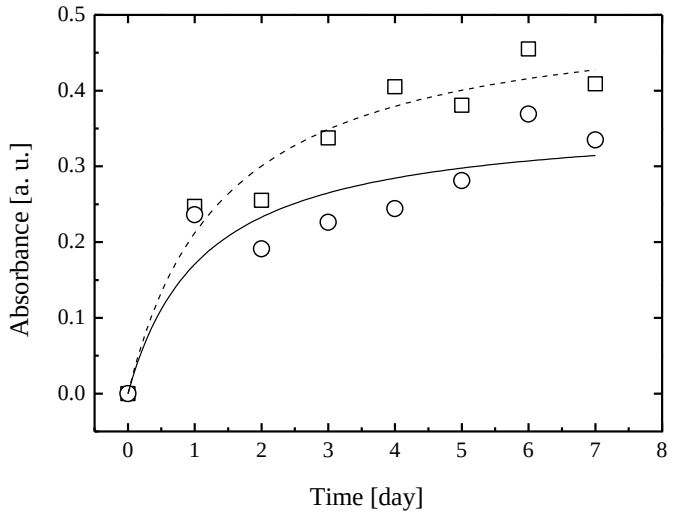

Figure 17. Reaction progress curves for: nanoreactors prepared at 8 ºC (□,---), nanoreactors prepared at room temperature (○,—). Data represent the average of three independent measurements with an error of 5%. Fits are shown as guides and not used for kinetic analyses.

The difference in the final concentration of the drug in the case of the control samples and the nanoreactor samples can be attributed to enzymatic activity. A significant difference in absorbance between nanoreactors prepared at room temperature and those prepared at 8 °C, as in the final cephalexin concentration, indicates that the temperature at which nanoreactors are prepared plays a major role in the final efficiency of the system. To corroborate this data, a further free enzyme activity assay based on penicillin G hydrolysis, catalysed by penicillin acylase and measured by colorimetric assay, was performed, see Figure 18. The activity of the enzyme stored under different conditions (8 °C and room temperature) was measured over time (five days). The penicillin acylase activity profiles after five days revealed that the retained activity of the enzyme was 79% for the sample stored at 8 °C and 65% for the sample stored at room temperature. This explains the difference in efficiency of nanoreactors prepared and stored at different

temperatures. The system can be further optimised by shortening the preparation and purification time and lowering the temperature.

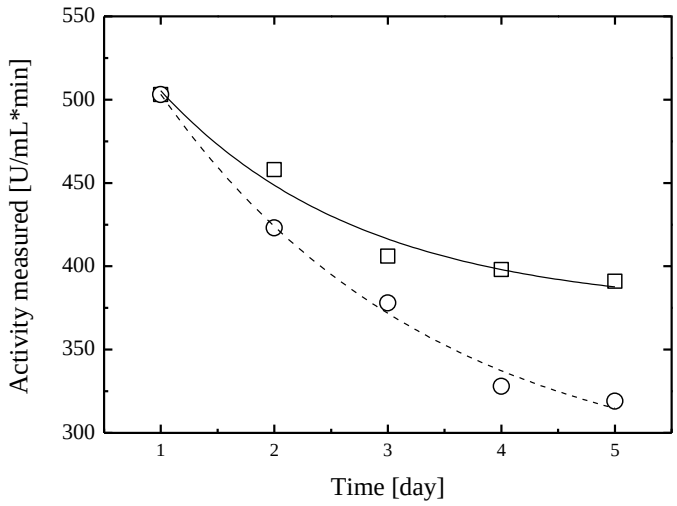

Figure 18. Penicillin acylase deactivation profiles in bulk solution during storage at 8 °C (□,—) and at room temperature (○,---), respectively.

3.4 Nanoreactor immobilization

Two strategies were employed to covalently immobilize polymeric nanoreactors on surfaces: attachment *via* an amino bond and attachment *via* a bifunctional aromatic coupling agent, as depicted in Figure 19. Silicon wafers (SiO_2) were used as a model surface, due to chemistry which is analogous to a number of different types of biomaterial surfaces, such as silicone rubber [166, 167]. Moreover, they have the advantage of relativly simple physical and antimicrobial analysis for characterization of the surface.

a)

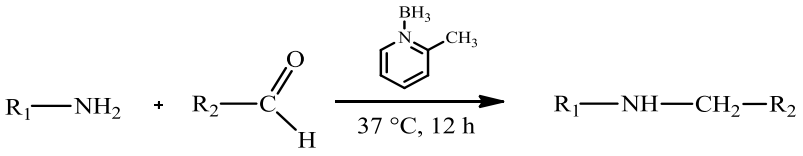

b)

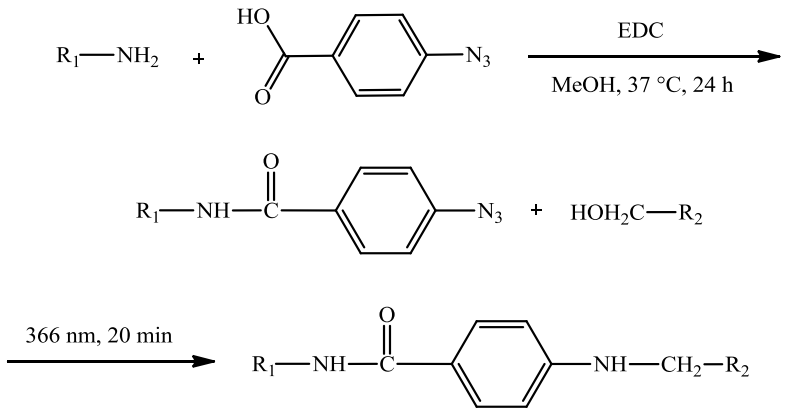

Figure 19. Schematic representation of: a) the chemistry as applied to nanoreactor immobilization *via* an amino bond; b) nanoreactor immobilization *via* a bifunctional aromatic coupling agent.

In the first strategy, an amino functionalized surface was immersed in an aqueous solution of PMOXA-*b*-PDMS-*b*-PMOXA nanoreactors made of aldehyde-terminated

block copolymer. The first step introduces amino functionalities onto the surface. This was done by silicon wafer modification with 3-aminopropyltriethoxysilane (APTS). In order to follow the surface functionalization process, contact angle and ATR-FTIR measurements were carried out. The second step is selective oxidation of the terminal hydroxyl groups to aldehydes. Analytical tests were used to confirm the presence of aldehyde groups, and ^{1}H-NMR and ATR-FTIR spectral analysis was performed to ensure that the polymer backbone stayed intact upon oxidation. The self-assembly properties of the oxidized polymer were studied by light scattering and TEM. To confirm nanoreactor immobilization, ATR-FTIR, AFM and SEM were employed.

In the second strategy, amino groups are also required for further surface functionalization with 4-azidobenzoic acid. Phenyl azides are highly photoreactive compounds commonly used to enable the attachment of proteins [168, 120, 169, 170].

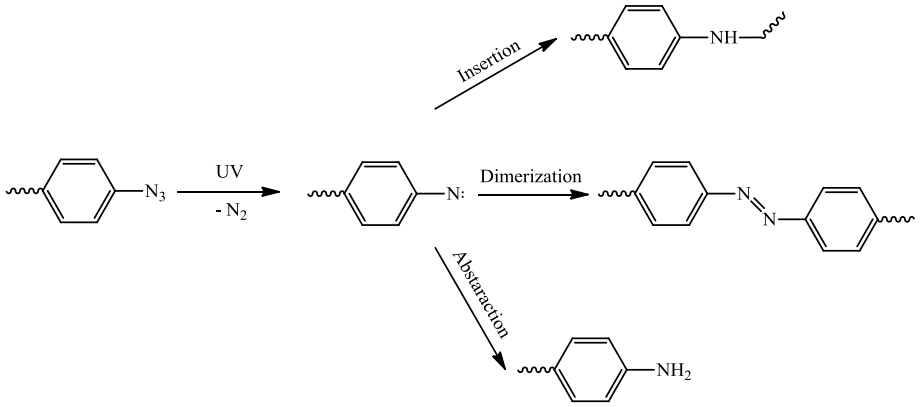

Figure 20. Scheme for the possible photochemical reactions of phenyl azide groups.

The usefulness of photo-cleavable azido linkers was demonstrated by immobilization of furanones [122] as well as antimicrobial cationic peptide [171] to obtain materials with antibacterial properties. Immobilization *via* photolinkers has become a popular method for the covalent attachment of polymers and biomolecules on surfaces due to its simplicity and versatility. Upon photolysis with ultraviolet light, organic azides generate nitrene radicals. The nitrene radical is an extremely reactive, intermediate species that can further react with neighbouring organic molecules to form a covalent bond through C-H, O-H or N-H insertion or abstraction, or C=C addition reactions [121] as depicted in

Figure 20. Azido-terminated surfaces were prepared by the functionalization of bare silicon wafer with 3-aminopropyltriethoxysilane followed by treatment with 4-azidobenzoic acid. Introduction of azido groups to the surface was confirmed by contact angle and ATR-FTIR measurements. Successful nanoreactor immobilization was studied by ATR-FTIR, AFM and SEM.

3.4.1 Surface amino functionalization (silanization) and characterization

To introduce amino groups onto silicon wafers, surfaces were immersed in a solution of 3-aminopropyltriethoxysilane under water-free and oxygen-free conditions. Afterwards, the excess of APTS was removed by rinsing in toluene, acetone and then ethanol. Changes in surface hydrophobicity were followed by H_2O contact angle measurements (Table 2). In contrast to the low contact angle of 40º, for unmodified silicon wafers the contact angle increased to 69º after amino modification of the surface. Increased hydrophobicity of the surface after modification indicates the presence of the amino groups, e. g. successful functionalization of the SiO_2 surface.

Table 2. Contact angle measurement.

Surface	***H_2O contact angle (º)***
SiO_2	40 ± 2.0
Amino functionalized SiO_2 surface	69 ± 1.8

Furthermore, the surfaces, namely a bare silicon wafer and a silanized silicon wafer, were analysed by ATR-FTIR and the spectra are presented in Figure 21. Peaks at 670 cm^{-1}, 730 cm^{-1}, and 1110 cm^{-1} correspond to the Si-O group. The peak at 1609 cm^{-1} is due to the deformation modes of the free amino groups. The peak at around 2700 cm^{-1} represents

the C-H stretch from alkyl groups in APTS. Peaks between 2000 cm^{-1} and 2500 cm^{-1} correspond to a residual amount of solvents.

For the silanized silicon wafer, in contrast to the unmodified silicon wafer, bands characteristic of 3-aminopropyltriethoxysilane were present, indicating that a silanization agent was attached to the surface during the reaction.

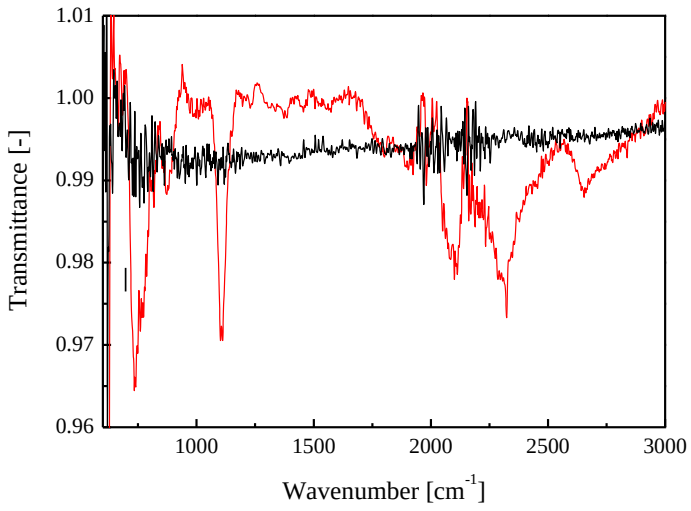

Figure 21. ATR-FTIR spectra of an unmodified silicon wafer (in black) and an amino functionalized silicon wafer (in red).

3.4.2 Polymer oxidation – introduction of aldehyde terminal groups

To introduce aldehyde groups to the end of the polymer, the polymer terminal hydroxyl groups were selectively oxidized to aldehydes by Dess-Martin oxidation [172, 173] as shown in Figure 22. Although reaction times of up to 2 h are described in the literature, in the case of polymers a considerably longer reaction time (24 h) was required. The oxidation was performed in DCM at room temperature. The solvent was removed by evaporation and residues were dissolved in ethanol. The product was purified by dialysis against ethanol.

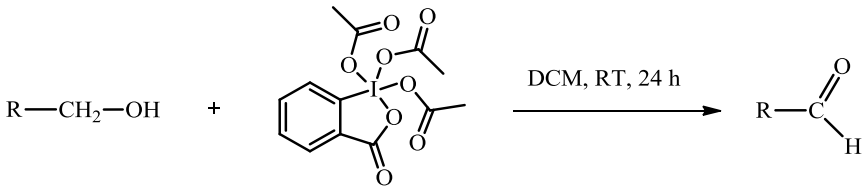

Figure 22. Scheme of Dess-Martin oxidation of primary alcohols to aldehydes.

Two analytical tests were applied to confirm successful oxidation of terminal hydroxyl groups to aldehyde functionalities – Brady's test and Tollens' test (details in the Experimental part). As a control sample, hydroxyl-terminated polymer was used. In the case of the control samples, no change of colour or precipitate was observed (Figure 45, Experimental part). For the Brady test, in the case of aldehyde-terminated polymer, a red precipitate confirmed the presence of the aldehyde groups. For the Tollens' test, a black precipitate was formed with the aldehyde-terminated polymer (Figure 46, Experimental part). Both analytical tests provided clear evidence of the successful oxidation of the terminal group.

The introduction of the functional groups to the polymers is generally more difficult than it is for smaller molecules, because of the occurrence of undesired secondary and side reactions. Since polymers contain various functional groups, it is of key importance to ensure that an applied functionalization procedure will not influence other functional groups or destroyed the backbone of the polymer. Therefore, ^{1}H-NMR spectral analysis was performed (Figure 23) to make certain that the oxidation did not influence the structure of the polymer. Two peaks corresponding to the PMOXA block: 2.0 – 2.2 ppm (***CH*$_3$**-CON<, 6H, b), 3.3 – 3.5 ppm (>N-***CH*$_2$**-***CH*$_2$**-N<, 8H, c), and one peak corresponding to the PDMS block 0 ppm (Si-***CH*$_3$**, 6H, a) did not change, clearly showing that the backbone of the oxidized polymer stayed intact.

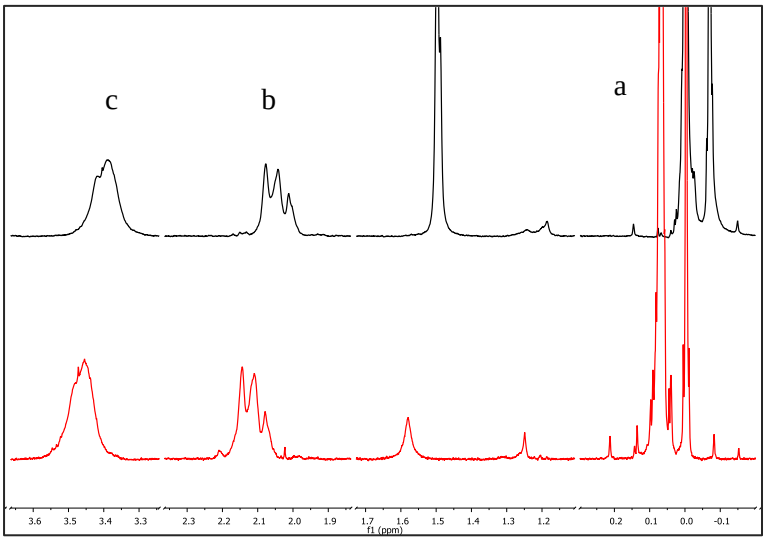

Figure 23. ^{1}H-NMR spectra of hydroxyl-terminated polymer (in black) and oxidized polymer (in red) in $CDCl_3$.

ATR-FTIR spectra of polymer before and after oxidation were also recorded and did not show any changes, suggesting that the oxidation did not alter the backbone of the polymer, as can be seen in Figure 24.

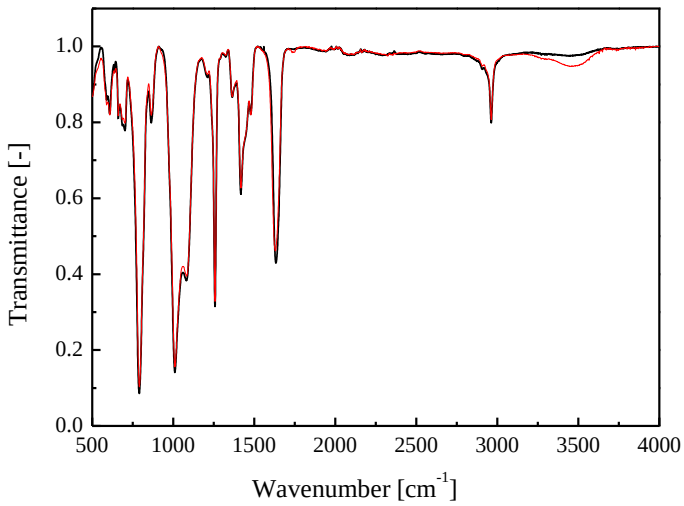

Figure 24. ATR-FTIR spectra of the polymer before (in black) and after oxidation (in red).

Next, dynamic light scattering (DLS) and transmission electron microscopy analysis of self-assembled nanoreactors made of unmodified and modified polymer were performed to ensure that oxidation of the terminal groups did not influence the self-assembly properties of the polymer. DLS results (Figure 25) for the self-assembled block copolymer before (smaller assemblies with hydrodynamic radii centred around 50 nm and bigger ones with 255 nm) and after oxidation (a major population with an average hydrodynamic radius of around 190 nm, and a minor one of around 50 nm) both exhibited bimodal distribution, demonstrating that the self-assembly properties of the polymer did not change upon introduction of the aldehyde groups. The observed differences in DLS results can be attributed to the quality of the polymeric film used for rehydration as well as rehydration itself. Because the polymeric films were not exactly the same, i. e. their homogeneity and thickness, and parameters of rehydration, for example speed of stirring, consequently the self-assembly did not proceed in exactly the same manner. Nevertheless, DLS measurements gave already a hint towards unchanged self-assembly of oxidized polymer.

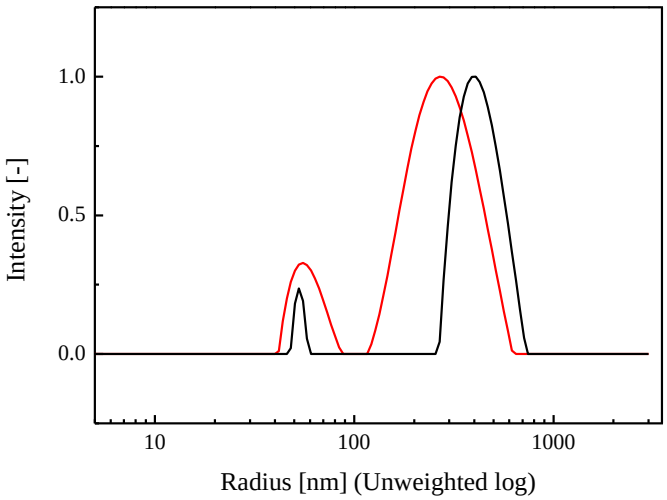

Figure 25. DLS size distribution at 90° for self-assembled nanoreactors made of unmodified polymer (in black) and oxidized polymer (in red).

To gain more insight into the morphology of the nanoreactors resulting from non-oxidized and oxidized polymer TEM was performed. TEM results also indicated clearly

that introduction of the terminal-aldehyde groups did not influence self-assembly of the block copolymer, since in both cases two populations of spherical objects were present, with sizes ranging between 50 nm and 200 nm. The spherical objects did not differ in size or shape, Figure 26.

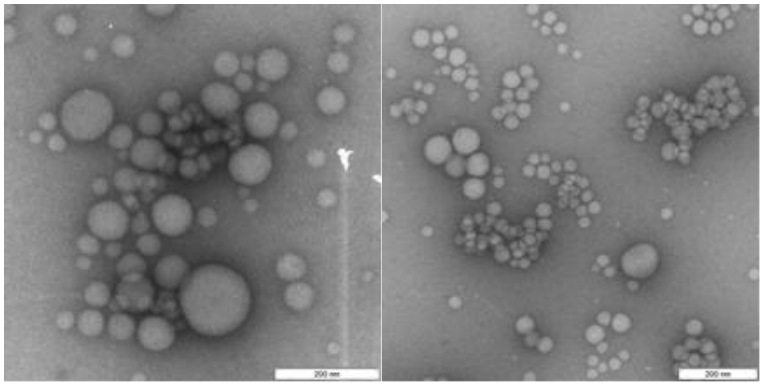

Figure 26. Representative TEM images of nanoreactors made of the hydroxyl-terminated (left image) and aldehyde-terminated (right image) block copolymer. Scale bar: 200 nm.

3.4.3 Nanoreactor immobilization *via* amino bond

The immobilization of nanoreactors was achieved by immersing the amino-functionalized surface in a solution of nanoreactors made of aldehyde terminated block copolymer containing the 2-picoline borane complex. The surfaces were rinsed with bidistilled water following incubation to remove unbound nanoreactors. Surfaces dried under a nitrogen stream were analysed by ATR-FTIR, SEM and AFM. Bare silicon wafers treated with a nanoreactor solution based on aldehyde terminated polymer, and silanized silicon wafers treated with a nanoreactor solution based on hydroxyl terminated polymer served as controls.

3.4.3.1 Characterization by ATR-FTIR

Spectra of nanoreactors made of polymer with aldehyde-terminal groups immobilized on amino functionalized silicon wafers were measured by ATR-FTIR (Figure 27). These clearly show the characteristic absorption bands of the polymer backbones (detailed peak assignment in Polymer synthesis and characterization part) detected on the silanized surface immersed in the solution containing nanoreactors made of aldehyde-terminated polymer. The non-covalently bound nanoreactors made of hydroxyl-terminated polymer were removed by washing. In contrast, the covalently immobilized nanoreactors could not be removed by rinsing with bidistilled water. The polymer backbone absorption bands therefore remained present as clear evidence of nanoreactor persistence (blue line). This experiment hints towards covalent immobilization of the nanoreactors made of aldehyde-terminated polymer on an aminated surface in the presence of the 2-picoline borane complex.

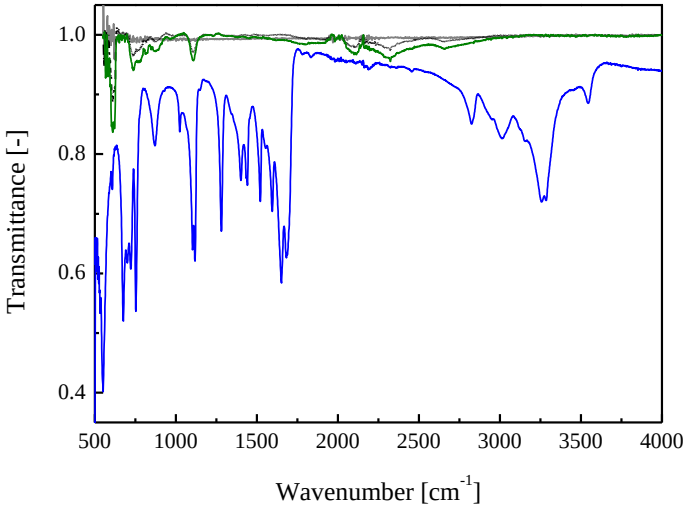

Figure 27. ATR-FTIR spectra of: bare silicon wafer (grey), APTS modified silicon wafer (black), APTS modified silicon wafer incubated with nanoreactors made of hydroxyl-terminated polymer (green), and APTS modified silicon wafer incubated with nanoreactors made of aldehyde-terminated polymer (blue).

3.4.3.2 Characterization by SEM

SEM images revealed that the surface was covered by spherical objects with diameters ranging from approx. 50 nm to 200 nm in an inhomogeneous manner. Rinsing the surface with bidistilled water did not remove covalently attached vesicles. In a control experiment nanoreactors formed by hydroxyl terminated polymer did not attach to the surface and were washed off by rinsing. The visible shrinkage of the nanoreactors was due to the drying procedure and to the high vacuum of the SEM set-up [80], which has been previously reported. The collapsed structures result from the fact that during the drying process water evaporates from the inner cavity of the vesicle. It is worth pointing out that the drying step took place after ten days of sample storage in bidistilled water. The overview image in Figure 28, in which aggregated and isolated structures are present, revealed non-homogenous coverage of the surface. This might be due to the fact that the hydroxyl functionalization of the polymer [136] as well as the oxidation of those hydroxyl groups [172] is not 100%. Therefore it is possible that not all of the nanoreactors being in contact with the amino groups of the surface were presenting aldehyde groups resulting in successful immobilization. In the zoom image (Figure 28), a collapsed vesicular structure is clearly seen, confirming the hollow nature of these particles. Covalent binding *via* an amine bond yielded a vesicular structure that did not disrupt for an extended period of time. These data indicated that treatment of amino-functionalizes surfaces with nanoreactors featuring aldehyde groups on their outer surface, under reducing conditions, can be covalently attached and the vesicular structure stays intact. The control samples, that is amino-functionalized surfaces immersed with nanoreactors based of hydroxyl terminated polymer in presence of 2-picoline borane, showed no immobilized structures and bare silicon wafers treated with nanoreactors based on aldehyde terminated polymer under reducing conditions did not reveal any attached structures in contrast to published findings on polymersomes immobilization *via* Schiff base [112]. The morphology of those control samples was identical to that of the amino silanized surface and bare silicon wafer surface which is homogenous without any object attached.

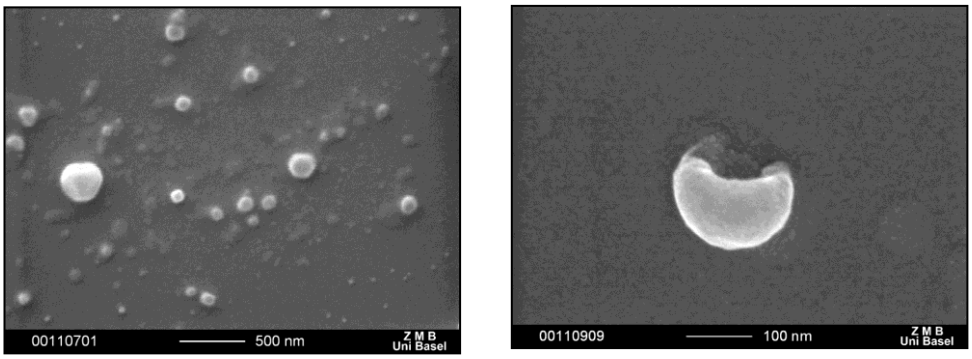

Figure 28. SEM images of nanoreactors covalently immobilized on amino functionalized silicon wafer surface. Left side: overview; Right side: zoom in image.

3.4.3.3 Characterization by AFM

Covalent attachment of the nanoreactors to the silanized silicon surface was also proved by AFM in air. Images recorded randomly throughout the surface of the sample show that the entirety was covered by spherical objects (Figure 29,a). The height of the assemblies based on the magnified height images and the corresponding cross-section profiles (Figure 29, c), was determined to be approximately 9 nm. Since the measured samples were dried before the measurement, the observed structures were collapsed, forming M-shaped profiles. The same morphology has been previously reported for immobilized and dried liposomes [174] and polymersomes [175]. The height of the collapsed vesicles should correspond to the thickness of two overlapped polymer layers; however, the AFM tip can affect and deform a soft, scanned surface, thereby resulting in heights a few nanometers lower than existent [176]. Thus, the thickness of the triblock copolymer membrane was estimated to be approx. 6 nm. This value is supported by cryo-TEM analysis of polymerized PMOXA-*b*-PDMS-*b*-PMOXA block copolymer vesicles which revealed a mean thickness of about 10 nm [100]. Furthermore, membranes assembled from poly(ethylene oxide)-*block*-poly(ethyl ethylene) diblock copolymers of comparable molecular weight resulted in a mean lamellar thickness of about 8 nm [39]. Structures attached to the surface were not homogenous, smaller as well as bigger objects were present. This was attributed to the fact that no extrusion was performed before

immobilization and final sample used for immobilization consisted of vesicles of diverse sizes as well as of micelles. The diameter of the objects ranged from 50 to 200 nm, which is in agreement with SEM data, and DLS results of the polymeric self-assemblies in solution. Fused nanoreactors were observed as bright aggregates, which are visible in the Figure 29, b. Similarly fused polymersomes were reported [175]. It is worth emphasizing that, even after ten days of storage in PBS buffer nanoreactors were still present on the surface, which means that they were covalently attached, did not disintegrate, and were stable against Brownian motion and convection. No objects were found on the control samples. A more detailed examination of control samples revealed that their roughness and morphology was identical to those of surfaces before immersion with nanoreactor solutions. AFM image of silanized silicon surface, Figure 30, presented a homogenous, smooth surface with negligible defects.

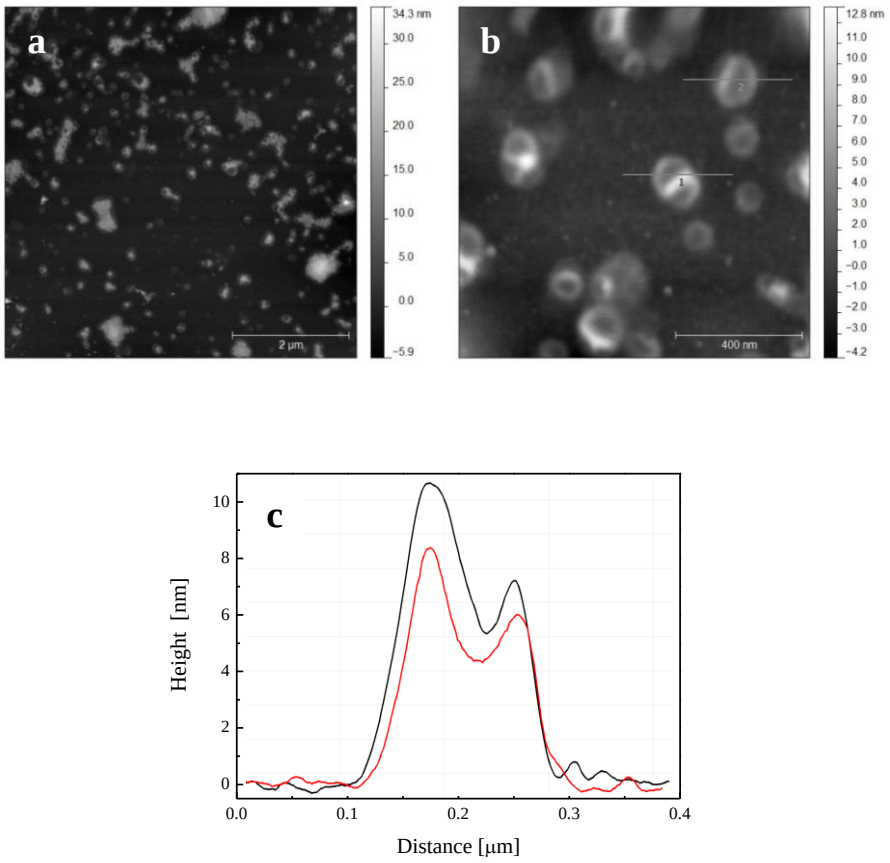

Figure 29. AFM height image of the polymer nanoreactors immobilized on aminated silicon surface. Scale bar (a) 2 µm; scale bar (b) 400 nm. (c) Corresponding to (b) cross section profiles.

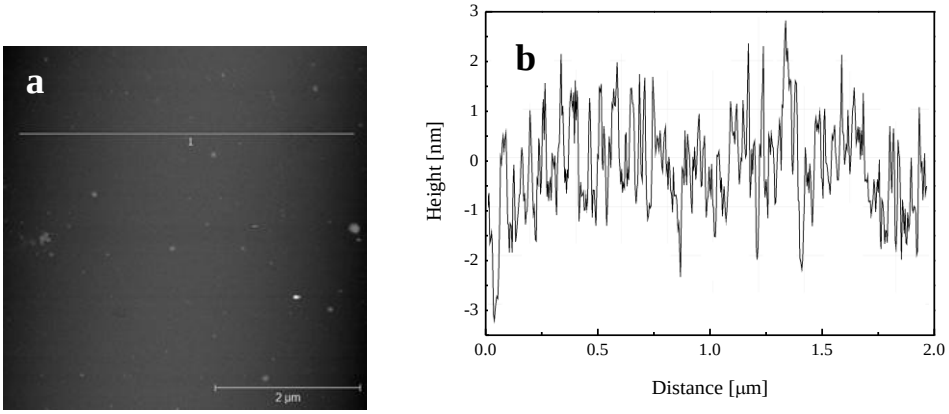

Figure 30. An AFM image of the amino functionalized silicon wafer surface showing homogenous, high uniformity and low roughness (~ 0.15 nm) (a) and the corresponding cross section (b). Scale bar: 2 µm.

3.4.3.4 Influence of immobilization on enzyme activity

The Dess-Martin oxidation resulted in aldehyde end groups so the self-assembled vesicles possessed aldehyde groups at their inner and outer surface. In principle it was possible that 2-picoline borane diffused to the inner cavity of the nanoreactors, where enzyme was encapsulated. To eliminate that enzyme amino groups reacted with the aldehyde moieties exposed on the inner surface of nanoreactors, resulting in reduced biocatalyst activity. To examine influence of 2-picoline borane complex on the activity of the enzyme a solution containing vesicles made of aldehyde terminated polymer and enzyme was incubated for 24 h at room temperature. Afterwards activity of the enzyme was measured by penicillin G hydrolysis test [177] in presence of a pH indicator. The assay measures the formation of the acidic products of penicillin G hydrolysis by following the decrease in absorbance. As a control sample a solution containing only enzyme and a solution containing enzyme and vesicles made of hydroxyl terminated polymer were used. Results are summarized in Figure 31. All of the samples exhibited comparable activity. The obtained results suggest that 2-picoline borane complex does not decrease activity of the enzyme.

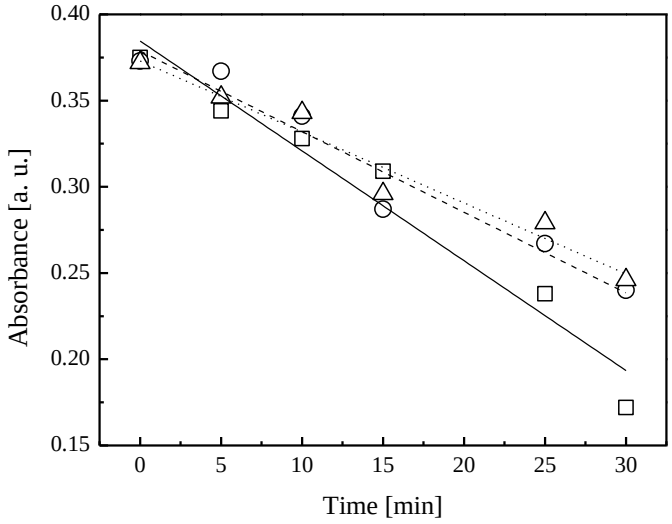

Figure 31. Enzymatic activity curves for: enzyme in presence of aldehyde-based nanoreactors (□,—), enzyme in presence of hydroxyl-based nanoreactors (○,---), solution containing enzyme only (Δ,···).

3.4.4 Nanoreactor immobilization *via* 4-azidobenozic acid

In general, the covalent immobilization was achieved by treatment of azido presenting surfaces with nanoreactor solution followed by UV irradiation to initiate the photo-cleavage. First, silanized silicon wafers were immersed with a solution of a bifunctional aromatic coupling agent, 4-azidobenzoic acid. Afterwards samples were washed with appropriate solvents to remove the excess of the azido linker. After drying under a nitrogen stream the functionalized surfaces were analysed by water contact angle and ATR-FTIR. Secondly, azido-functionalised surfaces were treated with nanoreactors solution followed by UV light irradiation to initiate the photo-cleavage of nanoreactors. Then the surfaces were extensively rinsed with bidistilled water to extract non-covalently adhered nanoreactors. To ensure that immobilization was indeed due to the photo-induced reaction of the bare surface azido groups with the block copolymer, control samples were prepared by treatment of silanized-surfaces with a nanoreactor solution in the same manner as described above.

3.4.4.1 Introduction of 4-azdiobenzoic acid on the surface

To alter the number of azido groups present on to surface the concentration of the photolinker (4-ABA) used for surface functionalization was adjusted. Experiments were carried out by treating the silanized silicon wafers with 4-ABA solution at various concentrations. A series of 4-ABA solutions were prepared by diluting the 4-ABA stock solution in methanol to give concentrations of 0.1 M, 0.01 M, and 0.001 M. Silanized silicon wafers were then treated with these solutions for 24 h, at 37 ºC and unbounded photolinker was subsequently washed off by rinsing with methanol and ethanol. Dried surfaces were examined by water contact angle. The contact angles values were obtained from a minimum of nine measurements on triplicate samples, and the results were averaged. All operations were carried out under dark conditions to avoid the azide photolinker decomposition. The freshly prepared silanized silicon wafer had a contact angle of 67°. Introduction of azido groups on the surface resulted in a contact angle of 91° for the most concentrated photolinker solution (C = 0.01 M), suggesting that the azido groups were introduced to the wafer surface. The value of contact angle gradually decreased with the dilution of 4-ABA solution used for functionalization, as presented in Table 3.

Table 3. Contact angle measurement.

Surface	***H_2O contact angle (º)***
Amino functionalized SiO_2 surface	67 ± 2.0
4-ABA + EDC, C = 0.1 M	91 ± 2.0
4-ABA + EDC, C = 0.01 M	80 ± 1.7
4-ABA + EDC, C = 0.001 M	72 ± 2.0

The lower number of azido groups present on the surfaces resulted in reduced hydrophobicity, which correlated with a decline of water contact angle. The detected gradual decrease in number of surface azido groups with dilution of the photolinker was previously studied in detail for fluorinated analogues of 4-ABA photolinker, which mediated immobilization of polystyrene [178] and furanones [122]. The contact angle measurements already hinted towards successful functionalization of the silanized silicon wafers with 4-ABA photolinker.

ATR-FTIR was used as a complementary analytical technique to characterize the functionalized surfaces and spectra are presented in Figure 32. The spectrum of azido-presenting surface (black line) contained peaks arising from azide group between 2000 cm^{-1} and 2300 cm^{-1} and phenyl ring stretching from C=C between 1500 cm^{-1} and 1600 cm^{-1} in contrast to the silanized silicon wafer (grey line). As expected, a complete photodecomposition of the azide species occurred upon UV-irradiation, as demonstrated by the disappearance of the corresponding azide peak [123] (blue line), which further proved to attachment of 4-ABA to the surface as well as its light-induced photoactivity.

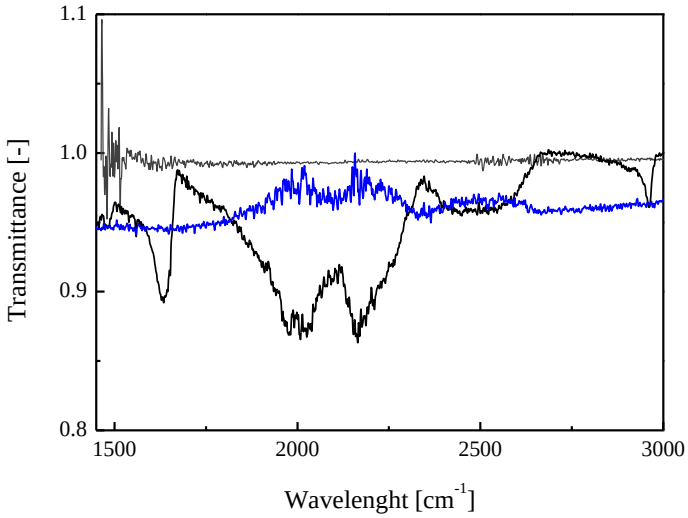

Figure 32. Section of ATR-FTIR spectrum of bare silicon wafer (in grey), silanized silicon wafer functionalized with 4-azidobenzoic acid (in black) and 4-azidobenzoic functionalized surface upon UV-irradiation (in blue).

3.4.4.2 Characterization by SEM and AFM

The surface morphology was studied by SEM and AFM. A series of surfaces were prepared by treatment of silanized silicon wafers with various solutions of the photolinker (0.1 M, 0.01 M and 0.001 M). Next, the surfaces were exposed to nanoreactor solutions and subsequently irradiated with UV light (366 nm, 20 min), the concentration of the block copolymer used for self-assembly was kept constant at 1 mg/ml. Finally, the samples were rinsed with bidestilled water to remove the unbound material, dried and analysed by SEM.

SEM images revealed that the surfaces were covered with dried, disrupted polymeric film, as can be seen in Figure 34. This fact was attributed to the change in the hydrophobicity of the surface. As the number of the surface azido groups decreased the hydrophobicity also decreased. It was reported that the photo-coupling reaction is dependent on the size of the immobilized molecules as well as on the number of azido groups present on the surface [178, 179]. At higher concentrations of the hydrophobic photolinker the hydrophobic external block of the block copolymer tries to minimize the contact area between the azido groups and the hydrophilic part of the polymer, which results in reorganization of the amphiphilic block copolymer, as is depicted in Figure 33.

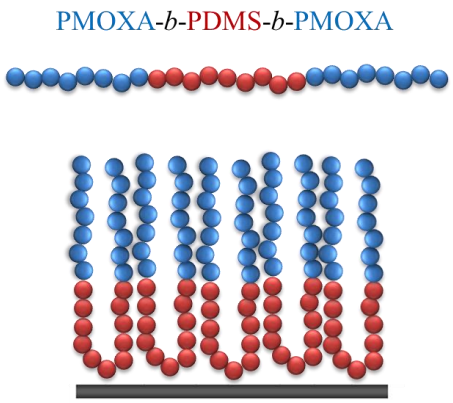

Figure 33. Schematic representation of the block copolymer rearrangement on surface functionalized with azido photolinker, resulting in surface with high hydrophobicity. This scheme does not depict the dimensions of the objects.

The unfavorable interactions between the hydrophobic surface and the hydrophilic chains of the polymer led to reassembly of the polymer molecules. The whole process is driven by the minimization of the free energy. The hydrophobic PDMS block was oriented downwards, while the hydrophilic PMOXA blocks were pointing upward. This same phenomenon of the reorientation of an amphihilic block copolymer was observed and reported for hydrophobic highly oriented pyrolytic graphite (water contact angle value 87.5º) [175]. It was found that is difficult to achieve nanoparticles attachment by azido-photolinker [124], however polymers, due to their big size, exhibit conformational freedom, and can be efficiently immobilized even at low concentration of azido-linker on the surface [178]. Dried, disrupted planar polymeric films are clearly seen in all of the SEM images (Figure 34), which is similar to the dewetted morphology of other dried planar polymeric films [180, 181, 182].

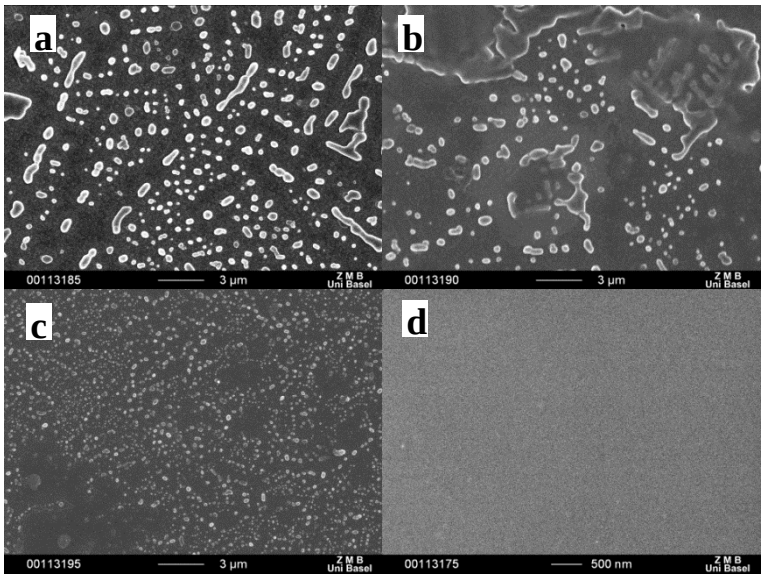

Figure 34. Representative SEM images of disrupted polymeric film on surfaces functionalized with 4-ABA solution at: (a) 0.1 M; (b) 0.01 M; (c) 0.001 M. (d) Bare silicon surface treated with nanoreactors solution, where no visible attached object on nanometer scale could be found.

To gain more insight AFM studies were conducted. The obtained results further confirmed the reassembly and planar film formation, as seen in Figure 35. AFM images showed that the surface was covered by an inhomogeneous polymeric film containing some defects. Since for those samples the dehydration and rupture of the dry polymeric film was not observed by AFM, so the earlier made assumption of the high vacuum of the SEM set-up (in the chapter 3.4.3.2 Characterization by SEM) leading to a significant change in film morphology was corroborated. The spots where the polymeric film is removed from the surface showed the same morphology and roughness as the 4-ABA functionalized surface. The mean thickness of this film was found to be approx. 2.5 nm.

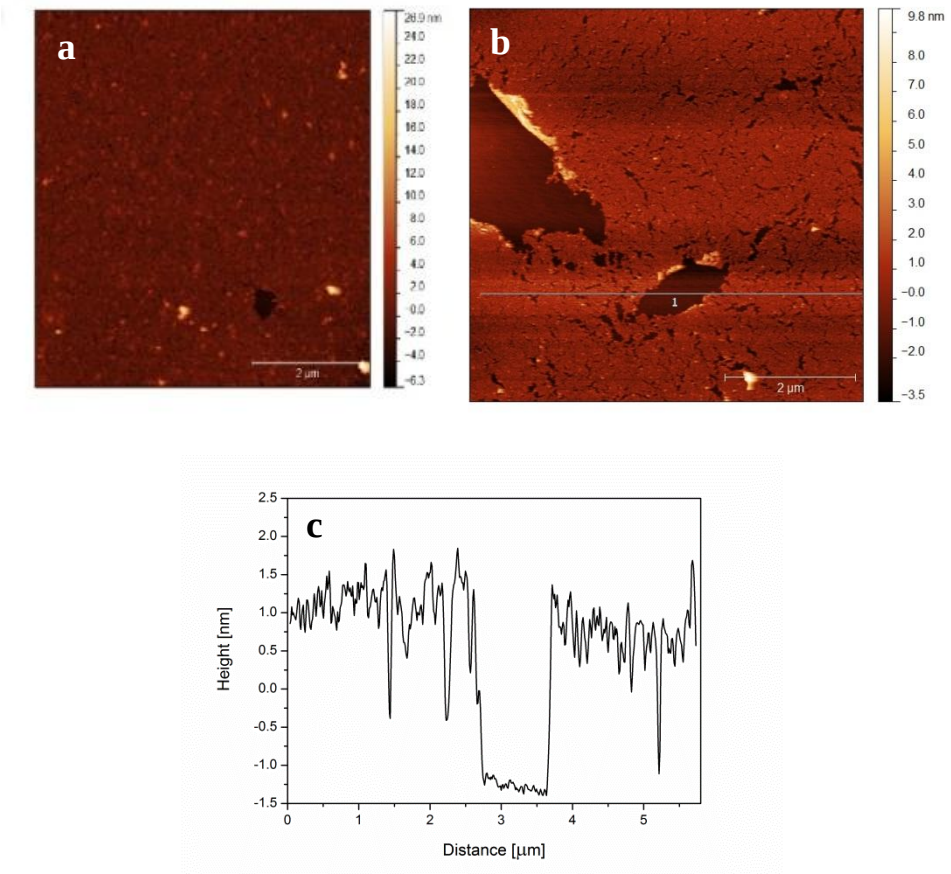

Figure 35. AFM images of 4-ABA functionalized surfaces treated with nanoreactors solution. The concentration of photlinker used for the surface functionalization corresponds to: (a) 0.01 M; (b) 0.1 M. Scale bar: 2 µm. (c) Cross section of (b).

The surfaces prepared by immersion of silanized silicon wafers in 0.001 M 4-ABA solution, were selected for further experiments. The experiments were accomplished by treating these surfaces with two nanoreactor solutions (0.5 mg/ml and 0.1 mg/ml). The lower concentration nanoreactor solution was selected in order to avoid their fusion, as previously described for liposomes [183] and polymersomes [175] attached to surface. Morphology, homogeneity, and roughness of the surface were studied by SEM and AFM.

For small molecules high concentration of azido groups is indispensable for the attachment. However in the case of polymers, which are big molecules and they have conformational freedom being a soft material, conformal contact of the polymer chains with the azido groups present on the surface is easily allowed [178]. Only one attachment point, that is only one azido group, is necessary to attach a polymer molecule to the surface. Because of the larger size of the polymer in comparison to that of the photolinker, the concentration of the surface azido groups can be diluted while still maintaining the covalent attachment of the polymer to the surface.

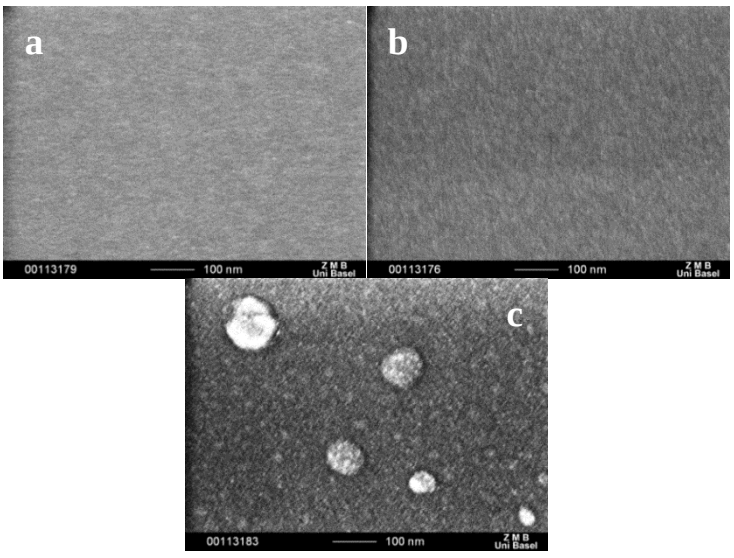

Figure 36. SEM images of: (a) 4-ABA functionalized surface; (b) control surface; (c) covalently immobilized nanoreactors by light-induced cleavage. Scale bars: 100 nm.

The hydrophilic–hydrophobic repulsion was minimized (by dilution of the photolinker used for the surface functionalization the number of 4-ABA molecules on the surface was

lower), while still ensuring covalent attachment of the polymer and lack of disruption to the vesicular structure. Vesicular shaped nanoreactors could be clearly distinguished in SEM image in Figure 36, c. Evidently, the covalently attached nanoreactors remained morphologically intact. In a control experiment, silanized surface exposed to nanoreactors solution and irritated with UV-light where completely washed off by rinsing.

AFM images (Figure 37, a and b) revealed non uniformly distributed, spherical features, absent in the case of more hydrophobic surfaces as described above. Figure 37, c shows representative examples of height images. After analysis of cross-section profiles of these spherical objects their average height was estimated to be approx. 9 nm. At the same surfaces, in regard to the photolinker concentration (0.001 M) used for functionalization, different immobilization efficiency was observed for the two nanoreactor solutions used for immobilization (0.5 mg/ml and 0.1 mg/ml). Surprisingly, in comparison to the more concentrated nanoreactor solution the density of surface coverage was significantly higher for less concentrated solution. For the surface immersed with nanoreactors at lower concentration, areas with tightly packed nanoreactors fused together as bigger aggregates could be recognized, Figure 37, b. Analogous behaviour was observed for surface immobilized liposomes [183] and polymersomes [175]. The diameters of the collapsed immobilized particles observed by AFM and SEM was consistent with the diameters of the corresponding nanoreactors measured by DLS, ranging from 50 nm to 200 nm. Additional experiments were conducted on bare silanized silicon wafers exposed to nanoreactors and treated with UV light, to prove that nanoreactor immobilization is due to the photocleavage from azido groups present on the surface. No nanoreactors remaining on the control surfaces were detected after rinsing with water and drying, as expected. In summary, these observations demonstrated that not only does the character of surface play a major role, but also the concentration of the immobilized material affects the outcome of the immobilization.

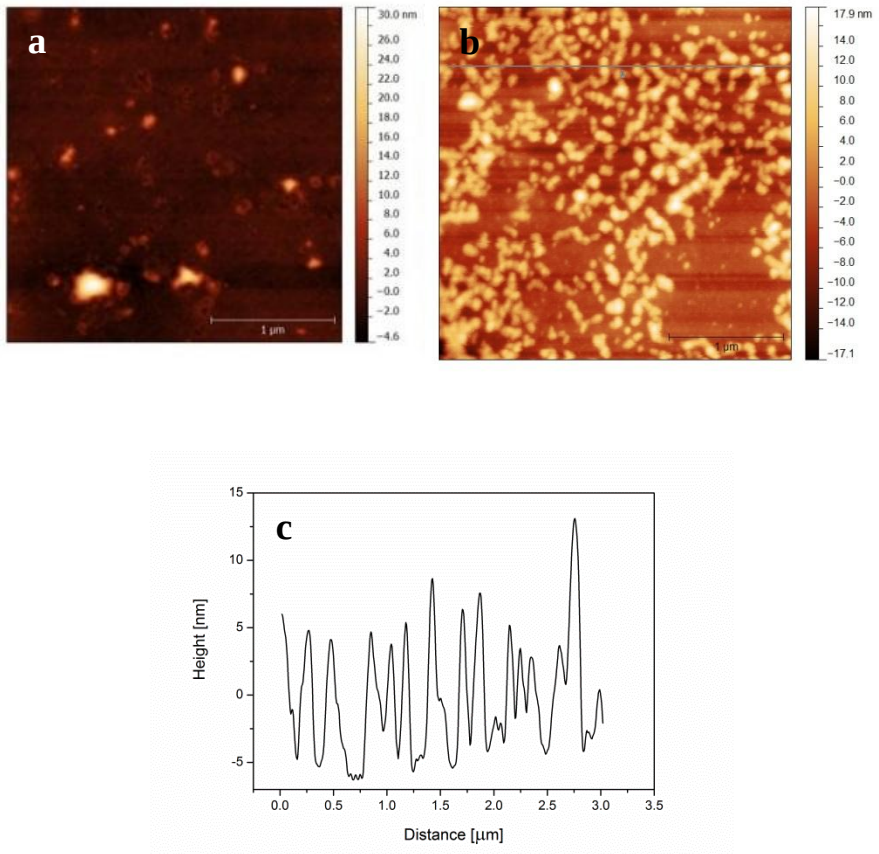

Figure 37. AFM images of covalently immobilized nanoreactors, obtained by photolinker presenting surface exposure to nanoreactor solution: (a) 0.5 mg/ml; (b) 0.1 mg/ml and cross section profiles (c), corresponding to (b). Scale bar: 1 µm.

3.5 Antibacterial properties of nanoreactors

The antibacterial characteristics of numerous dental and medical materials are conventionally examined using the agar diffusion test. However it is important to point out that to date, standardized and comprehensive tests on antibacterial activity of nanoparticles have not been formulated. The number of bacteria used in the antimicrobial potency tests is greatly higher than that met in real life surgical practice. The antimicrobial potency of antibiotic synthesizing nanoreactors against the model strain was tested using various methods: dilution test, disc diffusion test, direct contact diffusion test, and scanning electron microscopy. First, the bacterial growth in presence of nanoreactors was examined in solution. Secondly, the bacteria were allowed to come into direct contact with the surfaces featuring immobilized nanoreactors so that the bacterial growth could be analysed.

The covalent attachment of nanoreactors to a surface was accomplished as described in the chapter Nanoreactor immobilization *via* amino bond. Attempts were made to evaluate the amount of drug produced by immobilized nanoreactors but due to the very low concentration of synthesized drug it was not possible with available techniques. The applied methods however, allowed qualitative analysis of the antimicrobial potency of surface covalently attached nanoreactors.

3.5.1 Antimicrobial activity assay in solution – dilution method

In dilution tests, microorganisms are tested for their ability to produce visible growth in solution in the presence of antimicrobial agents in liquid media. In general, the mixture, consisting of microorganisms, nutrient medium and antibacterial agent, is incubated at 37 °C, for 24 hours with gentle agitation. The bacterial growth was monitored spectrophotometrically through optical density (OD) changes measured at 600 nm. The increase of optical density indicates growth.

The following samples were tested: nanoreactors, non-permeable polymersomes with the enzyme encapsulated, and solution composed of substrates only. The experiments also included a positive control (solution of medium and antibiotic, $C_{cephalexin}$ = 4 μg/ml) and a

negative control (solution of medium with bacteria). The negative control indicated the microbial growth in the absence of antimicrobial agent. A 1 ml of Mueller-Hinton broth (MHB), placed in a sterile plate, was inoculated with 20 µl of standardized *E. coli* suspension. The final number of cells was adjusted to give a final concentration ~ 10^4 CFU/ml. Then, 200 µl of appropriate solution, containing PGME (81.4 mM) and 7-ADCA (46.7 mM) in sterile PBS buffer, was added. After 24 h of incubation at 37 °C and 100 rpm the optical density was measured. The shaking was applied to minimize aggregation and settlement of the components as well as to ensure good mass transfer over the incubation period. Results are summarized in Table 4.

Table 4. Optical density at 600 nm after 24 h incubation at 37 °C

Sample	OD_{600}
nanoreactors	0.072
non-permeable polymersomes	2.254
substrates solution	2.174
solution of antibiotic	0.051
bacteria in absence of any additives	2.211

A visible decrease in turbidity after incubation was observed for all of the samples except the nanoreactor solution and the sample featuring antibiotic. A strong antibacterial effect for bacteria incubated with nanoreactors was evident. The bacterial growth in the case of non-permeable polymersomes and substrates solution was comparable with the bacterial growth observed for the sample consisting only of bacteria. The increase in the turbidity of these samples, which resulted from the uninhibited growth of the *E. coli* cells, was visible by eye, Figure 38, whereas the inhibition of bacterial growth was reduced in the case of nanoreactors due to the enzymatic activity of the nanoreactors and resulting drug production. This data provides a clear evidence of antimicrobial potency of drug-synthesizing nanoreactors in solution.

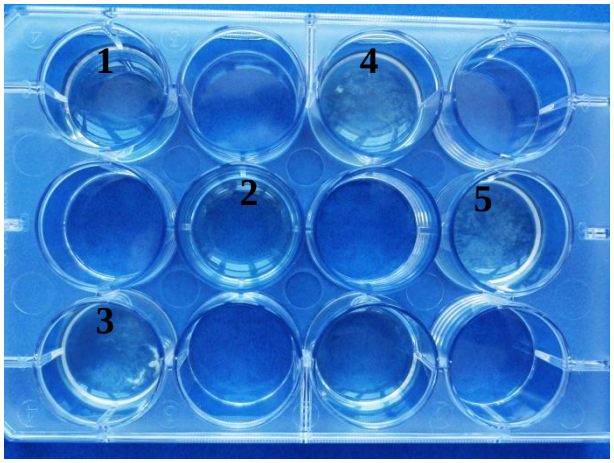

Figure 38. Picture of wells containing: (1) antibiotic; (2) nanoreactors; (3) substrates; (4) non-permeable polymersomes; (5) bacteria solution; after 24 h incubation at 37 ºC.

3.5.2 Antimicrobial activity assay – disc diffusion test

In the diffusion test the bacteria is cultured onto the surface of an agar plate. A sterile filter disc is applied to the surface of the plate. Then a sample containing antimicrobial agent is loaded onto the disc and the antibiotic is allowed to diffuse into the adjacent medium. Zones of inhibition are measured after the incubation indicating constrain of microbial growth.

The antimicrobial activity of the penicillin acylase loaded nanoreactors was analyzed measuring the bacterial growth in presence of nanoreactors adsorbed on a paper disc surface. Two solutions of nanoreactors were prepared – at room temperature and at 8 °C. A 100 μL of *E. coli* suspension, the optical density of which was adjusted photometrically, was cultured on a Muller-Hinton agar plate. Next, sterile paper discs were placed on inoculated agar. On each disc a 10 μl sample of mixture containing substrates (C_{PGME} = 81.4 mM, $C_{7\text{-}ADCA}$ = 46.7 mM) and nanoreactors was applied. Mixtures containing substrates only and substrates with non-permeable polymersomes served as controls, to prove that antimicrobial properties are not due to the substrates themselves or enzyme leakage. The samples were tested once daily over seven days applying the identical procedure. After 24 h incubation at 37 °C, bacterial growth on the

plates was examined by visual observation and the diameter of the zones of inhibition was measured with a ruler graduated to 0.5 mm.

Antibiotic synthesized by the enzyme encapsulated in the nanoreactors inhibited bacterial growth, while no inhibition of bacterial growth was observed in the case of substrates only and for non-permeable polymersomes containing enzyme (Table 5 and Figure 39).

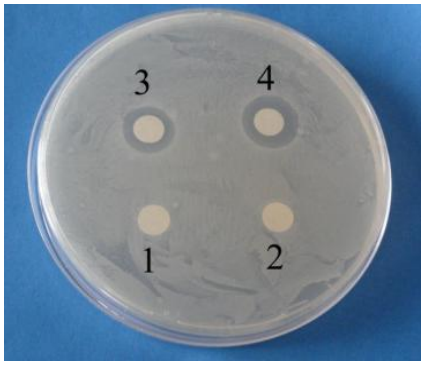

Figure 39. Picture of MHB agar plate inoculated with bacteria. Inhibition zones: (1) not permeable polymersomes; (2) substrates solution; (3) nanoreactors prepared at room temperature; (4) nanoreactors prepared at 8 °C; after incubation for 24 h at 37 °C. No zones of inhibition were observed around control (1) or substrate discs (2).

As expected, in the case of nanoreactors prepared at 8 °C the inhibition zones were larger than for nanoreactors prepared at room temperature, at which activity diminishes. This is due to the higher activity of the encapsulated enzyme. This correlates with deactivation of penicillin acylase over time for two different temperatures which was discussed in the chapter Enzymatic activity of nanoreactors. The obtained data corresponded to the cephalexin synthesis reaction curves (Figure 17). The decrease in the bacterial growth was attributed to the antibiotic synthesis and release.

Table 5. Inhibition zones in mm

Day	*Substrates*	*Polymersomes without OmpF*	*Nanoreactors prepared at RT*	*Nanoreactors prepared at 8 °C*
1	0	0	0	13.0
2	0	0	12.5	14.5
3	0	0	14.5	17.5
4	0	0	15.0	20.0
5	0	0	17.0	21.5
6	0	0	18.0	19.0
7	0	0	15.5	18.5

3.5.3 Direct contact surface test

The following surfaces were prepared and tested: surface immobilized nanoreactors, surface immobilized non-permeable polymersomes, silanized silicon surfaces, and bare silicon surfaces. The antimicrobial potency of immobilized nanoreactors was assessed by direct contact of the surface with bacterial cells. Bacterial strain *E. coli* XL Gold was streaked onto MHB agar plate and incubated overnight at 37 °C. A single colony was cultured overnight in 10 ml of MHB medium. The optical density of the resulting culture was adjusted to OD_{600} = 0.08 – 0.1 which corresponds to 1 x 10^8 CFU/ml. Surfaces were placed in 1 ml of reaction mixture ($C_{7\text{-ADCA}}$= 46.7 mM, C_{PGME} = 81.4 mM) in sterile PBS buffer and incubated for 24 h at 37 °C with agitation at 100 rpm. Afterwards the surfaces were placed active-side-down onto Mueller-Hinton agar plates previously inoculated with *E. coli* cells. After incubation for 24 h at 37 °C surfaces were examined by visual observation. An exact estimation of the drug produced by nanoreactors was not achievable with the available techniques. The surfaces were tested for seven days applying an identical procedure.

The antimicrobial potency of nanoreactors was proved by the presence of inhibition zones, which are characteristic of release of bactericidal agents, around surfaces functionalized with nanoreactors, as can be seen in Figure 40 a. This shows that the substrates present in the aqueous medium diffused through the polymeric wall to the interior cavity of the nanoreactors, where they were converted by the enzyme into the drug. Subsequently, the drug diffused back out of the nanoreactor and inhibited bacterial growth around the nanoreactor surface, which is reflected by the appearance of the inhibition halos. In contrast, the surface immobilized non-permeable polymersomes, silanized silicon surfaces, and bare silicon surfaces did not display any inhibition zones, Figure 40 b. The lack of the inhibition region, implies that bacteria were still able to grow around surfaces with non-permeable polymersomes. This suggests that the polymersomes themselves exhibit no antibacterial activity. This experiment also made certain that the antimicrobial properties of the surfaces were not due to leaching of enzyme from polymersomes to solution. The lack of inhibition zones around control surfaces with merely immobilized, non-permeable polymersomes, indicates that penicillin acylase does not leach from the polymersomes. Inhibition zones persisted for five days around the nanoreactor functionalized surfaces. The presence of these inhibition zones around surfaces with immobilized nanoreactors, characteristic of the release of bactericidal agents, proves that penicillin acylase-loaded nanoreactors are enzymatically active and efficiently catalyze antibiotic synthesis.

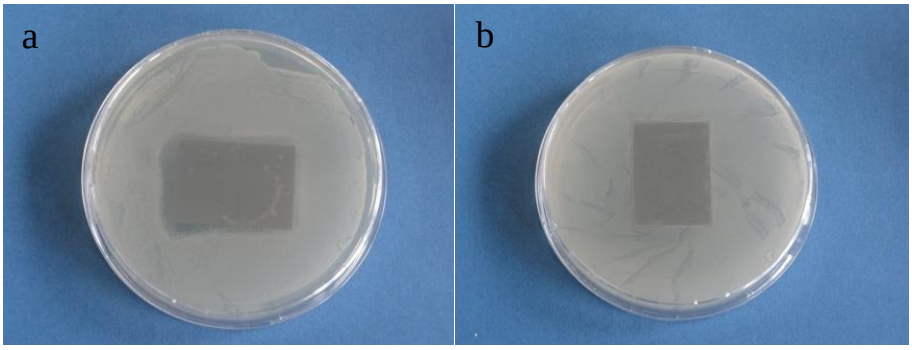

Figure 40. A representative picture of: (a) an inhibition zone around silanized silicon surfaces with immobilized nanoreactors; (b) silanized silicon surfaces with immobilized non-permeable polymersomes.

3.5.4 Scanning electron microscopy

The growth of microorganisms, following direct contact of the surface with the bacterial suspension, was detected with SEM. We investigated whether the immobilization of nanoreactors exhibited antimicrobial activity by the direct observation of bacterial adhesion and proliferation on the surfaces. As before, immobilized nanoreactors on silanized silicon wafers were incubated in the presence of substrates and bacteria. Silanized silicon wafers, and silanized silicon wafers bearing immobilized, non-permeable polymersomes were incubated in bacterial suspension, serving as a control. After 24 h incubation and washing to remove non-adhered bacteria, the surfaces were analysed by SEM (Figure 41). Visual inspection of the obtained images revealed that the enzymatic activity of the nanoreactors resulted in a drop of the *E. coli* cells when compared to the corresponding control surfaces. A significantly lower number of bacterial cells on surfaces with immobilized nanoreactors, as compared to controls, was attributed to the production and synthesis of cephalexin by the nanoreactors. Considerable decline in bacterial adhesion and proliferation in the case of immobilized nanoreactors proved their antibacterial potency.

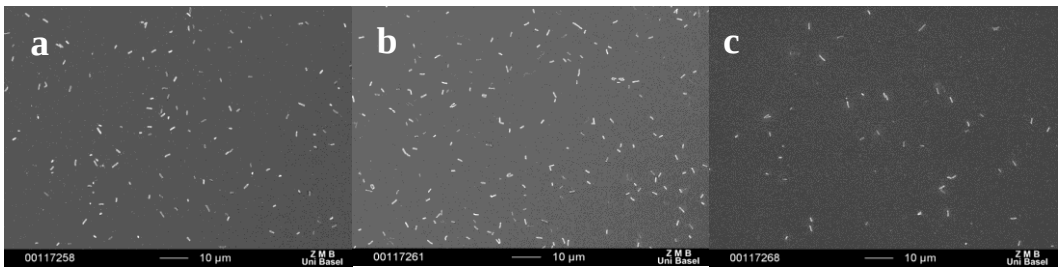

Figure 41. SEM images of *E. coli* attached to: a) silanized silicon surface; b) surface with non-permeable polymersomes; c) surface with immobilized nanoreactors. Scale bar: 10 µm.

In summary, these data demonstrate that nanoreactors immobilized on a surface synthesize antibiotic that is capable of inhibiting bacterial growth.

4 Conclusion and outlook

In this thesis enzymatically active nanoreactors that are based on an amphihilic block copolymer and their immobilization as well as antibacterial potency are described. PMOXA-*b*-PDMS-*b*-PMOXA block copolymer was synthesized and characterized in terms of block lengths and molecular weight. The obtained polymer was characterized by different analytical techniques such as ^{1}H-NMR, GPC and ATR-FTIR. The self-assembly of this polymer was studied with TEM and LS. The applied vesicle preparation method yielded self-assemblies with spherical shapes. Based on the data obtained by LS and TEM, the coexistence of two populations, vesicles as well as micelles, was concluded. Long term stability of polymeric vesicles was demonstrated, making them perfect candidates for biomedical applications.

An enzyme encapsulated in polymeric vesicles was protected from proteolytic degradation and retained its activity. The encapsulation efficiency agreed well with values published in literature. Also, the channel protein was inserted in the polymeric membrane, allowing for permeability. The resulting nanoreactors were active under physiological conditions. It was demonstrated that the catalytic activity is due to the encapsulated enzyme and that the final efficiency of the nanoreactors depends on the preparation parameters, i.e. time and temperature. Further studies should be focused on enhancement of the efficiency of the nanoreactors in regard to their enzymatic activity by employment of more stable enzymes.

Two different immobilization strategies were developed. The first, involving the reaction of the amino groups present on the surface with the aldehyde groups exposed on the outer shell of the nanoreactors, formed a Schiff base. The Schiff base was reductively aminated to yield a stable amino bond. A chemical modification was applied to introduce the aldehyde functionalities at the ends of the block copolymer. The selected modification procedure resulted in the required functionalities without disturbing the backbone of the polymer. The modification did not influence the self-assembly properties of the polymer. ATR-FTIR, SEM and AFM experiments were conducted in order to follow nanoreactor immobilization on the surface. The obtained results suggested that the attachment approach led to covalent immobilization and preserved the vesicular structure of the nanoreactors. Immobilized nanoreactors proved to be stable over several days. Investigations of attached nanoreactor density and its control are still to be carried out.

For the second immobilization strategy, a simple, fast, mild procedure was developed to prepare immobilized nanoreactors on surfaces *via* a UV-light activated photolinker. Activation of the surface was carried out by attaching a photoactive functional group 4-azidobenzoic acid to the surface. UV-irradiation of the photolinker transformed its azido groups into a highly reactive nitrene, which bonded with the hydroxyl groups present on the polymer surface.

The method that we developed allows for the immobilization of nanoreactors without chemical modification of the block copolymers and, in addition, no specific functional groups on the polymer are required for the attachment, which obviates modification of the polymer. The SEM and AFM data revealed that the nanoreactors were functionalized in a covalent, stable manner on the photolinker functionalized surface. The attachment efficiency was studied relative to the photolinker concentration used for the surface functionalization and the concentration of polymer. In addition, it was found that the surface properties influence the outcome of the immobilization. Since photolinker-mediated polymersome immobilization has never been studied, further studies must be focused on exploring various azido linkers with regard to their hydrophobicity to obtain more control over immobilization and enhanced immobilization yield. The good, time-dependent stability of the covalently attached nanoreactors seems a promising approach to a localized drug-delivery system. These developed immobilization methods could serve to attach biomolecules to nanoreactor surface. As a consequence, this work might have impact on diverse research fields such as drug delivery and biosensing.

To examine the antibacterial properties of the nanoreactors in bulk and on a surface, tests involving a model *E. coli* strain were performed. It was evident that these nanoreactors are enzymatically active in bulk and on a surface, synthesizing a drug on demand, and doing so efficiently to inhibit bacterial growth.

In summary, a novel system was designed and prepared based on covalently immobilized polymeric nanoreactors that were enzymatically active and able to efficiently synthesize an antibiotic on-demand.

5 Experimental part

All chemicals and solvents were purchased from Sigma Aldrich or Fluka (Sigma Chemical Co., USA) at the highest purity grade and used as received, unless otherwise stated.

5.1 Synthesis of poly(2-methyloxazoline)-*block*-poly(dimethylsiloxane)-*block*-poly(2-methyloxazoline) ($PMOXA_{16}$-$PDMS_{72}$-$PMOXA_{16}$) block copolymer

Block copolymers were synthesized by cationic ring opening living polymerization (CROP) according to a modified literature procedure [136]. Poly(dimethylsiloxane) (α,ω-bis(3-hydroxypropyl)poly(dimethylsiloxane)) (PDMS) pre-polymer (nominal *Mw* = 5600 g/mol, n = 72) was purchased from Sigma-Aldrich. All glassware was dried for at least 24 h at 120 °C. PDMS (1 eq) was pre-dried under high vacuum for 48 h at 60 – 80 °C. After cooling the PDMS to room temperature, 60 ml of anhydrous hexane and pyridine (3 eq, <0.005% water) were added *via* syringe under an argon flow. The reaction mixture was then cooled to -10 °C and trifluoromethanesulfonic anhydride (3 eq) in approximately 20 ml anhydrous hexane was added dropwise with a dropping funnel over 1 h under argon. The mixture was allowed to react for 1 h while the temperature was kept between -10 and -4 °C, before the solvent was removed under high vacuum. To the remaining material a fresh portion (60 ml) of dry hexane was added. The whole mixture was filtered through a glass filter (porosity G4) under argon in order to remove the insoluble salt resulting from pyridine and TfSA. The hexane was removed by high vacuum to yield a pale, yellow, oily, bifunctional macroinitator. Activated PDMS was dissolved in a mixture of anhydrous chloroform and acetonitrile (7 : 3) (<0.005% water) 100 ml. Next, 2-methyl-2-oxazoline (freshly distilled over calcium hydride, two excess units per side) was added slowly under argon flow to the reaction vessel. The solution was warmed to 40 °C and the polymerization proceeded with vigorous stirring for 72 h. After cooling the mixture to room temperature, the polymerization was terminated by addition of 0.5 M KOH and stirred for a further 4 h. The solvent mixture was removed by rotary evaporation. The remaining solid was dissolved in chloroform and non-reacted

PDMS was removed by precipitation with cold hexane at least twice. The product was recovered by filtration and purified by subsequent ultrafiltration in an ethanol-water mixture (Millipore Ultrafiltration Stirred Cell 76 mm, 300 ml). The solvents were evaporated under reduced pressure and the product was dried under high vacuum. The polymer was characterized by ^{1}H-NMR, GPC and ATR-FTIR spectroscopy.

5.1.1 Characterization by ^{1}H-NMR

^{1}H-NMR spectra were recorder with a Bruker DPX-400 spectrometer (Bruker, Switzerland). Deuterated chloroform was used as solvent (99.8% D, 0.1% TMS). Spectra were analyzed with MestReNova 7.0.3 software (Mestrelab Research SL, Spain). The molecular weight of the polymer obtained based on ^{1}H-NMR was 8323 g/mol.

Detailed peak assignments for the block copolymer:
^{1}H-NMR (400 MHz, $CDCl_3$): δ [ppm] = 0 ppm (Si-***CH$_3$***, 6H), 0.5 ppm (Si-***CH$_2$***-CH_2, 4H), 1.5 – 1.6 ppm (Si-CH_2-***CH$_2$***-CH_2, 4H), 2.0 – 2.2 ppm (***CH$_3$***-CON<, 6H), 3.3 – 3.5 ppm (>N-***CH$_2$***-***CH$_2$***-N<, 8H).

Detailed peak assignments for the pre-polymer:
^{1}H-NMR (400 MHz, $CDCl_3$): δ [ppm] = 0 ppm (Si-***CH$_3$***, 6H), 0.5 ppm (Si-***CH$_2$***-CH_2, 4H), 1.5 – 1.6 ppm (Si-CH_2-***CH$_2$***-CH_2, 4H), 1.9 – 2.0 ppm (-***OH***), 3.4 ppm (Si-CH_2-CH_2-***CH$_2$***-O-CH_2, 4H), 3.5 ppm (O-***CH$_2$***-CH_2-OH, 4H), 3.6 ppm (O-CH_2-***CH$_2$***-OH, 4H).

5.1.2 Characterization by gel permeation chromatography

The molecular weight of the block copolymer was determined by GPC using a Viscotek GPCmax system equipped with a PLgel 10 µm column, with THF as eluent (flow rate: 1 ml/min) at 40 °C and recorded by refractive-index (RI) and UV detection. Narrow polystyrene standards (PSS Polymer Standards Service, Germany) were used to calculate *Mn*, *Mw*, and the polydispersity index (*PDI*) of the block copolymer and the pre-polymer.

The molecular weight of the polymer used, by GPC, was *Mn* = 7988 g/mol and the *PDI* = 1.83.

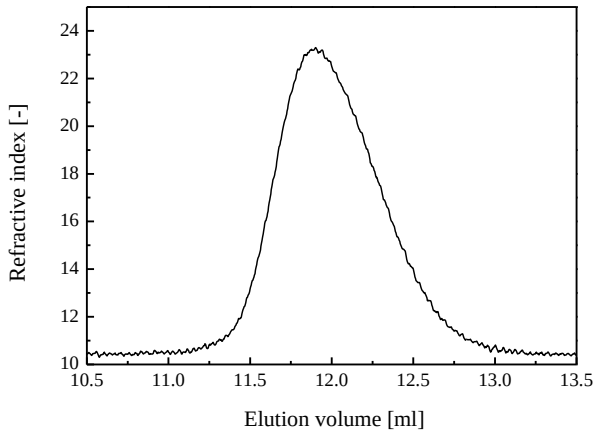

Figure 42. Gel permeation chromatogram of PMOXA-*b*-PDMS-*b*-PMOXA dissolved in THF. Refractive index detector.

5.1.3 Characterization by attenuated total reflectance Fourier transform infrared spectroscopy

ATR-FTIR measurements were acquired using an ALPHA spectrometer (Bruker, Germany) equipped with Platinum ATR QuickSnapTM A220/D-01 sampling modules and a single reflection diamond ATR accessory. Spectra were recorded over 128 scans and at resolution of 2 cm^{-1}, in the range between 4000 cm^{-1} and 450 cm^{-1}.

5.1.4 Dynamic and static light scattering

Dynamic and static light scattering experiments were performed at 293 K ± 0.05 K using an ALV-Langen Goniometer equipped with a frequency doubled He-Ne laser (wavelength 633 nm). The apparatus allows measurement at scattering angles of between 30° and 150°. Samples were measured in 10 mm diameter cylindrical quartz cells. Cells were then mounted in a thermostated optical matching bath (toluene bath). Vesicle

samples were prepared according to the film rehydratation method. A series of dilutions (at least of 5) were then prepared from the original solution of vesicles. Typically, polymer concentrations ranged from 1 mg/ml to 0.1 mg/ml. An ALV-5000/E Multiple Tau Digital Correlator was used to calculate the photon intensity, and an autocorrelation function was used to calculate vesicle size. DLS data were analyzed *via* the CONTIN algorithm.

A hydrodynamic radius (*Rh*) of around 165 nm was estimated from dynamic light scattering. Dividing the radius of gyration (*Rg*), derived from static light-scattering experiments, by the hydrodynamic radius, from dynamic light scattering, yields a value close to one (*Rg/Rh* = 1.09). Static light scattering indicated a vesicle molecular weight of 16 x 106 g/mol.

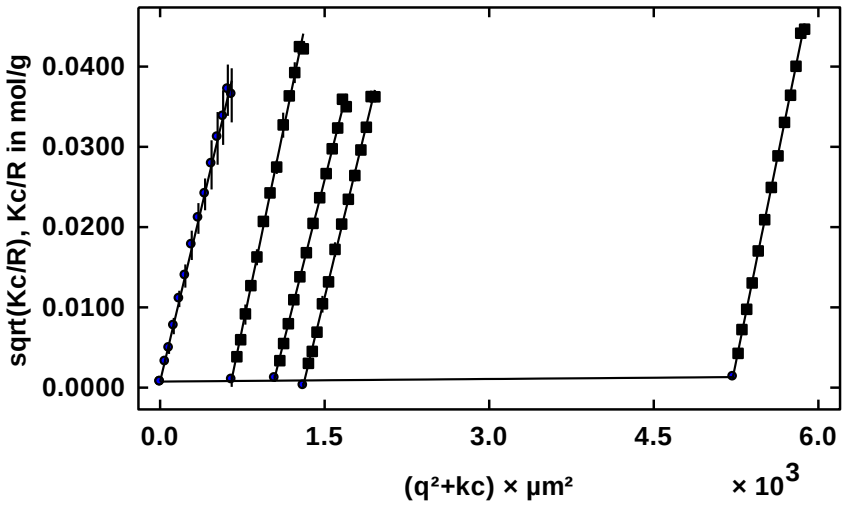

Figure 43. Zimm plots of PMOXA-*b*-PDMS-*b*-PMOXA vesicles solution in water, extrapolated to zero angle and concentration

5.2 Transmission electron microscopy

TEM images were taken on a Philips EM 400 (Philips Electronics, Netherlands) operated at 80 kV, equipped with a Megaview III charge-coupled device camera (CCD) and controlled with Morgagni 268D control and image acquisition software. The sample was

deposited on a glow-discharged, parlodion-and carbon-coated, 200 mesh copper grid and incubated for 1 min, before the droplet was blotted on filter paper. Afterwards, the samples were negatively stained with a 2% uranyl acetate solution.

5.3 Scanning electron microscopy

SEM images were taken on a Hitachi S-4800 FEG (Hitachi, Ltd., Japan) operated at 5 kV accelerating voltage. Solutions of polymeric vesicles were deposited on a clean silicon wafer by drop drying. The wafer was rinsed three times with double-distilled water and dried under argon flow. The surface was coated with 3 nm of sputtered platinum.
SEM images were taken by Eva Bieler of the ZMB, University of Basel.

5.4 Atomic force microscopy

AFM images were recorded with an Agilent 5100 AFM/SPM microscope (PicoLe System, Molecular Imaging) in ambient air in a tapping mode. Measurements were performed by using silicon cantilevers (PPP-NCHR, Nanosensors) with a nominal spring constant of 42 N/m and a mean tip radius of 7 nm. Images were collected with a resolution of 512 x 512 pixels at the scan rate of 0.5 line/s, and then analyzed with Gwyddion software.

5.5 UV-Vis spectroscopy

Measurements were performed on a Thermo Scientific NanoDrop 2000c UV-Vis spectrophotometer (Thermo Fisher Scientific, USA) equipped with a xenon flash lamp. Spectra were recorded between 200 nm and 800 nm with a slit width of 1 nm, absorbance precision ± 0.002 and a wavelength accuracy of 1 nm.

5.6 Contact angle measurements

Contact angles were determined by the static sessile drop method using a contact angle goniometer fully computer-controlled instrument CAM 100 (KSV, Germany). Multiple drops of ultrapure water were placed on each surface using a micro-syringe. The measurements were carried out under constant ambient conditions and constant drop size (3 µl). The angle between the droplet and the surface was measured with a 50 mm lens (Japan). CAM 100 imaging software was used to calculate the contact angle. A minimum of nine measurements were made on triplicate samples. No change in the measured contact angle was observed during a 1 min measurement

5.7 Channel protein extraction and purification

The outer membrane protein F (OmpF) was expressed in BL21 (DE3) Omp8 *Escherichia coli* cells [184]. An lysogeny broth (LB) sterile plate with 100 µl/mg ampicillin was inoculated with the Omp8 strain and allowed to grow overnight. Next, colonies were taken and mixed with 10 ml of ampicillin containing (100 µl/ml) LB medium to prepare a pre-culture. The pre-culture was mixed with 350 ml of LB containing ampicillin (100 µl/ml) in a 1 litre flask and vigorously shaken (250 rpm) at 37 ºC until the culture reached the mid-log phase of growth (OD_{600} = 0.5 – 0.8). The expression of OmpF was induced by the addition of 1 M IPTG, yielding a final concentration of 0.4 mM. After six hours, cells were centrifuged at 5000 rpm for 30 min at 4 ºC. The pellet was collected and stored at -20 ºC. The cell pellet was resuspended in 10 ml per 1 g cell pellet in breaking buffer (20 mM Tris-Cl pH 8.0, 2.5 mM $MgCl_2$, 0.1 mM $CaCl_2$). Then, 100 µl of freshly prepared RNase A (10 mg/ml) and 10 µl DNase I (1 U/µl) were added per 10 ml buffer. The mixture was homogenized. Next, 1 ml 20% SDS per 10 ml cell suspension was added and incubated for 1 h at 60 ºC with gentle stirring. The mixture was centrifuged at 22 000 rpm at 4 ºC for 60 min. The pellet was washed with 20 mM phosphate buffer pH 7.4 to remove residual SDS. 0.125% Octyl-POE in 20 mM phosphate buffer pH 7.4 was added to 5 ml/g cell pellet. The mixture was homogenized and incubated at 37 ºC for 1 h and centrifuged at 40 000 rpm at 4 ºC for 40 min. The final extraction was done by homogenization of pellet with 3% Octyl-POE in 20 mM phosphate buffer pH 7.4

followed by incubation for 1 h at 37 ºC and centrifugation at 40 000 rpm at 20 ºC for 40 min. OmpF purity was examined with a 12% SDS-PAGE gel (Figure 44). The concentration was estimated by UV-Vis spectrometry at 280 nm against 3% Octyl-POE in 20 mM phosphate buffer pH 7.4. The measured concentration was 1.7 mg/ml.

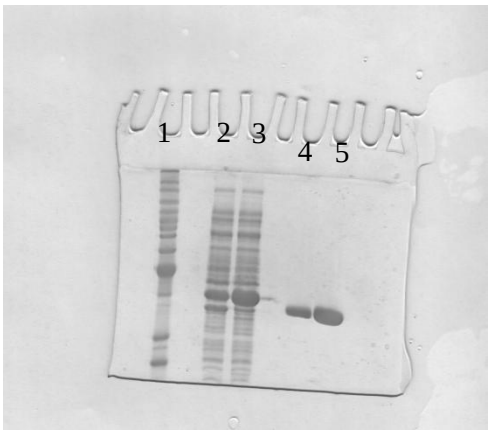

Figure.44. Purity analysis of OmpF by 12% SDS-PAGE. Ladder (1); pre-extracted OmpF (2, 3); diluted OmpF (0.5 mg/ml) (4); concentrated OmpF (1.7 mg/ml) (5).

5.8 Penicillin acylase

The penicillin acylase from *E. coli* (MW = 70 kDa) was purchased from ASA Spezialenzyme GmbH (Germany) and was used without further purification. The enzyme concentration was determined by BCA (Bicinchoninic Acid) Protein® Assay Kit (Thermo Scientific, USA).

5.8.1 Spectrophotometric assay of penicillin acylase activity

A modified colorimetric enzyme assay was used to determine penicillin acylase activity [177]. The assay measures the formation of the acidic products of penicillin G hydrolysis by following the decrease in pH using lackmus as an indicator. The change in pH induced by

the formation of the acidic products was followed at 584 nm, reflecting a change in the colour of the indicator. The activity measured is directly proportional to the amount of enzyme added to the assay, exhibiting a linear relationship with an R^2 value of 0.991 ± 0.004. One unit of activity is defined as the amount of enzyme that will produce 1 µmol of phenylacetic acid equivalents per min under the assay conditions used. The activity of the enzyme working solution was A = 503 U/min*ml.

5.9 Preparation of nanoreactors

In order to study the effect of temperature on enzyme activity during vesicle preparation and purification, samples were prepared at both 8 °C and at room temperature.
The penicillin acylase encapsulating nanoreactors were prepared *via* the film rehydration method. The general procedure is as follow: 10 mg of $PMOXA_{16}$-$PDMS_{72}$-$PMOXA_{16}$ polymer was dissolved in 150 µl ethanol and OmpF was added at the desired molecular ratio of protein to polymer (100 µg porin/10 mg polymer). The mixture was dried by rotary evaporation under reduced pressure at 40 °C. The resulting film was rehydrated with 2 ml of phosphate buffered saline (PBS; 137 mM NaCl, 2.7 mM KCl, 10 mM Na_2HPO_4, 1.7 mM KH_2PO_4, pH 7.4) solution containing 100 µM of *E. coli* penicillin acylase (2.2 mg/ml) and stirred for 24 h, respectively, at 8 °C and at RT, resulting in the formation of self-assembled nanoreactors. Non-encapsulated protein was removed by dialysis against PBS buffer (pH 7.4) at, respectively, 8 °C and RT for three days (cellulose membrane from Spectrapor®, MWCO 300 kDa). As control samples, vesicles with encapsulated enzyme but without channel protein were used.
Samples that were examined by SEM and AFM were prepared in bidistilled water instead of buffer in order to avoid salts precipitating during the drying process.

5.10 Encapsulation efficiency assay

Encapsulation efficiency was determined quantitatively using size exclusion chromatography (SEC, Sepharose 2B 60 – 200 µm bead diameter). Amount of non-

encapsulated enzyme was determined using the BCA Protein Assay kit (Thermo Scientific, USA).

5.11 Cephalexin synthesis and spectrophotometric assay

Reaction was carried out in PBS buffer pH 7.4 at 37 °C ± 1 °C for seven days. The concentrations of PGME and 7-ADCA in the reaction mixture were 81.4 mM and 46.7 mM, respectively. The concentration of cephalexin was estimated using UV-Vis spectroscopy by the modified method described in [164]. The method involves conversion of penicillins to the corresponding highly absorbing piperazine-2,5-dione derivatives by heating in an alkaline (carbonate buffer pH 9.2) sorbitol-zinc ion solution, and followed by incubation with 1 M NaOH solution. Since an intact β-lactam ring and a free amino group in the side-chain of the drug molecule are required, no interference due to 7-ADCA and PGME was observed. Changes in absorbance were followed at 388 nm. The procedure of the assay in general was as follows: 100 µl of analysed sample was mixed with 100 µl sorbitol-zinc ion solution (in carbonate buffer pH 9.2) and heated on a heating block at 60 °C for 10 min. 100 µl of 1 M NaOH was then added and mixed thoroughly. A sample of PBS buffer was treated exactly as the analysed sample and used as the reference. The cephalexin concentration in analysed samples was calculated by a standard curve ($R^2 = 0.998$).

5.12 Silicon wafers

Silicon wafers, single-side polished (orientation: N/Phos < 100 >, thickness: 525 ± 25 µm, resistance: 1 – 30 Ω/cm) were purchased from Si-Mat Silicon Materials (Landsberg am Lech, Germany). Silicon wafers were cut into 1 cm x 1 cm pieces. They were cleaned ultrasonically in acetone, dichloromethane and ethanol for 1 h each and then dried under a stream of nitrogen. Wafers were placed for 15 min in a UV/ozone (UVO) chamber (λ = 180 nm). Surfaces were finally placed in an oven (2 h, 120 °C).

Silicon wafers used for the antimicrobial activity testes (single-side polished, orientation: P, thickness: 150 ± 0.625 mm, resistance: 1 – 20 Ω/cm, 35 mm x 25 mm) were purchased from CrysTec (CrysTec GmbH, Germany). The cleaning procedure was as described above.

5.13 Amino functionalization (silanization) of silicon wafers

Functionalization of the wafers was performed according to the modified procedure described previously in [111]. Cleaned and dry surfaces were immersed in 5% (v/v) 3-aminopropyltriethoxysilane 99% (APTES) solution in toluene (anhydrous, 99.9%) for 4 h at room temperature under a dry argon atmosphere. Then, surfaces were washed several times with toluene, acetone, and ethanol, dried (80 °C, 2 h) and used directly for experiments.

5.14 .Dess-Martin oxidation of the hydroxyl, terminal groups of the polymer

The terminal OH groups were selectively oxidized to aldehydes by Dess-Martin oxidation. A round bottom flask was charged with polymer (1 eq) and Dess-Martin periodinane (2.4 eq). The oxidation was performed in DCM at room temperature for 24 h. The solvent was evaporated and residues were dissolved in ethanol. The product was purified by dialysis against ethanol at room temperature for 48 h. Ethanol was exchanged at least three times, a cellulose membrane was used (Spectrapor® with MWCO 1 kDa).

5.15 Analytical tests employed to confirm the presence of aldehyde groups

Brady’s test. Brady's positive test is signaled by a yellow or red precipitate (dinitrophenylhydrazone). A drop of 2,4-dinitrophenylhydrazine reagent (in 95% ethanol) was added to ~ 50 mg of polymer, shaken vigorously, and the solution was allowed to stand for 15 minutes. A reddish precipitate was formed in the case of a modified polymer.

Tollens' test. Tollens' reagent was prepared in the following manner: 0.2 M silver nitrate solution was mixed with a drop of 3 M sodium hydroxide solution and 2.8% ammonia solution, which was added dropwise with constant shaking until the precipitate of silver oxide dissolved. A drop of freshly prepared solution of Tollens' reagent was added to polymer samples and gently heated. In the presence of aldehyde groups a black precipitate was formed.

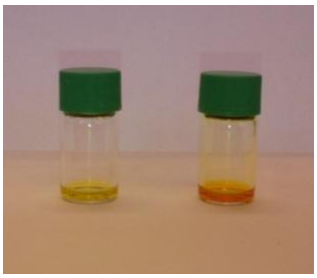

Figure 45. Pictures of aldehyde-terminated (right side) and hydroxyl-terminated polymer (left side) after Brady's test.

Figure 46. Pictures of aldehyde terminated (right side) and hydroxyl terminated (left side) polymer after the Tollen's test

5.16 Nanoreactor immobilization *via* amino bond on the silanized silicon wafer

The silanized surfaces were immersed in a solution of 1 mg/ml aldehyde-PMOXA-*b*-PDMS-*b*-PMOXA-aldehyde nanoreactors in PBS buffer (pH 7.4) containing a 0.25% (w/v) 2-picoline borane complex, at 37 °C. After 12 h of reaction, the samples were extensively rinsed with bidistilled water and dried under a stream of nitrogen.

5.17 Nanoreactor immobilization *via* bifunctional aromatic coupling agent

Silanized silicon wafers were immersed with solutions (0.1 M, 0.01 M and 0.001 M) in methanol of 4-azidobenzoic acid (~0.5 M in *tert*-butyl methyl ether) and EDC (0.1 M, 0.01 M and 0.001 M, respectively) at 37 °C for 24 h, with gentle stirring, in darkness. Afterwards the surfaces were washed with methanol and ethanol, and dried. The functionalized surfaces were placed in a chamber containing a solution of nanoreactors and irradiated under UV light at 366 nm for 20 min.

5.18 Bacterial culture and antimicrobial activity experiments

An *E. coli* XL10 Gold strain from Stratagene was used. The solutions for the bacterial experiments, BactoTM Agar and BBLTM Mueller-Hinton II broth, were purchased from BD (Becton, Dickinson and Company, USA).
Inoculum was prepared according to the following procedure. The bacteria were grown on MHB agar plates at 37 °C ± 1 °C until the stationary phase was reached. The working bacteria concentration was reached through consecutive dilutions (in sterile 0.91% w/v solution of NaCl) and was evaluated by measuring the suspension's optical density at 600 nm (1 cm light path) using a spectrophotometer. The inoculum was standardized to have a concentration of 1×10^8 CFU/ml. A correlation between absorbance by means of colony forming units per ml (CFU/ml) – 1×10^8 CFU/ml corresponds to $OD_{600} = 0.08 – 0.1$. In order to check whether the MIC was reached by the nanoreactors, 10 µl of reaction mixture were applied to the sterile discs, placed on Mueller-Hinton agar plates and subcultured with the *E.coli* strain. Subsequently, plates were incubated at 37 °C ± 1 °C for 24 h. Bacterial growth on the plates was examined by visual observation of the plates and the diameter of the zones of inhibition was measures with a ruler graduated to 0.5 mm.

The minimum inhibitory concentration is defined as the lowest concentration of antibiotic at which there is no visible growth of the organism. MIC of reference strains *E.coli* are:

NCTC (The National Collection of Type Cultures) 10418 4 – 16 mg/ml, ATCC (America Type Culture Collection) 25922 8 – 30 mg/ml. Inhibition zone diameter for a 30 μg cephalotin disc was 15 – 21 mm according to National Committee for Clinical Laboratory Standards.

5.18.1 Dilution method

To 1 ml sterile MHB medium, containing bacterial suspension (the inoculum was standarize to ~ 10^4 CFU/ml), 200 μl volume of a was added. The mixtures were incubated at 37 °C ± 1 °C, for 24 h with 100 rpm stirring speed. The bacterial growth was monitored through optical density changes measured at 600 nm. A mixture of 1 ml sterile MHB medium and 220 μl volume of PBS sterile buffer was used as reference.

5.18.2 Diffusion method

In the test, the bacteria were inoculated onto the surface of an agar plate. A sterile filter disc was applied to the surface of the plate. Then, a 10 μl of sample was loaded onto discs and the antibiotic was allowed to diffuse into the adjacent medium. Zones of inhibition of bacterial growth were present around the antibiotic discs when the MIC was achieved.

5.19 Antimicrobial properties of immobilized nanoreactors

5.19.1 Direct contact inhibition zone assay

35 mm x 25 mm silicon wafers (CrysTec, Germany) were silanized and nanoreactors were immobilized on them as described above. Surfaces were placed in individual sterile plates and 1 ml of PBS buffer pH 7.4 containing 81.4 mM PGME and 46.7 mM 7-ADCA, were added to each plate. Plates were incubated for 24 h at 37 °C with 100 rpm agitation.

Wafers were then washed with sterile PBS buffer and placed active-side-down onto Mueller-Hinton agar plates previously inoculated with 100 µl of *E. coli* with OD_{600} = 0.08 – 0.1. Plates were incubated for 24 h at 37 °C.

5.19.2 Scanning electron microscopy

E. coli (stored in 30% (v/v) glycerol solution at -80 °C) were grown overnight on sterile Mueller-Hinton agar plates at 37 °C. A pre-culture was obtained by inoculation of Mueller-Hinton broth and grown at 37 °C with rotary agitation at 250 rpm until the OD_{600} = 0.08 – 0.1. The test surfaces were placed in individual sterile plates and 1 ml of MHB containing 81.4 mM PGME and 46.7 mM 7-ADCA was added to each plate, as well as 10 µl of the bacterial suspension. Plates were incubated for 24 h at 37 °C with 120 rpm agitation. Afterwards the surfaces were washed with sterile PBS buffer to remove non-adhered bacteria. Test surfaces were then placed in 2.5% (v/v) glutaraldehyde solution for 4 h at room temperature – the fixation step. Subsequently, surfaces were sequentially placed in various ethanol solutions (30%, 50%, 70%, 90% and 100%) for 15 minutes each, to dehydrate bacteria. The samples were freeze-dried and coated with Au.

6 References

1. Hetrick, E. M.; Schoenfisch, M. H., Reducing implant-related infections: active release strategies. *Chemical Society Reviews* **2006,** *35* (9), 780-789.

2. Darouiche, R. O., Antimicrobial Approaches for Preventing Infections Associated with Surgical Implants. *Clinical Infectious Diseases* **2003,** *36* (10), 1284-1289.

3. Osmon, J. M. S. a. D. L., Prostetic joint infections. In *Infections Associated With Indwelling Medical Devices*, 3rd edition ed.; Bisno, F. A. W. a. A. L., Ed. ASM Press: Washington, 2000; pp 173-209.

4. A. Virk, D. R. O., Prostheticjoint infection. In *CurrTreatOptionsInfectDis*, 2001; Vol. 3, pp 287–300.

5. Darouiche, R. O., Treatment of Infections Associated with Surgical Implants. *New England Journal of Medicine* **2004,** *350* (14), 1422-1429.

6. Khardori, N.; Yassien, M., Biofilms in device-related infections. *Journal of Industrial Microbiology & Biotechnology* **1995,** *15* (3), 141-147.

7. Campoccia, D.; Montanaro, L.; Arciola, C. R., The significance of infection related to orthopedic devices and issues of antibiotic resistance. *Biomaterials* **2006,** *27* (11), 2331-2339.

8. Costerton, J. W., Overview of microbial biofilms. *J Ind Microbiol* **1995,** *15* (3), 137-40.

9. Costerton, J. W.; Lewandowski, Z.; Caldwell, D. E.; Korber, D. R.; Lappin-Scott, H. M., Microbial biofilms. *Annu Rev Microbiol* **1995,** *49*, 711-45.

10. Peyton, B. M.; Characklis, W. G., Microbial biofilms and biofilm reactors. *Bioprocess Technol* **1995,** *20*, 187-231.

11. Yuehuei H. An, R. J. F., *Handbook of bacterial adhesion: principles, methods and applications* Humana Press Inc: 2000.

12. Gristina, A. G., Biomaterial-Centered Infection - Microbial Adhesion Versus Tissue Integration. *Science* **1987,** *237* (4822), 1588-1595.

13. Poelstra, K. A.; Barekzi, N. A.; Rediske, A. M.; Felts, A. G.; Slunt, J. B.; Grainger, D. W., Prophylactic treatment of gram-positive and gram-negative abdominal implant infections using locally delivered polyclonal antibodies. *Journal of Biomedical Materials Research* **2002,** *60* (1), 206-215.

14. Schneeberger, P. M.; Smits, M. H. W.; Zick, R. E. F.; Wille, J. C., Surveillance as a starting point to reduce surgical-site infection rates in elective orthopaedic surgery. *Journal of Hospital Infection* **2002,** *51* (3), 179-184.

15. Nablo, B. J.; Rothrock, A. R.; Schoenfisch, M. H., Nitric oxide-releasing sol–gels as antibacterial coatings for orthopedic implants. *Biomaterials* **2005,** *26* (8), 917-924.

16. Kingshott, P.; Wei, J.; Bagge-Ravn, D.; Gadegaard, N.; Gram, L., Covalent Attachment of Poly(ethylene glycol) to Surfaces, Critical for Reducing Bacterial Adhesion. *Langmuir* **2003,** *19* (17), 6912-6921.

17. Kaper, H. J.; Busscher, H. J.; Norde, W., Characterization of poly(ethylene oxide) brushes on glass surfaces and adhesion of Staphylococcus epidermidis. *J Biomater Sci Polym Ed* **2003,** *14* (4), 313-24.

18. Nagel, J. A.; Dickinson, R. B.; Cooper, S. L., Bacterial adhesion to polyurethane surfaces in the presence of pre-adsorbed high molecular weight kininogen. *J Biomater Sci Polym Ed* **1996,** *7* (9), 769-80.

19. Jucker, B. A.; Harms, H.; Zehnder, A. J., Adhesion of the positively charged bacterium Stenotrophomonas (Xanthomonas) maltophilia 70401 to glass and Teflon. *J Bacteriol* **1996,** *178* (18), 5472-9.

20. Dathe, M.; Nikolenko, H.; Meyer, J.; Beyermann, M.; Bienert, M., Optimization of the antimicrobial activity of magainin peptides by modification of charge. *FEBS Letters* **2001,** *501* (2–3), 146-150.

21. Ofek, I.; Hasty, D. L.; Sharon, N., Anti-adhesion therapy of bacterial diseases: prospects and problems. *FEMS Immunology & Medical Microbiology* **2003,** *38* (3), 181-191.

22. Wu, P.; Grainger, D. W., Drug/device combinations for local drug therapies and infection prophylaxis. *Biomaterials* **2006,** *27* (11), 2450-2467.

23. Smith, A. W., Biofilms and antibiotic therapy: Is there a role for combating bacterial resistance by the use of novel drug delivery systems? *Advanced Drug Delivery Reviews* **2005,** *57* (10), 1539-1550.

24. Vorndran, E.; Spohn, N.; Nies, B.; Rossler, S.; Storch, S.; Gbureck, U., Mechanical properties and drug release behavior of bioactivated PMMA cements. *J Biomater Appl* **2012,** *26* (5), 581-94.

25. Høiby, N.; Bjarnsholt, T.; Givskov, M.; Molin, S.; Ciofu, O., Antibiotic resistance of bacterial biofilms. *International Journal of Antimicrobial Agents* **2010,** *35* (4), 322-332.

26. Bertazzoni Minelli, E.; Della Bora, T.; Benini, A., Different microbial biofilm formation on polymethylmethacrylate (PMMA) bone cement loaded with gentamicin and vancomycin. *Anaerobe* **2011,** *17* (6), 380-383.

27. Penner, M. J.; Duncan, C. P.; Masri, B. A., The in vitro elution characteristics of antibiotic-loaded CMW and Palacos-R bone cements. *The Journal of Arthroplasty* **1999,** *14* (2), 209-214.

28. Torholm, C.; Lidgren, L.; Lindberg, L.; Kahlmeter, G., Total Hip Joint Arthroplasty with Gentamicin-impregnated Cement: A Clinical Study of Gentamicin Excretion Kinetics. *Clinical Orthopaedics and Related Research* **1983,** *181*, 99-106.

29. Bunetel, L.; Segui, A.; Cormier, M.; Percheron, E.; Langlais, F., Release of gentamicin from acrylic bone cement. *Clinical pharmacokinetics* **1989,** *17* (4), 291-7.

30. Hendriks, J. G.; Neut, D.; van Horn, J. R.; van der Mei, H. C.; Busscher, H. J., Bacterial survival in the interfacial gap in gentamicin-loaded acrylic bone cements. *J Bone Joint Surg Br* **2005,** *87* (2), 272-6.

31. El-Harouny, M. A.; Zalata, A. A.; Naser, M. E.; Abo El-Atta, H. M.; El-Shawaf, I. M.; Mostafa, T., Long-term ofloxacin testicular toxicity: an experimental study. *Andrologia* **2010,** *42* (2), 92-96.

32. Huh, A. J.; Kwon, Y. J., "Nanoantibiotics": a new paradigm for treating infectious diseases using nanomaterials in the antibiotics resistant era. *Journal of controlled release : official journal of the Controlled Release Society* **2011,** *156* (2), 128-45.

33. Israelachvili, J. N.; Mitchell, D. J.; Ninham, B. W., Theory of self-assembly of lipid bilayers and vesicles. *Biochimica et biophysica acta* **1977,** *470* (2), 185-201.

34. Zhang, L.; Eisenberg, A., Multiple Morphologies of "Crew-Cut" Aggregates of Polystyrene-b-poly(acrylic acid) Block Copolymers. *Science* **1995,** *268* (5218), 1728-1731.

35. Won, Y.-Y.; Brannan, A. K.; Davis, H. T.; Bates, F. S., Cryogenic Transmission Electron Microscopy (Cryo-TEM) of Micelles and Vesicles Formed in Water by Poly(ethylene oxide)-Based Block Copolymers. *The Journal of Physical Chemistry B* **2002,** *106* (13), 3354-3364.

36. Antonietti, M.; Förster, S., Vesicles and Liposomes: A Self-Assembly Principle Beyond Lipids. *Advanced Materials* **2003,** *15* (16), 1323-1333.

37. Kauzmann, W., Some Factors in the Interpretation of Protein Denaturation. In *Advances in Protein Chemistry*, C.B. Anfinsen, M. L. A. K. B.; John, T. E., Eds. Academic Press: 1959; Vol. Volume 14, pp 1-63.

38. Motornov, M.; Roiter, Y.; Tokarev, I.; Minko, S., Stimuli-responsive nanoparticles, nanogels and capsules for integrated multifunctional intelligent systems. *Progress in Polymer Science* **2010,** *35* (1–2), 174-211.

39. Discher, B. M.; Won, Y.-Y.; Ege, D. S.; Lee, J. C.-M.; Bates, F. S.; Discher, D. E.; Hammer, D. A., Polymersomes: Tough Vesicles Made from Diblock Copolymers. *Science* **1999,** *284* (5417), 1143-1146.

40. Shi, J.; Votruba, A. R.; Farokhzad, O. C.; Langer, R., Nanotechnology in Drug Delivery and Tissue Engineering: From Discovery to Applications. *Nano Lett.* **2010,** *10* (9), 3223-3230.

41. Al-Jamal, W. T.; Kostarelos, K., Liposomes: From a Clinically Established Drug Delivery System to a Nanoparticle Platform for Theranostic Nanomedicine. *Accounts of Chemical Research* **2011,** *44* (10), 1094-1104.

42. Torchilin, V., Liposomes in Drug Delivery

Fundamentals and Applications of Controlled Release Drug Delivery. Siepmann, J.; Siegel, R. A.; Rathbone, M. J., Eds. Springer US: 2012; pp 289-328.

43. Nardin, C.; Meier, W., Hybrid materials from amphiphilic block copolymers and membrane proteins. *Reviews in Molecular Biotechnology* **2002,** *90* (1), 17-26.

44. Kumar, M.; Grzelakowski, M.; Zilles, J.; Clark, M.; Meier, W., Highly permeable polymeric membranes based on the incorporation of the functional water channel protein Aquaporin Z. *Proceedings of the National Academy of Sciences* **2007,** *104* (52), 20719-20724.

45. De Vocht, C.; Ranquin, A.; Willaert, R.; Van Ginderachter, J. A.; Vanhaecke, T.; Rogiers, V.; Versées, W.; Van Gelder, P.; Steyaert, J., Assessment of stability, toxicity and immunogenicity of new polymeric nanoreactors for use in enzyme replacement therapy of MNGIE. *Journal of Controlled Release* **2009,** *137* (3), 246-254.

46. Choucair, A.; Lim Soo, P.; Eisenberg, A., Active Loading and Tunable Release of Doxorubicin from Block Copolymer Vesicles. *Langmuir* **2005,** *21* (20), 9308-9313.

47. Wu, J.; Eisenberg, A., Proton Diffusion across Membranes of Vesicles of Poly(styrene-b-acrylic Acid) Diblock Copolymers. *Journal of the American Chemical Society* **2006,** *128* (9), 2880-2884.

48. Kim, K. T.; Cornelissen, J. J. L. M.; Nolte, R. J. M.; van Hest, J. C. M., A Polymersome Nanoreactor with Controllable Permeability Induced by Stimuli-Responsive Block Copolymers. *Advanced Materials* **2009,** *21* (27), 2787-2791.

49. Kim, K. T.; Meeuwissen, S. A.; Nolte, R. J.; van Hest, J. C., Smart nanocontainers and nanoreactors. *Nanoscale* **2010,** *2* (6), 844-58.

50. Brinkhuis, R. P.; Rutjes, F. P. J. T.; van Hest, J. C. M., Polymeric vesicles in biomedical applications. *Polymer Chemistry* **2011,** *2* (7), 1449-1462.

51. Egli, S.; Schlaad, H.; Bruns, N.; Meier, W., Functionalization of Block Copolymer Vesicle Surfaces. *Polymers* **2011,** *3* (1), 252-280.

52. Esser-Kahn, A. P.; Odom, S. A.; Sottos, N. R.; White, S. R.; Moore, J. S., Triggered Release from Polymer Capsules. *Macromolecules* **2011,** *44* (14), 5539-5553.

53. Wang, Z. G., Curvature instability of diblock copolymer bilayers. *Macromolecules* **1992,** *25* (14), 3702-3705.

54. Zhang, L.; Yu, K.; Eisenberg, A., Ion-Induced Morphological Changes in "Crew-Cut" Aggregates of Amphiphilic Block Copolymers. *Science* **1996,** *272* (5269), 1777-1779.

55. Yu, Y.; Zhang, L.; Eisenberg, A., Morphogenic Effect of Solvent on Crew-Cut Aggregates of Apmphiphilic Diblock Copolymers. *Macromolecules* **1998,** *31* (4), 1144-1154.

56. Burke, S.; Shen, H.; Eisenberg, A., Multiple vesicular morphologies from block copolymers in solution. *Macromolecular Symposia* **2001,** *175* (1), 273-284.

57. Reeves, J. P.; Dowben, R. M., Formation and properties of thin-walled phospholipid vesicles. *Journal of Cellular Physiology* **1969,** *73* (1), 49-60.

58. Lee, J. C. M.; Bermudez, H.; Discher, B. M.; Sheehan, M. A.; Won, Y.-Y.; Bates, F. S.; Discher, D. E., Preparation, stability, and in vitro performance of vesicles made with diblock copolymers. *Biotechnol. Bioeng.* **2001,** *73* (2), 135-145.

59. Oku, N.; Scheerer, J. F.; MacDonald, R. C., Preparation of giant liposomes. *Biochimica et Biophysica Acta (BBA) - Biomembranes* **1982,** *692* (3), 384-388.

60. Kremer, J. M. H.; Van der Esker, M. W.; Pathmamanoharan, C.; Wiersema, P. H., Vesicles of variable diameter prepared by a modified injection method. *Biochemistry* **1977,** *16* (17), 3932-3935.

61. Moscho, A.; Orwar, O.; Chiu, D. T.; Modi, B. P.; Zare, R. N., Rapid preparation of giant unilamellar vesicles. *Proceedings of the National Academy of Sciences* **1996,** *93* (21), 11443-11447.

62. Olson, F.; Hunt, C. A.; Szoka, F. C.; Vail, W. J.; Papahadjopoulos, D., Preparation of liposomes of defined size distribution by extrusion through polycarbonate membranes. *Biochimica et Biophysica Acta (BBA) - Biomembranes* **1979,** *557* (1), 9-23.

63. Ollivon, M.; Walter, A.; Blumenthal, R., Sizing and separation of liposomes, biological vesicles, and viruses by high-performance liquid chromatography. *Analytical Biochemistry* **1986,** *152* (2), 262-274.

64. Oku, N.; MacDonald, R. C., Differential effects of alkali metal chlorides on formation of giant liposomes by freezing and thawing and by dialysis. *Biochemistry* **1983,** *22* (4), 855-863.

65. Seung, S. L. N.; Young, R. N., Preparation of a diblock copolymer of isobutyl vinyl ether and 2-methyl-2-oxazoline. *Journal of Polymer Science: Polymer Letters Edition* **1979,** *17* (4), 233-240.

66. Seung, S. L. N.; Young, R. N., Polymerization of styrene oxide initiated by iodine and preparation of styrene oxide-2-methyl-2-oxazoline block copolymer. *Journal of Polymer Science: Polymer Letters Edition* **1980,** *18* (2), 89-96.

67. Simionescu, C.; Rabia, I.; Crişan, Z., Triblock copolymers of 2-methyl-2-oxazoline and poly(ethyleneglycoladipate). *Polymer Bulletin* **1982,** *7* (4), 217-222.

68. Simionescu, C.; Rabia, I., Triblock copolymers of 2-substituted-2-oxazoline and poly(ethylene oxide). *Polymer Bulletin* **1983,** *10* (7-8), 311-314.

69. Dai, Z.; Dähne, L.; Donath, E.; Möhwald, H., Downhill Energy Transfer via Ordered Multichromophores in Light-Harvesting Capsules. *The Journal of Physical Chemistry B* **2002,** *106* (44), 11501-11508.

70. Prinos, J.; Panayiotou, C., Glass transition temperature in hydrogen-bonded polymer mixtures. *Polymer* **1995,** *36* (6), 1223-1227.

71. Yilgor, I.; Steckle, W. P.; Yilgor, E.; Freelin, R. G.; Riffle, J. S., Novel triblock siloxane copolymers: Synthesis, characterization, and their use as surface modifying

additives. *Journal of Polymer Science Part A: Polymer Chemistry* **1989,** *27* (11), 3673-3690.

72. Yilgör, İ.; McGrath, J., Polysiloxane containing copolymers: A survey of recent developments. In *Polysiloxane Copolymers/Anionic Polymerization*, Springer Berlin Heidelberg: 1988; Vol. 86, pp 1-86.

73. Mathur, A. B.; Collier, T. O.; Kao, W. J.; Wiggins, M.; Schubert, M. A.; Hiltner, A.; Anderson, J. M., In vivo biocompatibility and biostability of modified polyurethanes. *Journal of Biomedical Materials Research* **1997,** *36* (2), 246-257.

74. Owen Michael, J., Siloxane Surface Activity. In *Silicon-Based Polymer Science*, American Chemical Society: 1989; Vol. 224, pp 705-739.

75. Zalipsky, S.; Hansen, C. B.; Oaks, J. M.; Allen, T. M., Evaluation of blood clearance rates and biodistribution of poly(2-oxazoline)-grafted liposomes. *Journal of Pharmaceutical Sciences* **1996,** *85* (2), 133-137.

76. Woodle, M. C., Controlling liposome blood clearance by surface-grafted polymers. *Advanced Drug Delivery Reviews* **1998,** *32* (1–2), 139-152.

77. Konradi, R.; Pidhatika, B.; Muhlebach, A.; Textor, M., Poly-2-methyl-2-oxazoline: A Peptide-like Polymer for Protein-Repellent Surfaces. *Langmuir* **2008,** *24* (3), 613-616.

78. Pidhatika, B.; Rodenstein, M.; Chen, Y.; Rakhmatullina, E.; Mühlebach, A.; Acikgöz, C.; Textor, M.; Konradi, R., Comparative Stability Studies of Poly(2-methyl-2-oxazoline) and Poly(ethylene glycol) Brush Coatings. *Biointerphases* **2012,** *7* (1), 1-15.

79. Woodle, M. C.; Engbers, C. M.; Zalipsky, S., New Amphipatic Polymer-Lipid Conjugates Forming Long-Circulating Reticuloendothelial System-Evading Liposomes. *Bioconjugate Chemistry* **1994,** *5* (6), 493-496.

80. Brož, P.; Benito, S. M.; Saw, C.; Burger, P.; Heider, H.; Pfisterer, M.; Marsch, S.; Meier, W.; Hunziker, P., Cell targeting by a generic receptor-targeted polymer nanocontainer platform. *Journal of Controlled Release* **2005,** *102* (2), 475-488.

81. Ranquin, A.; Versées, W.; Meier, W.; Steyaert, J.; Van Gelder, P., Therapeutic Nanoreactors: Combining Chemistry and Biology in a Novel Triblock Copolymer Drug Delivery System. *Nano Lett.* **2005,** *5* (11), 2220-2224.

82. Adams, N.; Schubert, U. S., Poly(2-oxazolines) in biological and biomedical application contexts. *Advanced Drug Delivery Reviews* **2007,** *59* (15), 1504-1520.

83. Hoogenboom, R., Poly(2-oxazoline)s: a polymer class with numerous potential applications. *Angewandte Chemie* **2009,** *48* (43), 7978-94.

84. Viegas, T. X.; Bentley, M. D.; Harris, J. M.; Fang, Z.; Yoon, K.; Dizman, B.; Weimer, R.; Mero, A.; Pasut, G.; Veronese, F. M., Polyoxazoline: Chemistry, Properties, and Applications in Drug Delivery. *Bioconjugate Chemistry* **2011,** *22* (5), 976-986.

85. Kobayashi, S.; Uyama, H.; Ihara, E.; Saegusa, T., Block copolymerization of tetrahydrofuran with cyclic imino ether: synthesis of a new nonionic polymer surfactant. *Macromolecules* **1990,** *23* (6), 1586-1589.

86. Odian, G., Ring-Opening Polymerization. In *Principles of Polymerization*, John Wiley & Sons, Inc.: 2004; pp 544-618.

87. Aranda-Espinoza, H.; Bermudez, H.; Bates, F. S.; Discher, D. E., Electromechanical limits of polymersomes. *Physical review letters* **2001,** *87* (20), 208301.

88. Discher, D. E.; Eisenberg, A., Polymer vesicles. *Science* **2002,** *297* (5583), 967-73.

89. Renggli, K.; Baumann, P.; Langowska, K.; Onaca, O.; Bruns, N.; Meier, W., Selective and Responsive Nanoreactors. *Advanced Functional Materials* **2011,** *21* (7), 1241-1259.

90. Caruso, F., Nanoengineering of Particle Surfaces. *Advanced Materials* **2001,** *13* (1), 11-22.

91. Antipov, A. A.; Sukhorukov, G. B.; Möhwald, H., Influence of the Ionic Strength on the Polyelectrolyte Multilayers' Permeability. *Langmuir* **2003,** *19* (6), 2444-2448.

92. Kreft, O.; Prevot, M.; Möhwald, H.; Sukhorukov, G. B., Shell-in-Shell Microcapsules: A Novel Tool for Integrated, Spatially Confined Enzymatic Reactions. *Angewandte Chemie International Edition* **2007,** *46* (29), 5605-5608.

93. Vriezema, D. M.; Hoogboom, J.; Velonia, K.; Takazawa, K.; Christianen, P. C. M.; Maan, J. C.; Rowan, A. E.; Nolte, R. J. M., Vesicles and Polymerized Vesicles from Thiophene-Containing Rod–Coil Block Copolymers. *Angewandte Chemie International Edition* **2003,** *42* (7), 772-776.

94. Nallani, M.; de Hoog, H.-P. M.; Cornelissen, J. J. L. M.; Palmans, A. R. A.; van Hest, J. C. M.; Nolte, R. J. M., Polymersome Nanoreactors for Enzymatic Ring-Opening Polymerization. *Biomacromolecules* **2007,** *8* (12), 3723-3728.

95. Kuiper, S. M.; Nallani, M.; Vriezema, D. M.; Cornelissen, J. J. L. M.; van Hest, J. C. M.; Nolte, R. J. M.; Rowan, A. E., Enzymes containing porous polymersomes as nano reaction vessels for cascade reactions. *Organic & Biomolecular Chemistry* **2008,** *6* (23), 4315-4318.

96. Koide, A.; Kishimura, A.; Osada, K.; Jang, W.-D.; Yamasaki, Y.; Kataoka, K., Semipermeable Polymer Vesicle (PICsome) Self-Assembled in Aqueous Medium from a Pair of Oppositely Charged Block Copolymers: Physiologically Stable Micro-/Nanocontainers of Water-Soluble Macromolecules. *Journal of the American Chemical Society* **2006,** *128* (18), 5988-5989.

97. Kishimura, A.; Koide, A.; Osada, K.; Yamasaki, Y.; Kataoka, K., Encapsulation of Myoglobin in PEGylated Polyion Complex Vesicles Made from a Pair of Oppositely Charged Block Ionomers: A Physiologically Available Oxygen Carrier. *Angewandte Chemie* **2007,** *119* (32), 6197-6200.

98. Cheng, Z.; Tsourkas, A., Paramagnetic Porous Polymersomes. *Langmuir* **2008,** *24* (15), 8169-8173.

99. Cheng, Z.; Thorek, D. L. J.; Tsourkas, A., Porous Polymersomes with Encapsulated Gd-Labeled Dendrimers as Highly Efficient MRI Contrast Agents. *Advanced Functional Materials* **2009,** *19* (23), 3753-3759.

100. Nardin, C.; Thoeni, S.; Widmer, J.; Winterhalter, M.; Meier, W., Nanoreactors based on (polymerized) ABA-triblock copolymer vesicles. *Chemical Communications* **2000,** (15), 1433-1434.

101. Nardin, C.; Widmer, J.; Winterhalter, M.; Meier, W., Amphiphilic block copolymer nanocontainers as bioreactors. *The European Physical Journal E: Soft Matter and Biological Physics* **2001,** *4* (4), 403-410.

102. Graff, A.; Sauer, M.; Van Gelder, P.; Meier, W., Virus-assisted loading of polymer nanocontainer. *Proceedings of the National Academy of Sciences of the United States of America* **2002,** *99* (8), 5064-8.

103. Axthelm, F.; Casse, O.; Koppenol, W. H.; Nauser, T.; Meier, W.; Palivan, C. G., Antioxidant Nanoreactor Based on Superoxide Dismutase Encapsulated in Superoxide-Permeable Vesicles. *The Journal of Physical Chemistry B* **2008,** *112* (28), 8211-8217.

104. Grzelakowski, M.; Onaca, O.; Rigler, P.; Kumar, M.; Meier, W., Immobilized Protein–Polymer Nanoreactors. *Small* **2009,** *5* (22), 2545-2548.

105. Tanner, P.; Onaca, O.; Balasubramanian, V.; Meier, W.; Palivan, C. G., Enzymatic Cascade Reactions inside Polymeric Nanocontainers: A Means to Combat Oxidative Stress. *Chemistry – A European Journal* **2011,** *17* (16), 4552-4560.

106. Vriezema, D. M.; Garcia, P. M. L.; Sancho Oltra, N.; Hatzakis, N. S.; Kuiper, S. M.; Nolte, R. J. M.; Rowan, A. E.; van Hest, J. C. M., Positional Assembly of Enzymes in Polymersome Nanoreactors for Cascade Reactions. *Angewandte Chemie International Edition* **2007,** *46* (39), 7378-7382.

107. Egli, S.; Nussbaumer, M. G.; Balasubramanian, V.; Chami, M.; Bruns, N.; Palivan, C.; Meier, W., Biocompatible Functionalization of Polymersome Surfaces: A New Approach to Surface Immobilization and Cell Targeting Using Polymersomes. *Journal of the American Chemical Society* **2011,** *133* (12), 4476-4483.

108. De Hoog, H.-P. M.; Arends, I. W. C. E.; Rowan, A. E.; Cornelissen, J. J. L. M.; Nolte, R. J. M., A hydrogel-based enzyme-loaded polymersome reactor. *Nanoscale* **2010,** *2* (5), 709-716.

109. Crescenzi, V.; Cornelio, L.; Di Meo, C.; Nardecchia, S.; Lamanna, R., Novel Hydrogels via Click Chemistry: Synthesis and Potential Biomedical Applications. *Biomacromolecules* **2007,** *8* (6), 1844-1850.

110. Li, F.; Ketelaar, T.; Cohen Stuart, M. A.; Sudholter, E. J. R.; Leermakers, F. A. M.; Marcelis, A. T. M., Gentle Immobilization of Nonionic Polymersomes on Solid Substrates. *Langmuir* **2007,** *24* (1), 76-82.

111. Huang, N.-P.; Csucs, G.; Emoto, K.; Nagasaki, Y.; Kataoka, K.; Textor, M.; Spencer, N. D., Covalent Attachment of Novel Poly(ethylene glycol)−Poly(dl-lactic acid) Copolymeric Micelles to TiO2 Surfaces. *Langmuir* **2001,** *18* (1), 252-258.

112. Domes, S.; Filiz, V.; Nitsche, J.; Frömsdorf, A.; Förster, S., Covalent Attachment of Polymersomes to Surfaces. *Langmuir* **2010,** *26* (10), 6927-6931.

113. Layer, R. W., The Chemistry of Imines. *Chemical Reviews* **1963,** *63* (5), 489-510.

114. Weber, P.; Ohlendorf, D.; Wendoloski, J.; Salemme, F., Structural origins of high-affinity biotin binding to streptavidin. *Science* **1989,** *243* (4887), 85-88.

115. Holmberg, A.; Blomstergren, A.; Nord, O.; Lukacs, M.; Lundeberg, J.; Uhlén, M., The biotin-streptavidin interaction can be reversibly broken using water at elevated temperatures. *ELECTROPHORESIS* **2005,** *26* (3), 501-510.

116. Alon, R.; Hershkoviz, R.; Bayer, E. A.; Wilchek, M.; Lider, O., Streptavidin blocks immune reactions mediated by fibronectin-VLA-5 recognition through an Arg-Gly-Asp mimicking site. *European Journal of Immunology* **1993,** *23* (4), 893-898.

117. Sato, S.; Sakamoto, T.; Miyazawa, E.; Kikugawa, Y., One-pot reductive amination of aldehydes and ketones with α-picoline-borane in methanol, in water, and in neat conditions. *Tetrahedron* **2004,** *60* (36), 7899-7906.

118. Ruhaak, L. R.; Steenvoorden, E.; Koeleman, C. A. M.; Deelder, A. M.; Wuhrer, M., 2-Picoline-borane: A non-toxic reducing agent for oligosaccharide labeling by reductive amination. *PROTEOMICS* **2010,** *10* (12), 2330-2336.

119. Sigrist, H.; Gao, H.; Wegmuller, B., Light-Dependent, Covalent Immobilization of Biomolecules on /`Inert/' Surfaces. *Nat Biotech* **1992,** *10* (9), 1026-1028.

120. Guire, P., [21] Photochemical immobilization of enzymes and other biochemicals. In *Methods in Enzymology*, Klaus, M., Ed. Academic Press: 1976; Vol. Volume 44, pp 280-288.

121. Sugawara, T.; Matsuda, T., Photochemical Protein Fixation on Polymer Surfaces via Derivatized Phenyl Azido Group. *Langmuir* **1995,** *11* (6), 2272-2276.

122. Al-Bataineh, S. A.; Luginbuehl, R.; Textor, M.; Yan, M., Covalent Immobilization of Antibacterial Furanones via Photochemical Activation of Perfluorophenylazide. *Langmuir* **2009,** *25* (13), 7432-7437.

123. Coll Ferrer, M. C.; Yang, S.; Eckmann, D. M.; Composto, R. J., Creating Biomimetic Polymeric Surfaces by Photochemical Attachment and Patterning of Dextran. *Langmuir* **2010,** *26* (17), 14126-14134.

124. Zhao, Y.; Xu, Z.; Wang, X.; Lin, T., Photoreactive Azido-Containing Silica Nanoparticle/Polycation Multilayers: Durable Superhydrophobic Coating on Cotton Fabrics. *Langmuir* **2012,** *28* (15), 6328-6335.

125. Poe, R.; Schnapp, K.; Young, M. J. T.; Grayzar, J.; Platz, M. S., Chemistry and kinetics of singlet pentafluorophenylnitrene. *Journal of the American Chemical Society* **1992,** *114* (13), 5054-5067.

126. Bräse, S.; Gil, C.; Knepper, K.; Zimmermann, V., Organic Azides: An Exploding Diversity of a Unique Class of Compounds. *Angewandte Chemie International Edition* **2005,** *44* (33), 5188-5240.

127. Liu, L.-H.; Yan, M., Simple Method for the Covalent Immobilization of Graphene. *Nano Lett.* **2009,** *9* (9), 3375-3378.

128. Bartlett, M. A.; Yan, M., Fabrication of Polymer Thin Films and Arrays with Spatial and Topographical Controls. *Advanced Materials* **2001,** *13* (19), 1449-1451.

129. Chen, G.; Ito, Y.; Imanishi, Y.; Magnani, A.; Lamponi, S.; Barbucci, R., Photoimmobilization of Sulfated Hyaluronic Acid for Antithrombogenicity. *Bioconjugate Chemistry* **1997,** *8* (5), 730-734.

130. Zhu, A.; Zhang, M.; Shen, J., Covalent immobilization of O-butyrylchitosan with a photosensitive hetero-bifunctional crosslinking reagent on biopolymer substrate surface and bloodcompatibility characterization. *Journal of Biomaterials Science, Polymer Edition* **2003,** *14* (5), 411-421.

131. Zhu, A.; Zhang, M.; Wu, J.; Shen, J., Covalent immobilization of chitosan/heparin complex with a photosensitive hetero-bifunctional crosslinking reagent on PLA surface. *Biomaterials* **2002,** *23* (23), 4657-4665.

132. Xu, G.; McLeod, H. L., Strategies for Enzyme/Prodrug Cancer Therapy. *Clinical Cancer Research* **2001,** *7* (11), 3314-3324.

133. Bagshawe, K. D.; Springer, C. J.; Searle, F.; Antoniw, P.; Sharma, S. K.; Melton, R. G.; Sherwood, R. F., A cytotoxic agent can be generated selectively at cancer sites. *British journal of cancer* **1988,** *58* (6), 700-703.

134. Smyth, T. P.; O'Donnell, M. E.; O'Connor, M. J.; St Ledger, J. O., β-Lactamase-Dependent Prodrugs—Recent Developments. *Tetrahedron* **2000,** *56* (31), 5699-5707.

135. Rodrigues, M. L.; Carter, P.; Wirth, C.; Mullins, S.; Lee, A.; Blackburn, B. K., Synthesis and β-lactamase-mediated activation of a cephalosporin-taxol prodrug. *Chemistry & Biology* **1995,** *2* (4), 223-227.

136. Nardin, C.; Hirt, T.; Leukel, J.; Meier, W., Polymerized ABA triblock copolymer vesicles. *Langmuir* **2000,** *16* (3), 1035-1041.

137. Kobayashi, S.; Uyama, H.; Narita, Y.; Ishiyama, J., Novel multifunctional initiators for polymerization of 2-oxazolines. *Macromolecules* **1992,** *25* (12), 3232-3236.

138. Kobayashi, S.; Iijima, S.; Igarashi, T.; Saegusa, T., Synthesis of a nonionic polymer surfactant from cyclic imino ethers by the initiator method. *Macromolecules* **1987,** *20* (8), 1729-1734.

139. Yilgor, I.; Yilgor, E., Thermal stabilities of end groups in hydroxyalkyl terminated polydimethylsiloxane oligomers. *Polymer Bulletin* **1998,** *40* (4), 525-532.

140. Cai, D.; Neyer, A.; Kuckuk, R.; Heise, H. M., Raman, mid-infrared, near-infrared and ultraviolet–visible spectroscopy of PDMS silicone rubber for characterization of

polymer optical waveguide materials. *Journal of Molecular Structure* **2010,** *976* (1–3), 274-281.

141. Kobayashi, S.; Masuda, E.; Shoda, S.; Shimano, Y., Synthesis of acryl- and methacryl-type macromonomers and telechelics by utilizing living polymerization of 2-oxazolines. *Macromolecules* **1989,** *22* (7), 2878-2884.

142. Lim Soo, P.; Eisenberg, A., Preparation of block copolymer vesicles in solution. *Journal of Polymer Science Part B: Polymer Physics* **2004,** *42* (6), 923-938.

143. Mayer, L. D.; Hope, M. J.; Cullis, P. R., Vesicles of variable sizes produced by a rapid extrusion procedure. *Biochimica et Biophysica Acta (BBA) - Biomembranes* **1986,** *858* (1), 161-168.

144. Jousma, H.; Talsma, H.; Spies, F.; Joosten, J. G. H.; Junginger, H. E.; Crommelin, D. J. A., Characterization of liposomes. The influence of extrusion of multilamellar vesicles through polycarbonate membranes on particle size, particle size distribution and number of bilayers. *International Journal of Pharmaceutics* **1987,** *35* (3), 263-274.

145. Hunter, D. G.; Frisken, B. J., Effect of Extrusion Pressure and Lipid Properties on the Size and Polydispersity of Lipid Vesicles. *Biophysical Journal* **1998,** *74* (6), 2996-3002.

146. Mui, B.; Chow, L.; Hope, M. J., Extrusion Technique to Generate Liposomes of Defined Size. In *Methods in Enzymology*, Nejat, D., Ed. Academic Press: 2003; Vol. Volume 367, pp 3-14.

147. Phale, P. S.; Philippsen, A.; Kiefhaber, T.; Koebnik, R.; Phale, V. P.; Schirmer, T.; Rosenbusch, J. P., Stability of Trimeric OmpF Porin: The Contributions of the Latching Loop L2†. *Biochemistry* **1998,** *37* (45), 15663-15670.

148. Stauch, O.; Schubert, R.; Savin, G.; Burchard, W., Structure of Artificial Cytoskeleton Containing Liposomes in Aqueous Solution Studied by Static and Dynamic Light Scattering. *Biomacromolecules* **2002,** *3* (3), 565-578.

149. Litvinchuk, S.; Lu, Z.; Rigler, P.; Hirt, T.; Meier, W., Calcein Release from Polymeric Vesicles in Blood Plasma and PVA Hydrogel. *Pharmaceutical Research* **2009,** *26* (7), 1711-1717.

150. Walde, P.; Ichikawa, S., Enzymes inside lipid vesicles: preparation, reactivity and applications. *Biomolecular Engineering* **2001,** *18* (4), 143-177.

151. O'Neil, C. P.; Suzuki, T.; Demurtas, D.; Finka, A.; Hubbell, J. A., A Novel Method for the Encapsulation of Biomolecules into Polymersomes via Direct Hydration. *Langmuir* **2009,** *25* (16), 9025-9029.

152. Parnell, A. J.; Tzokova, N.; Topham, P. D.; Adams, D. J.; Adams, S.; Fernyhough, C. M.; Ryan, A. J.; Jones, R. A. L., The efficiency of encapsulation within surface rehydrated polymersomes. *Farad. Discuss.* **2009,** *143*, 29-46.

153. Balasubramanian, V.; Onaca, O.; Ezhevskaya, M.; Van Doorslaer, S.; Sivasankaran, B.; Palivan, C. G., A surprising system: polymeric nanoreactors containing a mimic with dual-enzyme activity. *Soft Matter* **2011,** *7* (12), 5595-5603.

154. Bruggink, A.; Roos, E. C.; de Vroom, E., Penicillin Acylase in the Industrial Production of β-Lactam Antibiotics. *Organic Process Research & Development* **1998,** *2* (2), 128-133.

155. Merino, E.; Balbás, P.; Recillas, F.; Becerril, B.; Valle, F.; Bolivar, F., Carbon regulation and the role in nature of the Escherichia coli penicillin acylase (pac) gene. *Molecular Microbiology* **1992,** *6* (15), 2175-2182.

156. Böck, A.; Wirth, R.; Schmid, G.; Schumacher, G.; Lang, G.; Buckel, P., The two subunits of penicillin acylase are processed from a common precursor. *FEMS Microbiology Letters* **1983,** *20* (2), 141-144.

157. Böck, A.; Wirth, R.; Schmid, G.; Schumacher, G.; Lang, G.; Buckel, P., The penicillin acylase from Escherichia coli ATCC11105 consists of two dissimilar subunits. *FEMS Microbiology Letters* **1983,** *20* (2), 135-139.

158. Rolinson, G. N., Forty years of beta-lactam research. *Journal of Antimicrobial Chemotherapy* **1998,** *41* (6), 589-603.

159. Schroën, C. G. P. H.; Fretz, C. B.; DeBruin, V. H.; Berendsen, W.; Moody, H. M.; Roos, E. C.; VanRoon, J. L.; Kroon, P. J.; Strubel, M.; Janssen, A. E. M.; Tramper, J., Modelling of the enzymatic kinetically controlled synthesis of cephalexin: Influence of diffusion limitation. *Biotechnol. Bioeng.* **2002,** *80* (3), 331-340.

160. Spratt, B. G., Distinct penicillin binding proteins involved in the division, elongation, and shape of Escherichia coli K12. *Proc Natl Acad Sci U S A* **1975,** *72* (8), 2999-3003.

161. Choi, W. G.; Lee, S. B.; Ryu, D. D. Y., Cephalexin synthesis by partially purified and immobilized enzymes. *Biotechnol. Bioeng.* **1981,** *23* (2), 361-371.

162. Schroën, C. G. P. H.; Nierstrasz, V. A.; Moody, H. M.; Hoogschagen, M. J.; Kroon, P. J.; Bosma, R.; Beeftink, H. H.; Janssen, A. E. M.; Tramper, J., Modeling of the enzymatic kinetic synthesis of cephalexin—Influence of substrate concentration and temperature. *Biotechnol. Bioeng.* **2001,** *73* (3), 171-178.

163. Okunuki, K., Denaturation and Inactivation of Enzyme Proteins. In *Advances in Enzymology and Related Areas of Molecular Biology*, John Wiley & Sons, Inc.: 2006; pp 29-82.

164. Bundgaard, H.; Larsen, C., A new spectrophotometric method for the selective determination of ampicillin, amoxycillin and cyclacillin in the presence of polymers and other degradation products. *J Pharm Biomed Anal* **1983,** *1* (1), 29-37.

165. Ospina, S. S.; Lopez-Munguia, A.; Gonzalez, R. L.; Quintero, R., Characterization and use of a penicillin acylase biocatalyst. *Journal of Chemical Technology & Biotechnology* **1992,** *53* (2), 205-213.

166. Kenefick, N. J.; Vaizey, C. J.; Malouf, A. J.; Norton, C. S.; Marshall, M.; Kamm, M. A., Injectable silicone biomaterial for faecal incontinence due to internal anal sphincter dysfunction. *Gut* **2002,** *51* (2), 225-228.

167. Hsiue, G.-H.; Lee, S.-D.; Chuen-Thuen Chang, P.; Kao, C.-Y., Surface characterization and biological properties study of silicone rubber membrane grafted with phospholipid as biomaterial via plasma induced graft copolymerization. *Journal of Biomedical Materials Research* **1998,** *42* (1), 134-147.

168. Fleet, G. W.; Knowles, J. R.; Porter, R. R., The antibody binding site. Labelling of a specific antibody against the photo-precursor of an aryl nitrene. *Biochem J* **1972,** *128* (3), 499-508.

169. Harmer, M. A., Photomodification of surfaces using heterocyclic azides. *Langmuir* **1991,** *7* (10), 2010-2012.

170. Nahar, P.; Wali, N. M.; Gandhi, R. P., Light-Induced Activation of an Inert Surface for Covalent Immobilization of a Protein Ligand. *Analytical Biochemistry* **2001,** *294* (2), 148-153.

171. Chen, R.; Cole, N.; Willcox, M. D. P.; Park, J.; Rasul, R.; Carter, E.; Kumar, N., Synthesis, characterization and in vitro activity of a surface-attached antimicrobial cationic peptide. *Biofouling* **2009,** *25* (6), 517-524.

172. Dess, D. B.; Martin, J. C., Readily accessible 12-I-5 oxidant for the conversion of primary and secondary alcohols to aldehydes and ketones. *The Journal of Organic Chemistry* **1983,** *48* (22), 4155-4156.

173. Speicher, A.; Bomm, V.; Eicher, T., Dess–Martin-Periodinan (DMP)

Dess–Martin-Periodinane (DMP). *Journal für Praktische Chemie/Chemiker-Zeitung* **1996,** *338* (1), 588-590.

174. Li, S. L.; Palmer, A. F., Structure of small actin-containing liposomes probed by atomic force microscopy: Effect of actin concentration & liposome size. *Langmuir* **2004,** *20* (19), 7917-7925.

175. Rakhmatullina, E.; Meier, W., Solid-Supported Block Copolymer Membranes through Interfacial Adsorption of Charged Block Copolymer Vesicles. *Langmuir* **2008,** *24* (12), 6254-6261.

176. (a) Yang, M.; Wang, W.; Yuan, F.; Zhang, X. W.; Li, J. Y.; Liang, F. X.; He, B. L.; Minch, B.; Wegner, G., Soft vesicles formed by diblock codendrimers of poly(benzyl ether) and poly(methallyl dichloride). *J Am Chem Soc* **2005,** *127* (43), 15107-15111; (b) Xie, D.; Jiang, M.; Zhang, G. Z.; Chen, D. Y., Hydrogen-bonded dendronized polymers and their self-assembly in solution. *Chem-Eur J* **2007,** *13* (12), 3346-3353.

177. Simons, H.; Gibson, T. D., Rapid continuous colorimetric enzyme assay for penicillin G acylase. *Biotechnology Techniques* **1999,** *13* (6), 365-367.

178. Liu, L.; Engelhard, M. H.; Yan, M., Surface and Interface Control on Photochemically Initiated Immobilization. *Journal of the American Chemical Society* **2006,** *128* (43), 14067-14072.

179. Kubo, T.; Wang, X.; Tong, Q.; Yan, M., Polymer-Based Photocoupling Agent for the Efficient Immobilization of Nanomaterials and Small Molecules. *Langmuir* **2011,** *27* (15), 9372-9378.

180. Leonard, D. N.; Russell, P. E.; Smith, S. D.; Spontak, R. J., Multiscale Dewetting of Low-Molecular-Weight Block Copolymer Ultrathin Films. *Macromolecular Rapid Communications* **2002,** *23* (3), 205-209.

181. Gu, X.; Raghavan, D.; Douglas, J. F.; Karim, A., Hole-growth instability in the dewetting of evaporating polymer solution films. *Journal of Polymer Science Part B: Polymer Physics* **2002,** *40* (24), 2825-2832.

182. Volegova, I.; Buzin, A., Morphology of ultrathin polymer films based on poly(ethylene oxide) blends. *Polymer Science Series A* **2007,** *49* (9), 1014-1019.

183. Jass, J.; Tjärnhage, T.; Puu, G., From Liposomes to Supported, Planar Bilayer Structures on Hydrophilic and Hydrophobic Surfaces: An Atomic Force Microscopy Study. *Biophysical Journal* **2000,** *79* (6), 3153-3163.

184. Prilipov, A.; Phale, P. S.; Van Gelder, P.; Rosenbusch, J. P.; Koebnik, R., Coupling site-directed mutagenesis with high-level expression: large scale production of mutant porins from E. coli. *FEMS Microbiology Letters* **1998,** *163* (1), 65-72.